E. TORUK

ATILIM UNIVERSITY 2023

STRUCTURAL PART DESIGN OPTIMIZATION OF RIGID SHEET METAL

THE GRADUATE SCHOOL OF NATURAL AND APPLIED SCIENCES
OF
ATILIM UNIVERSITY

EMRE TORUK

A MASTER OF SCIENCE THESIS
IN
THE DEPARTMENT OF MECHANICAL ENGINEERING

DECEMBER 2023

STRUCTURAL PART DESIGN OPTIMIZATION OF RIGID SHEET METAL

A THESIS SUBMITTED TO
THE GRADUATE SCHOOL OF NATURAL AND APPLIED SCIENCES
OF
ATILIM UNIVERSITY

BY

EMRE TORUK

IN PARTIAL FULFILLMENT OF THE REQUIREMENTS
FOR
THE DEGREE OF MASTER OF SCIENCE
IN
THE DEPARTMENT OF MECHANICAL ENGINEERING

DECEMBER 2023

Approval of the Graduate School of Natural and Applied Sciences, Atilim University

_____

Prof. Dr. Ender Keskinkılıç
Director

I certify that this thesis satisfies all the Requirements as a thesis for the degree of **Master of Science in Mechanical Engineering, Atilim University.**

_____

Prof. Dr. Sadık Engin Kılıç
Head of Department

This is to certify that we have read the thesis '' STRUCTURAL PART DESIGN OPTIMIZATION OF RIGID SHEET METAL'' submitted by ''EMRE TORUK'' and that in our opinion it is fully adequate, in scope and quality, as a thesis for the degree of Master of Science.

_____

Asst. Prof. Dr. Hakan Kalkan
Co-Supervisor

_____

Prof. Dr. Bilgin Kaftanoğlu
Supervisor

Examining Committee Members:

Prof. Dr. Ahmet Hakan Argeşo
Manufacturing Engineering Department, Atilim University _____

Prof. Dr. Bilgin Kaftanoğlu
Manufacturing Engineering Department, Atilim University _____

Prof. Dr. Haluk Darendeliler
Mechanical Engineering Department, METU _____

Asst. Prof. Dr. Hakan Kalkan
Manufacturing Engineering Department, Atilim University _____

Asst. Prof. Dr. Bahram Lotfi
Mechanical Engineering Department, Atilim University _____

Date: 25.12.2023

I hereby declare that all information in this document has been obtained and presented in accordance with academic rules and ethical conduct. I also declare that, as required by these rules and conduct, I have fully cited and referenced all material and results that are not original to this work.

Name, Last Name: Emre Toruk

Signature:

ABSTRACT

STRUCTURAL PART DESIGN OPTIMIZATION OF RIGID SHEET METAL

Toruk, Emre

MSc, Department of Mechanical Engineering

Supervisor : Prof. Dr. Bilgin Kaftanoğlu

Co-Supervisor : Asst. Prof. Dr. Hakan Kalkan

December 2023, 128 pages

Metal forming methods are widely used all over the world. Metal is shaped by using a wide variety of methods, especially in the aerospace and automotive industries. Hydraulic forming method, which is one of the metal forming methods, has been one of the preferred methods because of its ease of production, reduction of the need for molds, and effective in the production of complex structures. This method, which aims to transmit pressure evenly by using the incompressible property of the liquid, distinguishes the hydraulic metal forming method from the traditional metal forming methods. One of the hydraulic metal forming methods, which also has varieties in itself, is the sheet metal hydroform (Flexform) method. The liquid trapped in a rubber-based chamber is pressurized, and the metal forming method is performed with the pressure exerted by the rubber diaphragm on the mold and sheet metal part. Although it makes the production of complex structures possible, problems such as wrinkling, pot formation, tearing and springback seen in other metal forming methods have also been valid for this method.

In this study, forming patterns were created on the sheet metal part by using the sheet metal hydroform method, and these patterns were examined numerically and experimentally. In this study, in which a three-dimensional diaphragm, two-dimensional mold and sheet metal part were used, many patterns were modeled and as

a result of the elastic analyzes made between the modeled patterns, the most durable forming pattern was selected, which provides the least bending. Analysis and design optimizations were made using the selected pattern, 0.60 mm thick titanium with CP2 titanium material. A maximum 10% thinning design restriction was determined, and a study was conducted to reduce springback as much as possible. Plastic analyzes were carried out using the finite element method and the optimization processes continued until the design constraints were met. Then, molds were manufactured for the experimental processes and the shaping process was carried out. After the part was shaped, the thinning, distortion and strength gained by the part were measured by the supporting 4 point. After the deflection measurements were made, the part was transferred to the 3D environment by laser scanning method, and the simulation and experimental product were compared geometrically in the computer environment.

Keywords: Sheet Metal Forming, Hydroforming, Thinning, Spring Back, Wrinkling, Tear, Flexforming

ÖZ

RİJİT SAC METAL YAPISAL PARÇA TASARIMI OPTIMIZASYONU

Toruk, Emre

Yüksek Lisans, Makine Mühendisliği Bölümü

Tez Yöneticisi : Prof. Dr. Bilgin Kaftanoğlu

Ortak Tez Yôneticisi : Dr. Öğretim Üyesi Hakan Kalkan

Aralık 2023, 128 sayfa

Metal şekillendirme yöntemleri tüm dünyada yaygın kullanılmaktadır. Özellikle havacılık ve otomotiv sektörlerinde çok çeşitli yöntemler kullanılarak metale şekil verilmektedir. Metal şekillendirme yöntemlerinden biri olan hidrolik şekillendirme yöntemi, üretim kolaylığı, kalıp ihtiyacının azaltılabilmesi, karmaşık yapıların üretiminde etkili olduğu için tercih edilen yöntemlerden biri olmuştur. Sıvının sıkıştırılamayan özelliği kullanılarak basıncın eşit olarak iletilmesini hedefleyen bu yöntem, hidrolik metal şekillendirme yöntemini geleneksel metal şekillendirme yöntemlerinden ayırmaktadır. Kendi içerisinde de çeşitleri olan hidrolik metal şekillendirme yöntemlerinden bir tanesi de sac metal hidroform (Flexform) yöntemidir. Kauçuk tabanlı bir haznede hapsedilen sıvı basınçlandırılarak, kauçuk diyaftamın kalıp ve sac parça üzerine uyguladığı basınç ile metal şekillendirme yöntemi yapılmaktadır. Karmaşık yapıların üretimini mümkün de kılsa, diğer metal şekillendirme yöntemlerinde görülen kırışma, pot oluşumu, yırtılma ve geri yaylanma gibi sorunlar, bu yöntem için de geçerli olmuştur.

Yapılan bu çalışmada sac metal hidroform yöntemi kullanılarak sac parça üzerinde şekillendirme desenleri oluşturulmuş, bu desenler sayısal ve deneysel olarak incelenmiştir. Üç boyutlu diyafram, iki boyutlu kalıp ve sac parçanın kullanıldığı bu çalışmada birçok desen modellenmiş ve modellenen desenler arasında yapılan elastik analizler sonucunda en az bükülmeyi sağlayan, en mukavemetli şekillendirme deseni

seçilmiştir. Seçilen desen, 0.60 mm kalınlığındaki titanyum CP2 malzemesi kullanılarak analiz ve tasarım optimizasyonları yapılmıştır. Maksimum %10 incelme tasarım kısıtlaması belirlenmiş, geri yaylanmayı mümkün olduğunca azaltmak amaçlı bir çalışma yapılmıştır. Sonlu elemanlar yöntemi kullanılarak plastik analizler gerçekleştirilmiş ve tasarım kısıtları yakalanıncaya kadar optimizasyon süreçleri devam etmiştir. Daha sonra deneysel işlemler için kalıplar üretilerek şekillendirme işlemi gerçekleştirilmiştir. Parça şekillendirildikten sonra parçada oluşan incelme, çarpılma ve mukavemet basit destekli kiriş yöntemiyle ölçülmüştür. Sehim ölçümleri yapıldıktan sonra ise, parça 3 boyutlu ortama lazer tarama yöntemi ile aktarılmış, simulasyon ile deneysel ürün bilgisayar ortamında geometrik olarak karşılaştırılmıştır.

Anahtar Kelimeler: Sac Metal Şekillendirme, Hidroform, İncelme, Geri Yaylanma, Kırışma, Yırtılma, Esnek Şekillendirme

To Mustafa Kemal ATATÜRK…

ACKNOWLEDGMENTS

First of all, I would like to thank the very valuable Prof. Dr. Bilgin KAFTANOĞLU and Dr. Hakan Kalkan, who guided me with their knowledge and experience throughout my thesis work. The guidance they showed throughout the process not only guided me throughout my thesis process, but also became invaluable experiences for the rest of my life.

I would also like to thank Turkish Aerospace Industries for the material and equipment support they provided during my thesis process. I would like to thank Dr.Serkan Toros, Dr.Remzi Ecmel, Dr.Hakan Yavaş, Sertaç Altınok, Enes Gebel, Berkay Doğan, Hasan Ökşit, Ramazan Sakarya and all TAI-MFCE employees for supporting this academic study throughout the process.

I would like to thank Özgür Bank who supported me with his experience and knowledge during the thesis.

I would like to thank my very valuable mother, Gönül Toruk, and my father, Mehmet Toruk, who provided me with all kinds of convenience, gave me all kinds of support, made me feel their support and showed patience throughout my master's degree process.

TABLE OF CONTENTS

LIST OF TABLE

LIST OF FIGURES

ABBREVIATIONS

MFCE	Metal Forming Center of Excellence
TAI	Turkish Aerospace Industry

CHAPTER 1

1. INTRODUCTION

1.1. Motivation

The strength and weight of the parts are the criteria that are taken into consideration when creating and developing parts in the aviation industry. Titanium material can provide both these features. In the aviation sector, there are patterns and mounting points on the part. So, it requires a metal forming process. Traditional metal forming methods such as punching and deep drawing are generally used in products where mass production is required. This is because the hydroform method is slower than conventional methods. However, the hydroforming method is very suitable for products where the volume of production is low [1]. Especially in the aviation industry, since the mold costs are very high, only male or female die manufacturing may be sufficient with this method, depending on the part form.

The flex-forming method was used in this study. In the Flexforming method, pressure is applied to the liquid in a closed chamber. There is a rubber diaphragm in the lower area of the closed chamber. The pressure is transmitted directly to the rubber diaphragm. Then, with the force created by the diaphragm on the sheet metal piece, the sheet metal piece takes the shape of the mold. In the flex-forming method, only male or female molds are used. Unlike traditional methods, a mold in which only geometry is processed can be produced without connecting apparatus or tools. For these reasons, mold costs are lower than the mold costs used in traditional methods. The disadvantage of this method is that very high pressures are required.

Problems such as wrinkling, tearing, breaking, and springback, which are frequently seen in other metal forming methods, are also seen in this production method. [2]

Considering both the advantages of the flex-forming method and the properties of the titanium material, it is possible to produce more durable and lighter materials. However, it requires a deep examination.

Figure 1.1 Flex-forming

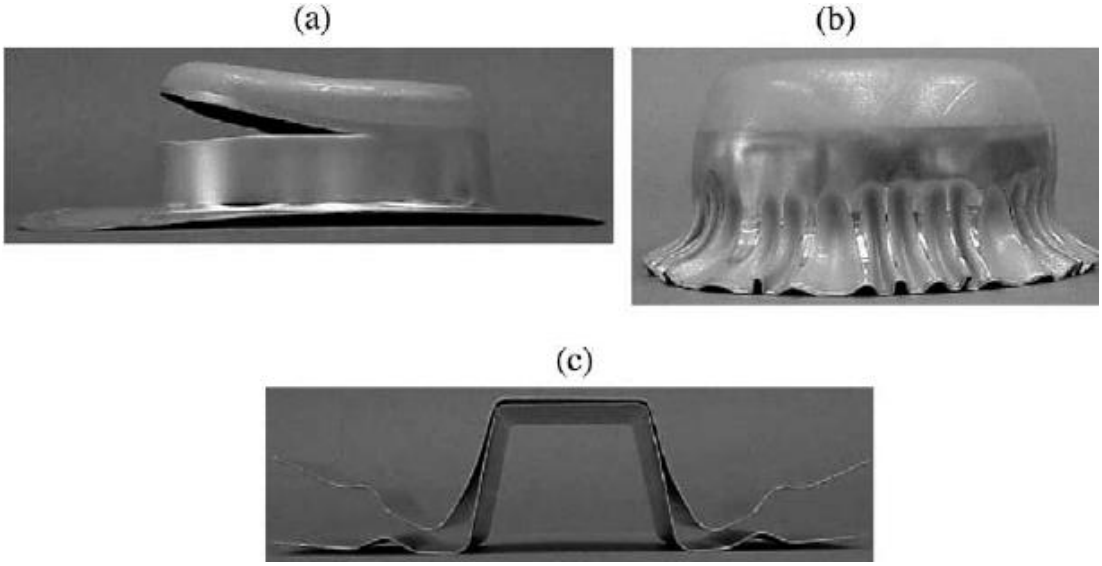

1.2

Figure 1.2 a-) Tearing b-) Wrinkling c-) Springback [3]

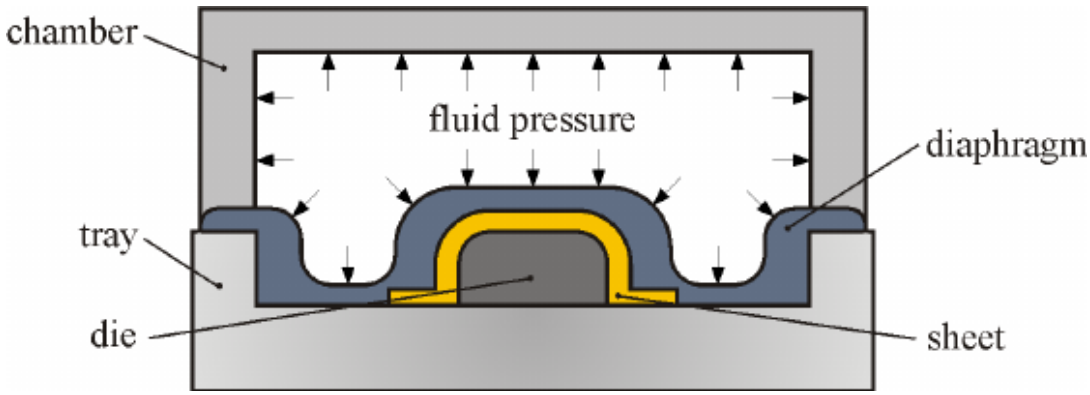

1.3

Figure 1.3 Flex-forming process [4]

1.2. Aim of This Study

In this study, it is aimed to create a pattern by using titanium CP2 material with flex-forming method. This pattern geometry, which will be applied on titanium material with a thickness of 0.6 mm, can cause thinning up to a maximum of 10%. In addition, it is aimed to make the part as stable, more rigid, low springback and warping as possible after shaping.

Both elastic and plastic analyzes were performed to determine and produce the final geometry. Elastic analyzes were performed to determine the deflection rate of the part. Elastic analyzes were carried out on the unformed sheet material. Different shaping patterns were designed on the part and elastic analyzes were carried out by accepting the sheet thickness as 0.6 mm as homogeneous. According to the results of this analysis, the pattern with the least deflection was accepted as the shaping pattern. Subsequently, material testing experiments and required tests were carried out. The coefficients to be used in the analysis were determined by performing friction tests for the titanium CP2 material. For elastic modulus and stress-strain relations, support was obtained from TAI library. Afterwards, plastic analyzes were performed and design optimizations were carried out until 10% thinning is achieved.

The simulation studies are compared with the experimental studies and the minimum deflection and springback, maximum strength and thinning below 10% will be

compared with the experimental results obtained from the simulation-design processes. According to the experimental results obtained, mold-analysis and design revision will be carried out.

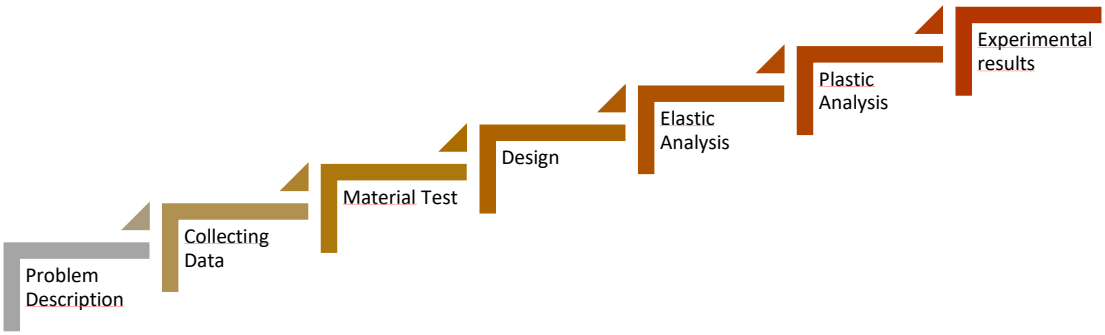

Figure 1.4 Project Steps

1.3. Content of the Study

There will be a total of 8 chapters in this study. In the Introduction section, general information about the process, thesis and objectives will be mentioned. In the second part, the literature review, the history of hydroforming will be mentioned and hydroforming methods will be mentioned. In addition, problems such as wrinkling, tearing, waring, springback, which are frequently encountered in sheet metal forming processes, will be introduced. In the third part, material tests and equipment used in these tests will be given. In the next section, Chapter 4, the design and elastic analysis cycles and the decision stages on which forming geometry to use will be discussed. The plastic analysis – design cycles of the geometry decided in Chapter 4 will be included and an examination will be made. In the same chapter, mold manufacturing stages and experimental results will be reviewed. In following part, chapter 5, the results will be examined and the analysis-experimental results will be interpreted. The other chapters are future works, references and appendix.

CHAPTER 2

2. SURVEY OF LITERATURE

2.1. Introduction

In this section, similar issues in the literature related to the study are discussed. In addition, information on the main subject are given. Hydroforming methods are studied. Common problems encountered in sheet metal forming are then be discussed. After giving information about sheet forming simulations and thickness distribution, the issues related to spring-back in place are examined.

2.2. History of Hydroforming Process

Hydroforming technologies enable the creation of complex metal parts with specific curves and even unusual shapes. They also enable the reduction of a product's component count, leading to cost savings and improved performance.[4] In this method, only single tool is using to shape the sheet part. In addition, due to the incompressibility of liquids, the pressure is transmitted equally to all points on the sheet metal part. Hydroforming methods can be examined under three main headings; Tube hydroforming, sheet hydroforming, shell hydroforming.

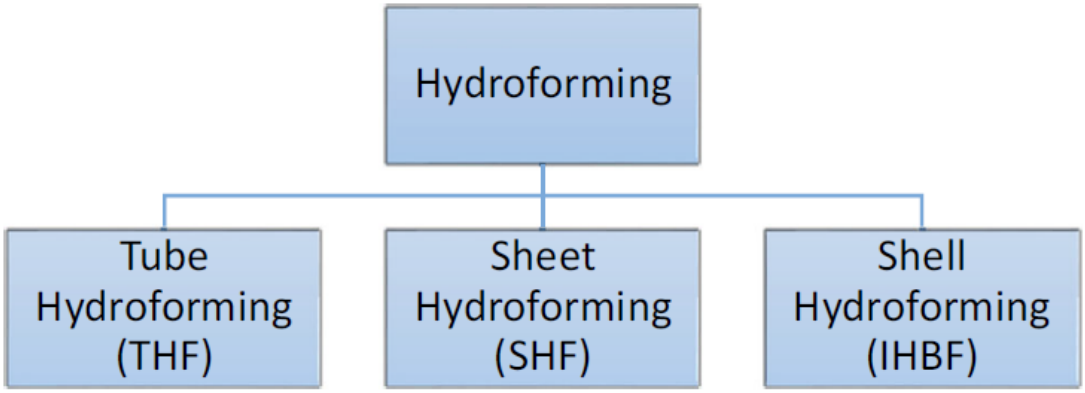

Figure 2.1 Hydroforming methods [5]

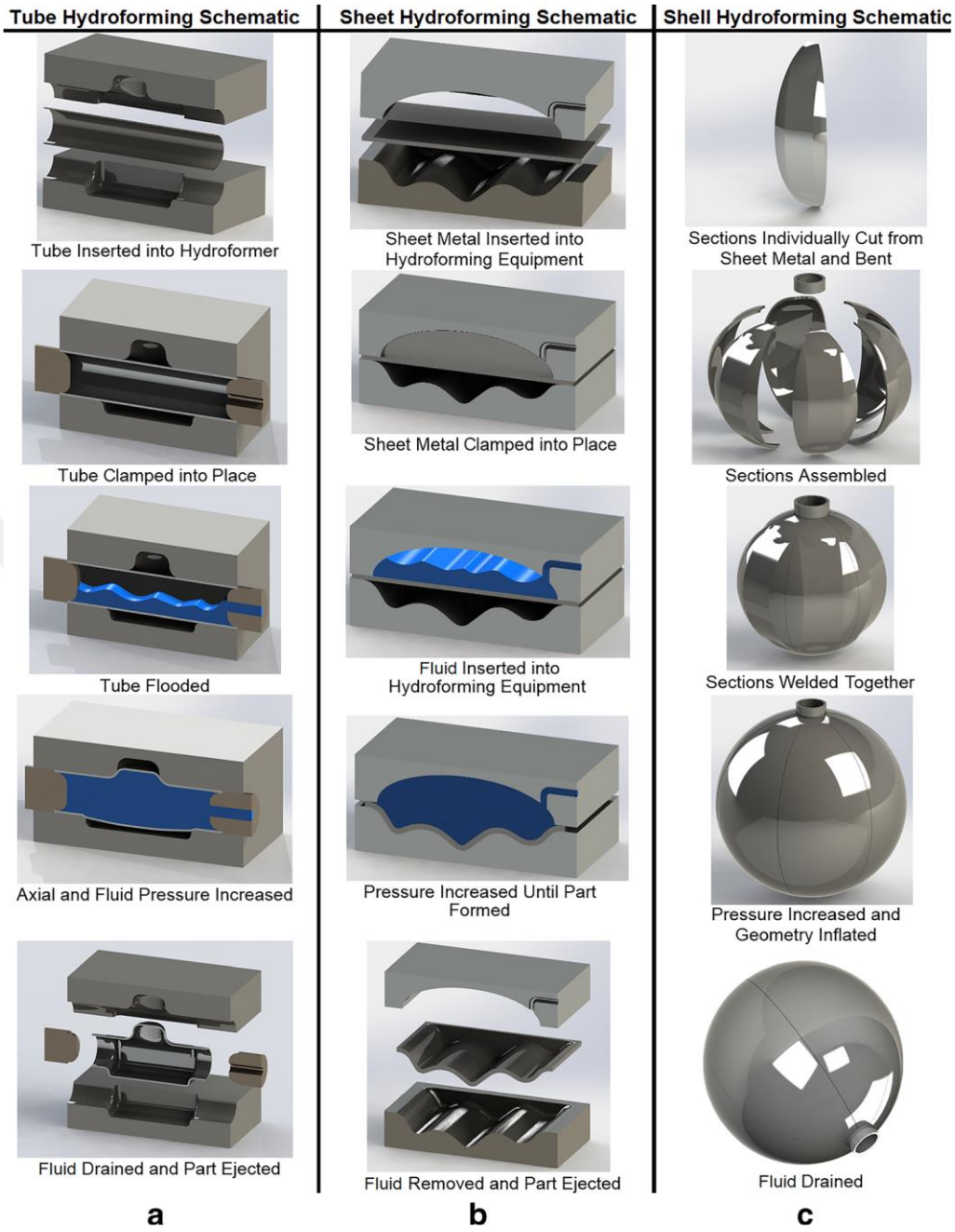

Figure 2.2 Shematic representation of Hydroforming process [5]

Although it is said that it was first tried in 1890 in some sources, the first studies with a patent were made in the early 1900s with an application made to the US patent office (BApparatus for forming serpentine hollow bodies) [6]. This first study was recorded as sheet hydroforming.

2.2.1. Sheet Hydroforming Process

2.2.1.1. Sheet hydroforming with punch (SHF-P)

Sheet hydroforming processes basically serve the same purpose as traditional sheet forming methods. Sheet hydroforming method is divided into many branches in itself. In punch sheet hydroforming, a pressure vessel is used instead of the female mold used in traditional methods. In opposition to the counter pressure in the pressure vessel that the pressurizing fluid creates, the sheet is dragged deeply to form on the punch surface [4]. The liquid in the pressure vessel, along with the movement of the punch, forces the sheet material to take the shape of the punch. A relief valve is used to stabilize the pressure at this time. This valve functions to keep the pressure constant.

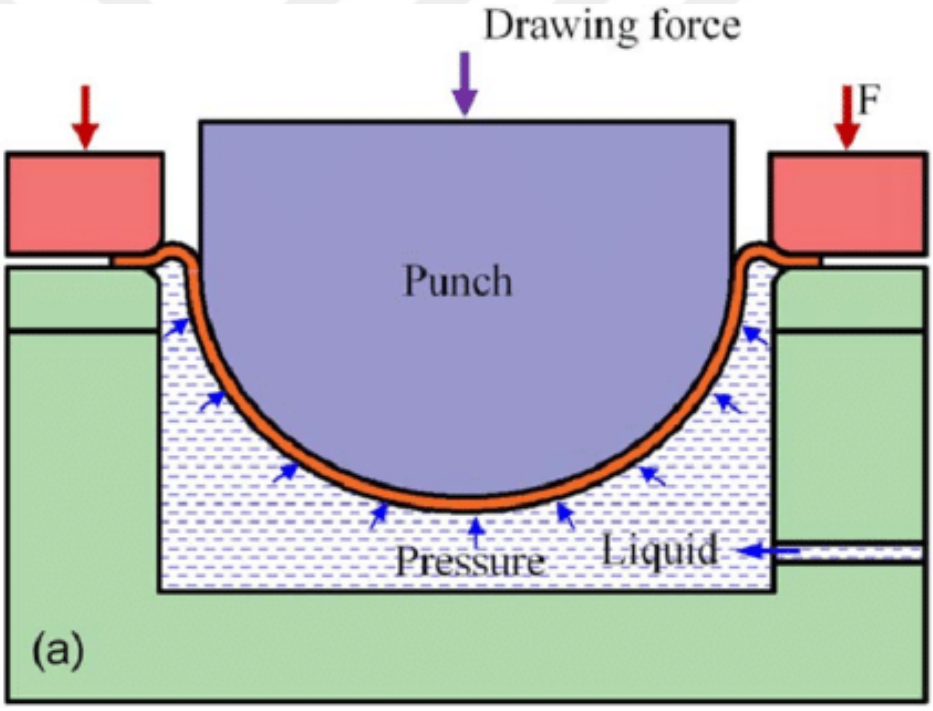

Figure 2.3 Sheet hydroforming with punch [7]

2.2.1.2. Sheet hydroforming with Die (SHF-D)

Hydroforming with a mold is also among the methods used. Unlike deep drawing, this time there is a fixed male or female pattern. During shaping, the intermediate plate acts to prevent fluid leaks.

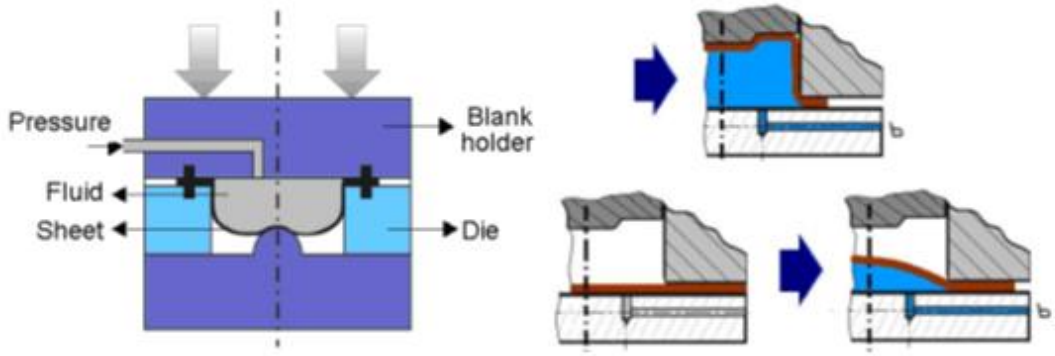

Figure 2.4 SHF-D Steps [8]

In this method, shaping takes place in 2 stages (Figure 2.4). First of all, the sheet material swells until it comes into contact with the mold, and the pressure is low at this stage. After the contact is made, the plastic forming process begins. By increasing the pressure, the sheet metal is forced to take the mold shape. Unlike the punch method, no liquid output is performed to stabilize the pressure. In order to keep the pressure constant, a continuous feeding is carried out with the help of pumps.

2.2.1.3. Flex-forming

Another method, Flex-forming, is the method that will also be used in this thesis. Parts such as liquid, rubber diaphragm, blank holder, blank are basically used. In addition, this method can save additional costs in production by providing the possibility of undercut (Figure 2.6)

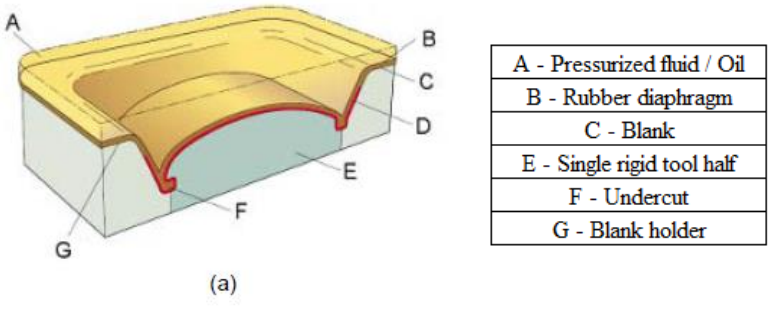

Figure 2.5 Flex-forming Scheme [8]

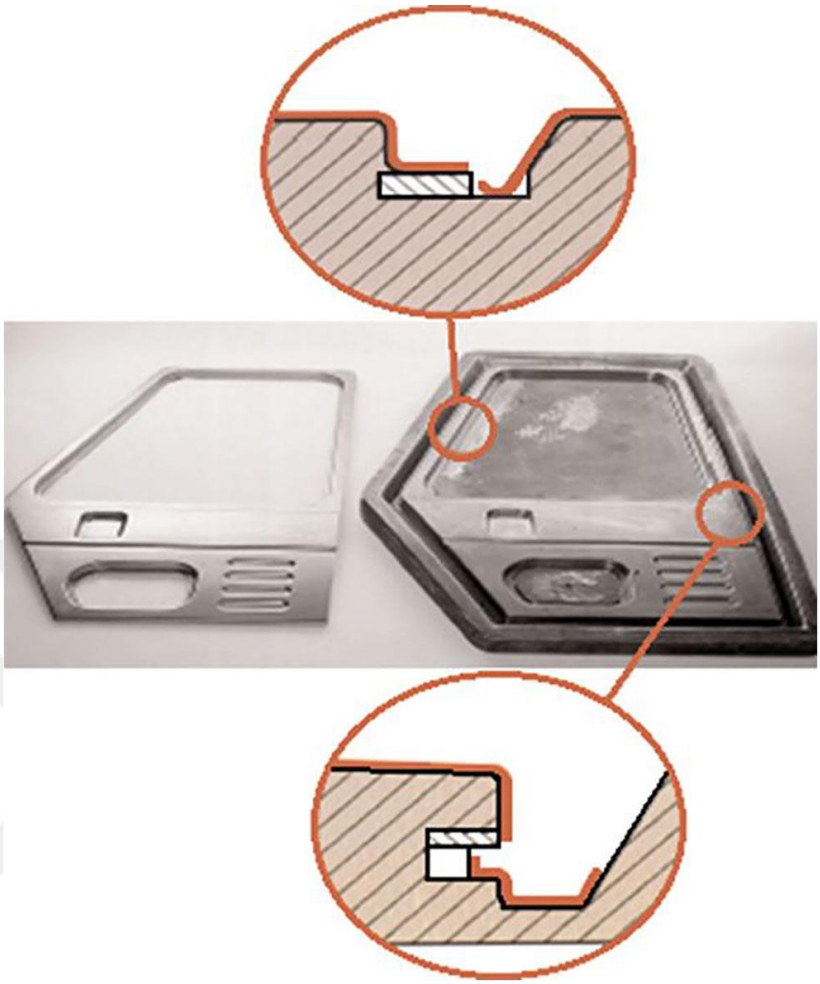

Figure 2.6 Undercut [9]

In the flex-forming method, the forming process is based on the pressure of the liquid. In this method, the liquid is trapped in a reservoir and the bottom area is closed with a rubber material. The aim here is to increase the production capability with equal pressure distribution by taking advantage of the flexibility of the rubber material (Figure.2.7).

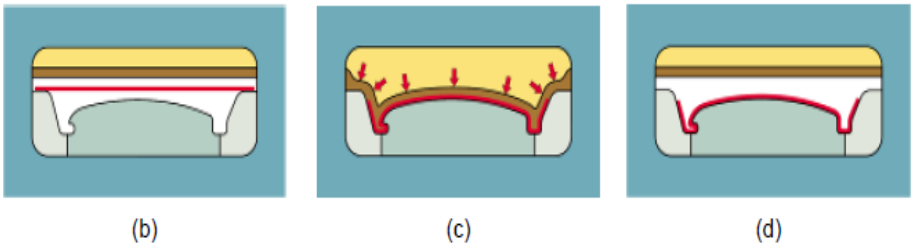

Figure 2.7 Flex-forming example [8]

The sheet material to be shaped is placed on the mold. Design details such as pins can be used in this placement phase. Then the liquid sealed with rubber material is pressurized and the diaphragm moves towards the sheet material. While the pressure is increased in a controlled way, the diaphragm starts to contact the sheet material. Due to the elastic structure of the diaphragm material, the sheet material starts to be plastered on the mold and is forced to take the shape of the mold. Thus, the diaphragm acts as a kind of male or female mold.

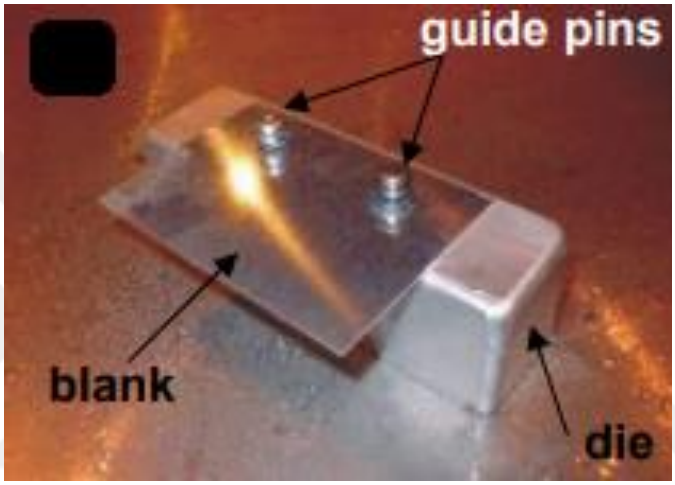

Figure 2.8 Guide pin to locate [10]

Thanks to the flexible feature of the diaphragm, it is also possible to produce multiple parts at the same time. In the same process, more than one mold can be placed in the hydroform press at the same time and the forming process can be performed. Especially in sectors where the variety of parts is high, this method can halve the mold manufacturing price for each molded part. The main reason for its use in the automotive and aviation industry is that it provides die manufacturing savings due to the wide product variety (Figure 2.9 and Figure 2.10).

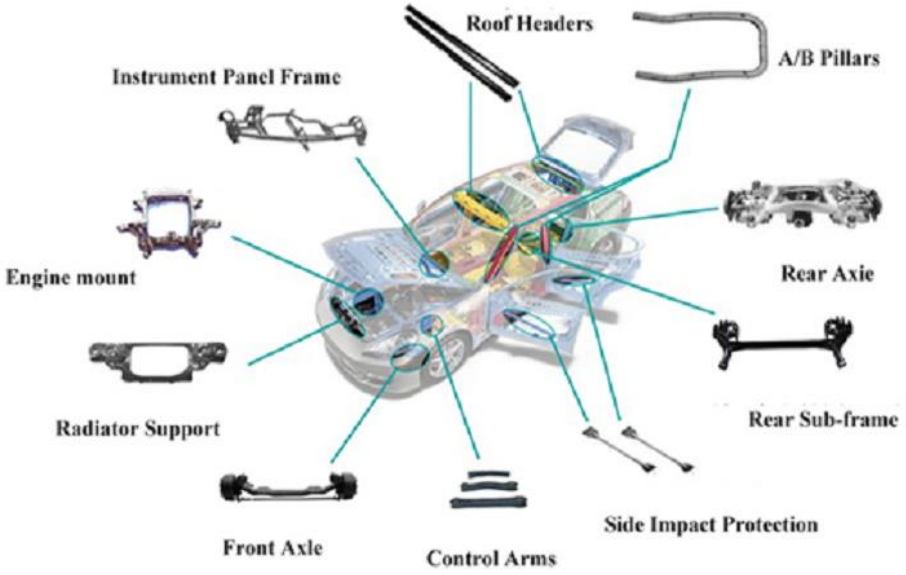

Figure 2.9-Automotive industry [11]

Figure 2.10 Automotive Parts [12]

2.2.1.4. Sheet Stretching hydroforming

The deep drawing method has also been one of the methods used because it provides advantages over other methods. The forming process is performed by applying the force to the sheet material with a hydraulic pressure. In this method, it can be performed both with a single mold or by using two molds. One of the molds is the mold that will directly force the sheet material to take shape. The other side is the region where the fluid pressure is created. By providing feeding from one side, the sheet material takes the shape of the mold. Since there is a continuous inlet of liquid, pressure stabilization is done by liquid feeding.

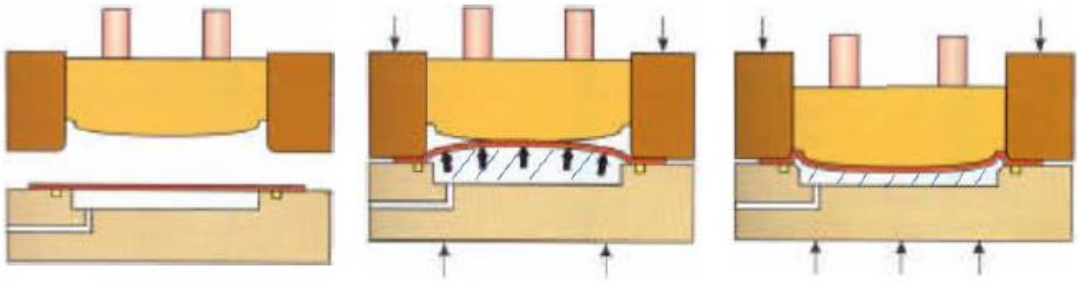

Figure 2.11 Sheet stretching example [13]

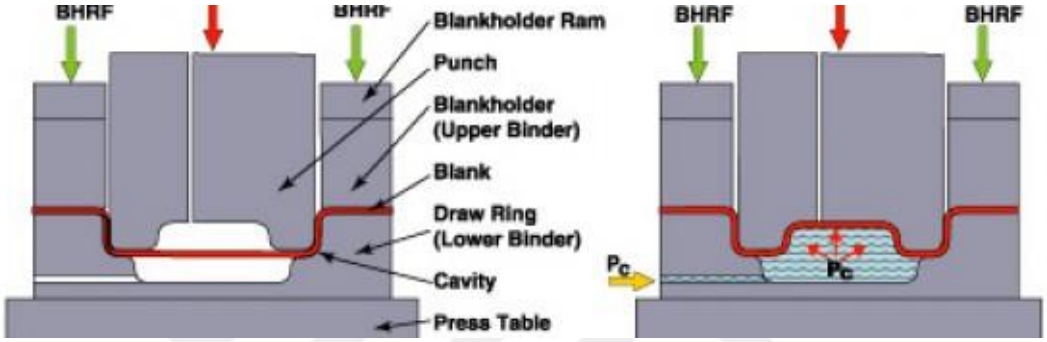

Figure 2.12 Sheet stretching example [14]

2.2.1.5. Rubber Diaphragm Forming

The forming method using the diaphragm is basically the same as liquid pressurization. The volume occupied by the liquid-filled chamber is covered by rubber material. Since the fluid pressure cannot be created, the stroke applies a downward movement as in the pressing process. Male or female molds are used. There are several variants of the diaphragm hydroforming method. Applications are named according to the method. The most well-known methods are Verson, Guerin, Marform and Hydroform.

After the mold movement is started, the rubber material placed in the upper mold acts as a male or female. The diaphragm, which takes the form of a mold, provides a high cost advantage. Thanks to its flexibility, it provides the opportunity to produce parts in different geometries at the same time. This method is known as the Guerin method. It is one of the oldest and most primitive methods.

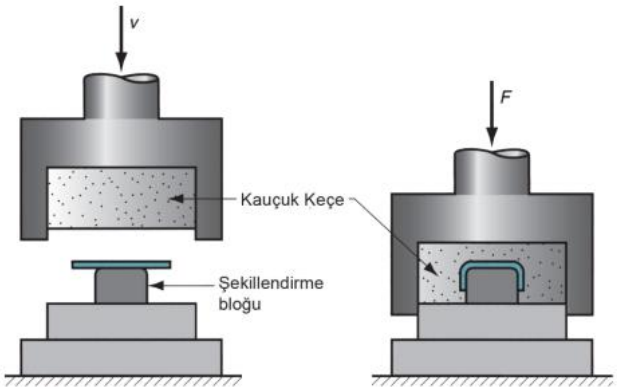

Figure 2.13 Rubber Diaphragm Forming [15]

2.2.2. Tube Hydroforming

The tube hydroforming method was first patented in the 1940s [16]. This method is used in many sectors such as automotive and white goods, especially in the oil and natural gas sectors. It is used in these sectors because it is a suitable method for the production of T-shaped pipes without welding and additional points.

Figure 2.14 Tube hydroforming [17]

The working principle of this method starts with placing a pipe in the mold. There is core on the right and left sides of the mold both to increase the pressure in the pipe and

to prevent liquid leaks. With the increase in pressure, the pipe begins to take the shape of the mold.

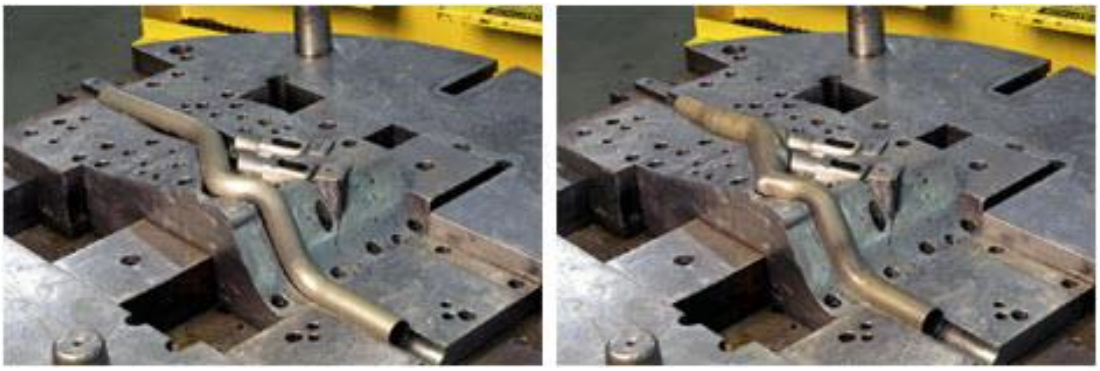

Figure 2.15 Tube hydroforming [18]

Depending on the mold geometry and material type, the pressure parameters vary as in other methods. This method is performed in 6 main steps (Figure 2.16). [19]

1- Positioning of tube; The standard size pipe is placed in the mold.
2- Closing of die: The upper and lower molds are closed, the cores touch the surfaces of the pipe.
3- Filling: Liquid is filled into the pipe.
4- Axial feeding: After the liquid is filled into the pipe, the cores start to move. It is the stage where pressure starts to build up on the pipe walls so that the pipe can take a mold shape by using the incompressibility feature of the liquid.
5- Forming fluid under pressure: Thanks to the pressure applied to the walls of the pipe, the pipe takes the shape of the mold.
6- Extraction of part: It is the stage where the shaping is completed and the part is removed from the mold.

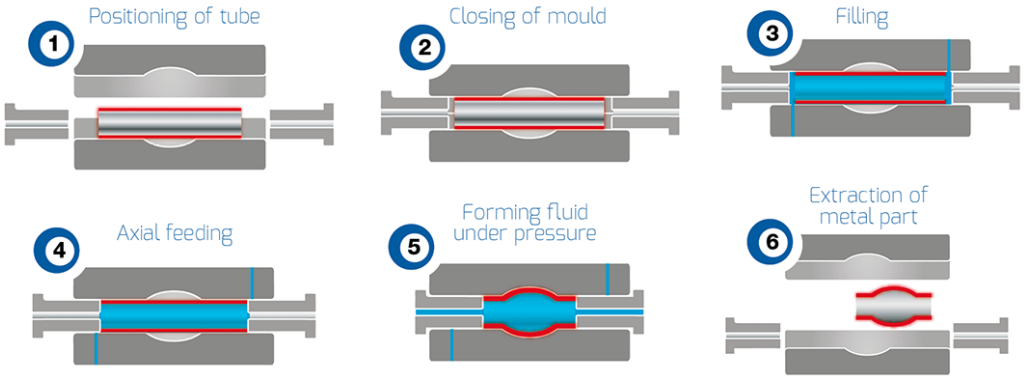

Figure 2.16 Tube hydroforming steps [19]

2.2.3. Shell Hydroforming

The hydraulic shell forming method is a method that emerged in the 1980s [20]. It has been used in engineering applications for the manufacture of high pressure parts such as large LPG tanks. After the liquid is filled into a closed volume, the pressure is increased and the required shape is given. This method can be applied with or without a mold, depending on the application.

Figure 2.17 Example of Shell Hydroforming [21]

Apart from engineering applications, it is also used for the production of decorative parts. Operations in the related picture (Figure 2.18);

1- The pieces are cut separately.
2- Then they are joined from the necessary welding points.
3- Liquid is filled into the shell geometry from a certain cross-section.
4- It is ensured to take the final shape by pressurizing.

Figure 2.18 Example of Shell Hydroforming [22]

There is only one point on which all these methods are based; Pressure. Shaping is carried out by increasing the pressure and aiming to distribute it equally to every point. Like every production method, hydroforming has its advantages and disadvantages. Its advantages can be listed as follows.

1- Parts have good surface quality
2- The wear rate of the tools is low.
3- The products are of high quality in terms of dimensional accuracy. It can be worked closer to the desired dimensional sensitivities.
4- They have superior mechanical properties. It is possible to manufacture parts with higher strength.
5- Decreases the amount of residual material.
6- Since the hydroforming method applies equal pressure to all parts of the part instead of applying point pressure, the thickness distribution is at more controllable levels compared to other methods.
7- It has a lower springback rate.
8- It is suitable for the production of complex parts.
9- Parts can be produced using a single mold. This advantage of the production method provides cost savings.
10- It reduces additional labor costs by saving from additional production methods such as welding.

It makes it possible to produce parts in more than one mold at the same time in sectors such as aviation and automotive, where product diversity is high.

In addition to all these advantages, the hydroforming method also has some disadvantages. These can be listed as follows.

1- Although it allows the production of complex parts or the production of more than one part at the same time, it is not very suitable for mass production. Production rates are much lower than traditional methods.
2- Material, equipment and maintenance costs are high. Presses or pumps that can reach high pressures are required for shaping.
3- It is difficult to keep the oil temperature constant throughout the process.

In metal forming, wrinkling refers to the formation of wrinkles or creases in sheet metal during the forming process. This can occur when the sheet metal is stretched beyond its elastic limit, causing the material to buckle and form wrinkles. Wrinkling can occur in a variety of metal forming processes, such as stamping, deep drawing, and roll forming. It is considered as a failure mode in metal forming process as it affects the final quality of the product, it also reduces the useful life of the die used in the process.

There are several factors that can contribute to wrinkling in metal forming, including the properties of the metal being used, the design of the die or tooling being used, and the process conditions such as the forming speed, the temperature, and the lubrication. To prevent wrinkling, metal formers often use techniques such as increasing the thickness of the metal, using a higher-strength alloy, reducing the forming speed, or using a different type of die or tooling.

2.3. Sheet Metal Formability

The purpose of sheet metal forming is to put the sheet material into a certain form. This design varies according to the purpose. A deep examination and analysis process is required to get the sheet metal into the desired form without breaking or cracking.

There are many parameters that directly affect sheet metal forming. Material thickness, grain structure, chemical composition, elastic modulus, yield strength value, UTS and fracture values are some of the most important values in shaping the material. Thin sheet material will be shaped with lower forces than a thick material. Because it is more flexible and has lower deformation resistance. Grain structure is also an

important parameter in plastic shaping. The force applied to the material in the plastic deformation zone causes deterioration in the grain structure and creates new dislocations. This is how shaping takes place.

There are several techniques used to form sheet metal, including:

- Bending: This process involves applying force to the sheet metal in order to cause it to bend along a particular axis. Folding and press braking equipment can be used for this (Figure 2.19).

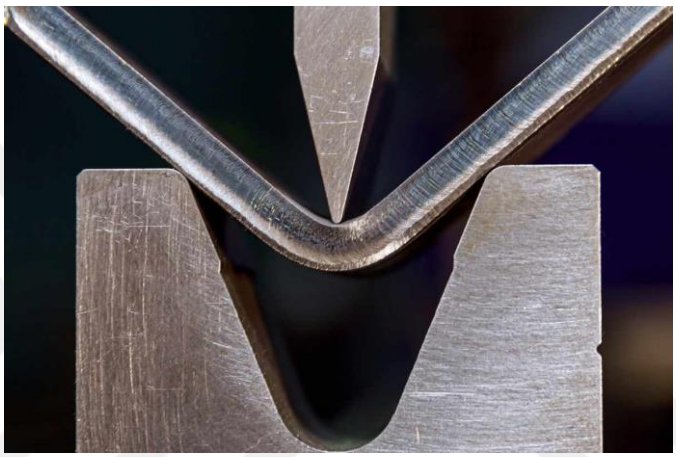

Figure 2.19 An Expample of Bending Operation [23]

- Deep Drawing: Using a die and a punch, the sheet metal is stretched to create a specific shape (Figure 2.20).

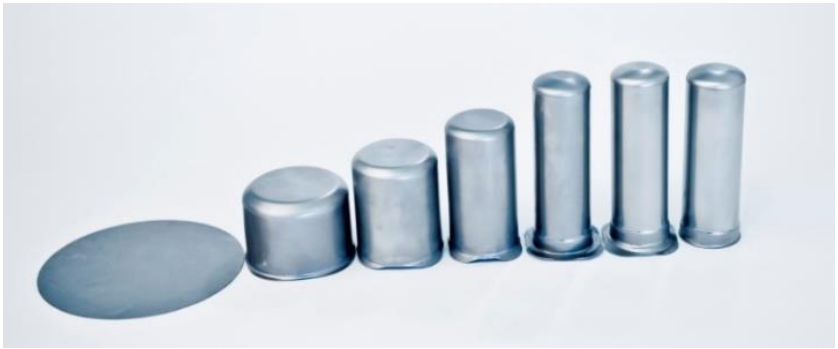

Figure 2.20 Deep Drawing steps [24]

- Stamping: where the sheet metal is cut and shaped using a stamping press. It can be also used to create holes or specific shape on sheet metal.

The following strategies can be used by manufacturers to increase formability. Annealing is a type of heat-treatment process. It directly affects the crystal structure of the material and increases its ductility. Friction is also a serious obstacle to shaping. By using suitable lubricants, friction is reduced between sheet metal and die. Thus, an easier shaping can be made.

To summarize, the mechanical and chemical properties of the material are directly effective in forming the sheet metal without breaking or cracking. In addition, additional methods are applied to increase formability.

Some common problems are observed during the forming of sheet metal. These problems occur in almost all sheet metal methods;

1. Wrinkling: The wrinklink condition occurs during the shaping of the material. A visible wave forms on the material. While the sheet material takes the shape of the male or female mold, material begins to be drawn from the edge areas. The excess thus formed causes wrinkling. Parameters such as unsuitable mold design, high forming speed, high material strength, thickness, low blank holder force are effective in this error (Figure 2.21).

Figure 2.21 An example of wrinkling [2]

2. Springback: The springback event is caused by the desire to return the material to its original state. Many properties such as material type, thickness, anisotropy, yield strength, young modulus, hardening, etc. are effective in the springback phenomenon and are a serious problem in shaping. It is a problem entirely caused by the elastic properties of the material. There are some common operations to prevent or reduce springback. Pre-stretching is a pre-process that prevents springback. Choosing a harder material or using a thicker

material will also reduce springback. Also, using a different shaping method can reduce springback (Figure 2.22).

Figure 2.22 An example of springback [2]

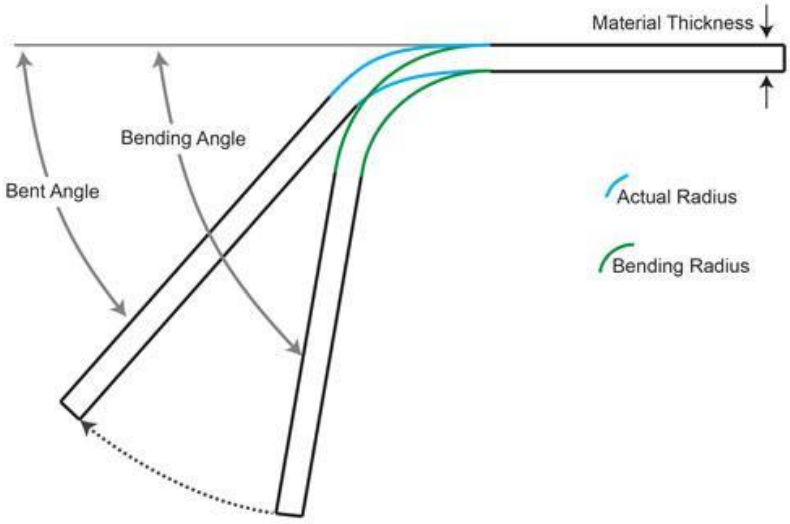

Figure 2.23 Springback radius [25]

3. Warping: Warping is a common problem that can occur in sheet metal forming, it happens when sheet metal deforms unevenly in different areas during the forming process. This can make the use of the product difficult or impossible. There can be many reasons for bending. However, it is basically caused by wrong mold design, uneven heating and cooling of the metal, etc. (Figure 2.24).

Figure 2.24 An example of warping [26]

4. Tearing: This occurs when the material splits or tears as it is being formed. This can be caused by improper tool design, high forming speeds, or high material strength.

Figure 2.25 An exmple of tearing [2]

5. Surface defects: This occurs when the surface of the material is damaged during the forming process. Crazing, folding, inclusion, patch, pitted surface, stratch are one of the examples of this problem.

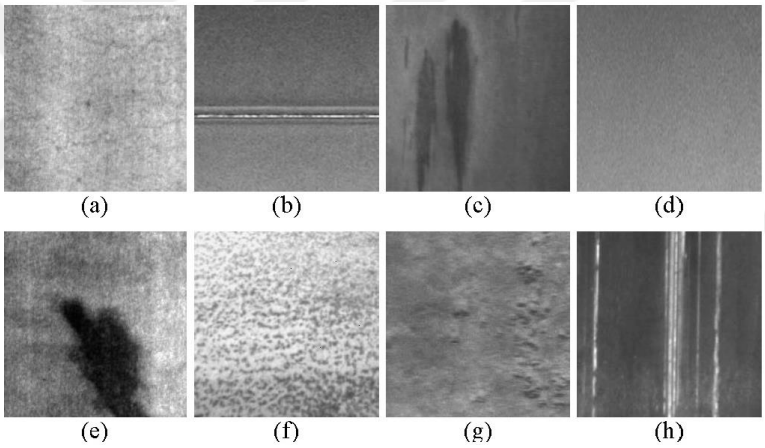

Figure 2.26 Examples of surface defects (a) crazing, b) folding, c) inclusion, d) original, e) patch, f) pitted surface, g) rolled-in scale, h) scratch) [27]

6. Surface finish: The surface finish of the final product is not up to the requirement.

2.4. Elasticity

Elasticity is a property of a material that describes its ability to return to its original shape after being stretched or deformed. When a material is stretched or deformed within its elastic limit, the material will return to its original shape when the load is removed.

The elasticity of a material can be described by its modulus of elasticity, which is a measure of a material's resistance to being stretched or compressed. Some of the common modulus of elasticity measurements are Young's modulus, Shear modulus and bulk modulus.

The most common modulus of elasticity measurement is Young's modulus, which is a measure of a material's ability to resist stretching or compression along one axis. Materials with a high Young's modulus, such as steel, are considered to be stiff, while materials with a low Young's modulus, such as rubber, are considered to be flexible.

Elasticity is a fundamental property of most materials, and is important in many engineering and construction applications. Understanding the elasticity of a material is crucial for designing structures that can withstand loads and forces without deforming permanently.

2.5. FEM (Finite Element Method)

The finite element method (FEM) is a mathematical problem solving technique that is frequently used in engineering and physics. FEM enables numerical solutions in complex metal forming processes and is the most frequently used method. It breaks down complex models into small pieces and calculates these small structures mathematically. The basic logic in this method is to divide a complex geometry into many simple, interconnected and small regions called finite elements. It simulates how the system will behave in real life using various loads and boundary conditions. The concepts called "finite element" are simple geometric shapes in 2 and three dimensions such as line, triangle, quadrilateral, hexagon. These simple geometric shapes are connected using nodes and finite elements are created. [28]

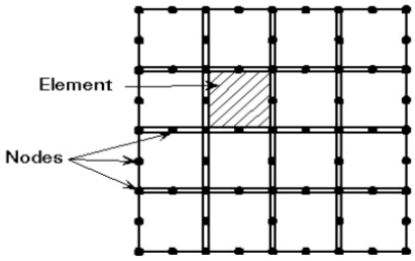

Figure 2.27 FEM Nodes and elements [29]

After the system is divided into small parts, it is solved using mathematical models to explain the real-life behavior of each element. The result is an estimate of how the system will behave in real life. [30]

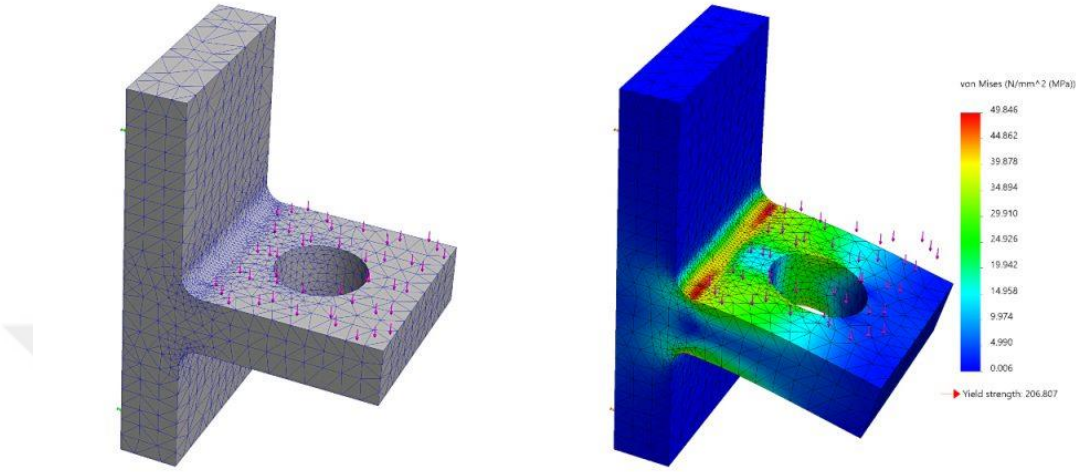

Figure 2.28 FEM modelling with mesh [31]

In a Finite Element Method setup, there are step in the solver program to get results. These are;

1- Simulation Type;

   This step is the first step of a simulation. First of all, it should be determined which simulation should be chosen according to the user problem. There are a lot of different simulation type. For instance, static, dynamic, implicit, explicit, thermal, CFD etc.

2- Geometry and Mesh;

   A geometry must be covered by a surface or volume mesh structure. Adaptive meshing is generally used in metal forming analyses. Adaptive meshing is generally used in metal forming analyses. The reason for this is the need to create a new mesh geometry when the metal changes shape. A network structure consists of nodes and elements. The connections between nodes create elements. Triangle and quadrilateral elements are generally used in 2D analyses. Tetrahedral and hexahedra are suitable for 3D analysis.

3- Material Properties;

Material Properties defines the material behavior under the load for a structural simulation. It contains Poisson Ratio, Elastic modulus and hardening curve. Additionally, material properties include material models, too. The material can be isotropic, anisotropic, orthotropic etc.

4- Contact Defining;

Defining the contact is necessary to understand the physical aspects of the problem for programming. At this stage, the identification of the specific parts that will come into contact with each other is determined. The coefficient of friction between the two materials can be defined at this stage.

5- Loads;

In a structural simulation, the load needs to be defined to program. The load can be point load or distributed load. Gravitational or non-gravity load can be added.

6- Boundary Conditions;

Constraints, DOF (Degree of Freedom) of the designed part must be defined. It is the phase of introducing the physics of the problem.

7- Solver Settings;

Solution method needs to be chosen in this section. Direct solver or iterative solvers can be selected. Convergence criteria also defines at this stage. It directly affects the accuracy of analysis and time.

8- Outputs;

This is the last stage of a simulation setup. Selection is made according to expectation and necessity.

2.5.1. Discretization

Discretization is defined as the process of discretization of continuous functions, models, and equations. This method is the first stage of preparing a suitable basis for a model to be solved in a computer environment.

2.5.2. Elements

In finite element method, three-dimensional or two-dimensional mesh elements can be used. Depending on the type of analysis, the structure is transferred to the simulation program in 2D or 3D. Within the scope of this study, 2-dimensional Hexahedron elements will be used for the mold and blank, and two-dimensional and three-dimensional Hexahedron elements will be used for the rubber membrane.

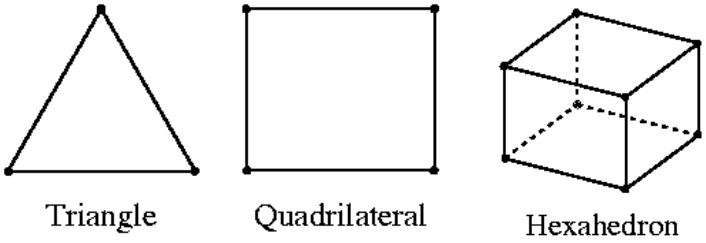

Figure 2.29 Element types in FEM [32]

Two-dimensional quadratic bounded elements are a bounded element used for analysis of structures. This element consists of 4 points to simulate the structure in real life. To increase the accuracy of the limited element method, small and numerous elements should be used whenever possible. Each point is a graphical tool that contains many data such as the thickness of the structure, material properties, loads. It creates a mathematical model by knitting the surface like a network with small elements. The stiffness of this element is formed using four-point Gaussian integration [33].

2.5.3. Adaptive Meshing

Adaptive meshing is a method used in the finite element method that allows the network structure to become thinner or thicker. In this method, the system dynamically updates the region with high error or to better solve the region where shaping will be done. In regions with good solutions, the number of elements is reduced and this provides significant savings in analysis time.

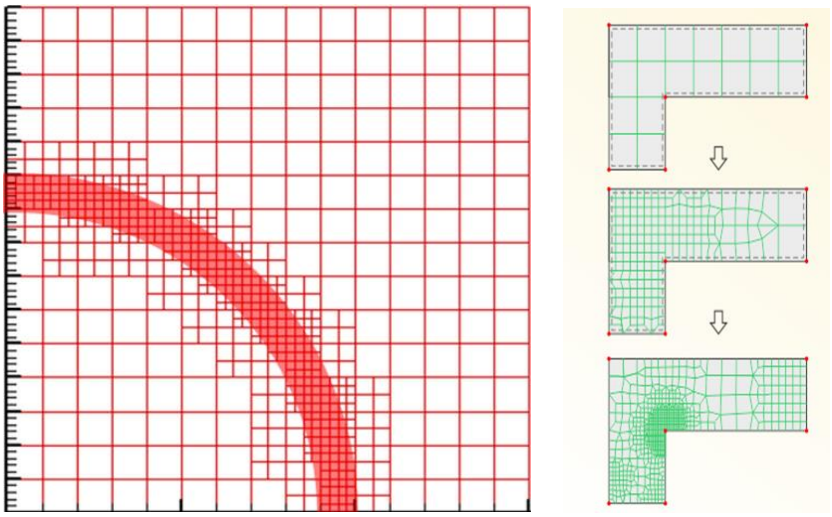

Figure 2.30 Adaptive meshing [30]

Refinement settings are used when determining element sizes. After adaptive meshing is applied, discontinuities may be observed in the network structure. New points are created to eliminate this situation. By connecting each point to each other, the discontinuity is eliminated and the relationship between the network structures is created.

Adaptive meshing can only be used in two-dimensional structures. If there is a three-dimensional element in the simulation (rubber diagram, etc.), adaptive meshing cannot be used.

2.5.4. Material Modelling

The material modeling process is one of the most important parts of the analysis process. It directly affects the simulation results. Geometry, mesh structure, boundary conditions, forces and material properties are the basic elements that make up a FEM analysis. Material modeling is carried out by transferring the results obtained from test data about the mechanical behavior of a material to the computer environment. This process is used to predict how the material reacts under load.

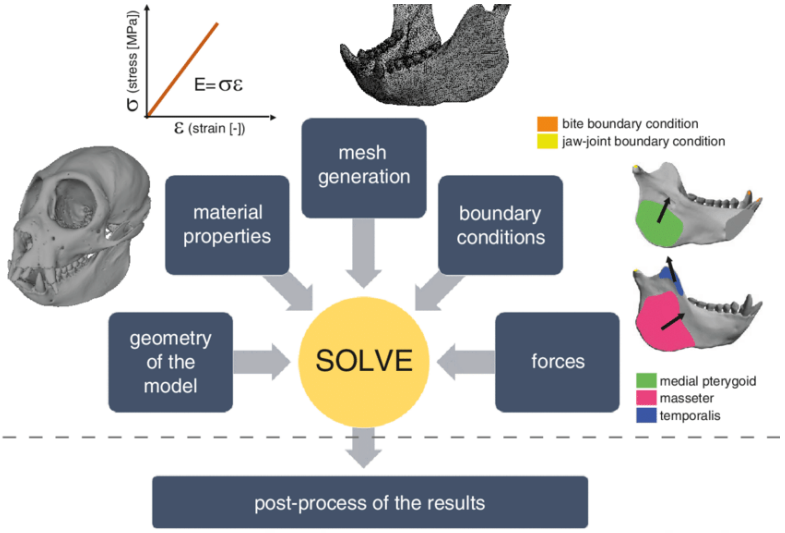

Figure 2.31 FEM steps [34]

The data obtained as a result of repeated tests carried out with test samples or test standards manufactured in accordance with the standards are transferred to the computer environment. For a study where structural analysis is performed, it is very important to accurately analyze the resistance of the material against the load under applied loads.

This technique is a very important technique that saves both time and money in solving many engineering problems as it helps predict the durability of materials.

Within the scope of this thesis, the study will be carried out using the elastic and plastic properties of the material. A forming pattern will be applied to increase the strength of a flat sheet metal plate. After this pattern is applied, the amount of springback will be kept to a minimum and the maximum thinning will be approximately 10%.

2.5.4.1. FLD (Forming Limit Diagram)

FLD (Forming limit diagram) is a graph that shows the behavior of the metal after forming in sheet metal forming processes, graphically with limit curves. It is divided into areas such as stretch, wrinkling trend, thinning and failure. According to the simulation results, the minor and major strain values on each material are determined and placed on the graph. FLC (Forming limit curve) consists of 3 different regions.

- Above the FLC is the failed zone (areas of fracture) [35]
- By moving down the FLC (by percentage of strain depending of material types, usually 10%), a marginal zone is defined from the initial FLC and the shifting FLC (area of incertitude between necking/failure and safe) [35]
- Zone below the shifting FLC is considered as a safe zone [35]

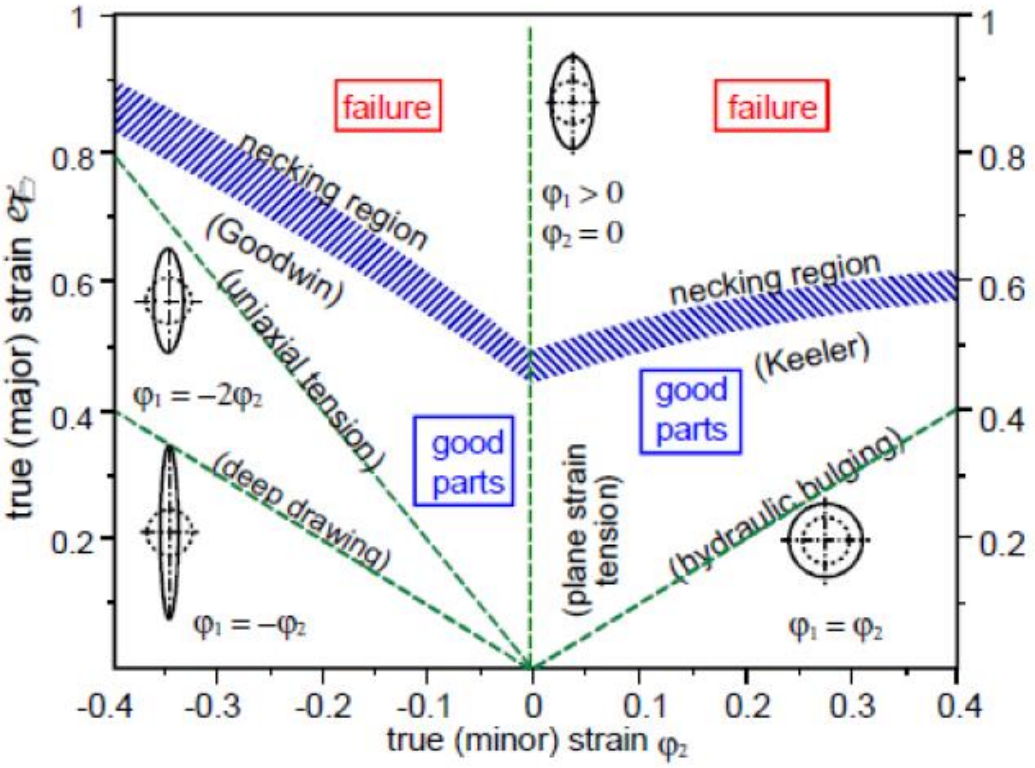

Figure 2.32 The region of FLD [35]

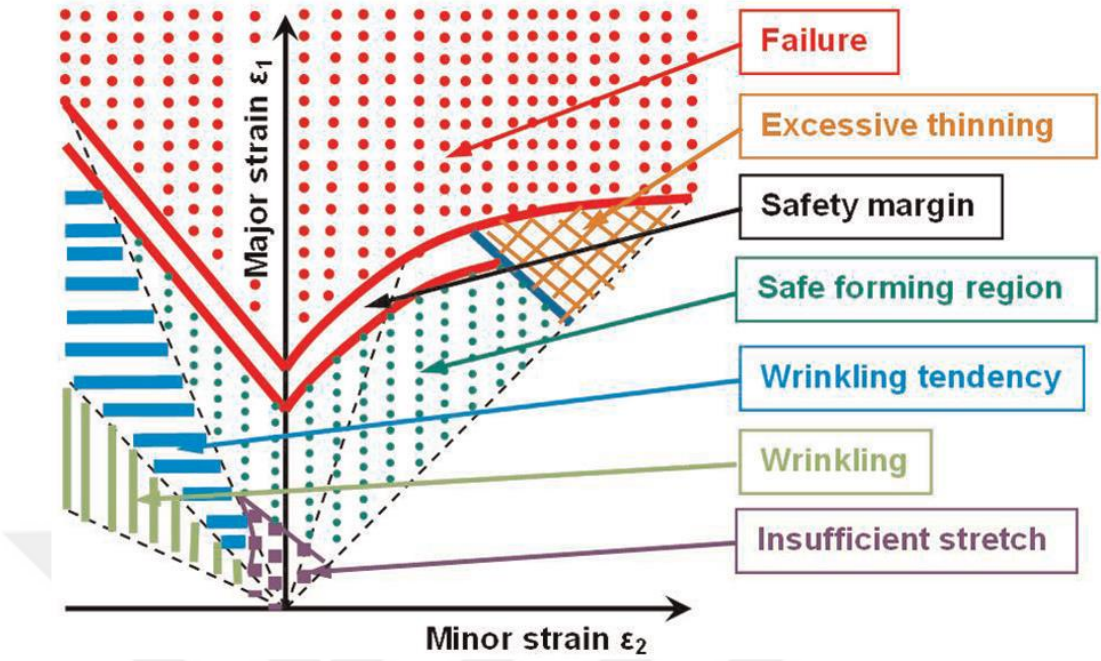

Figure 2.33 The region of FLD [36]

Part samples conforming to standards are used to create the FLD graph, and testing with each sample determines a forming limit curve in the graph. It is known as the nakazima test.

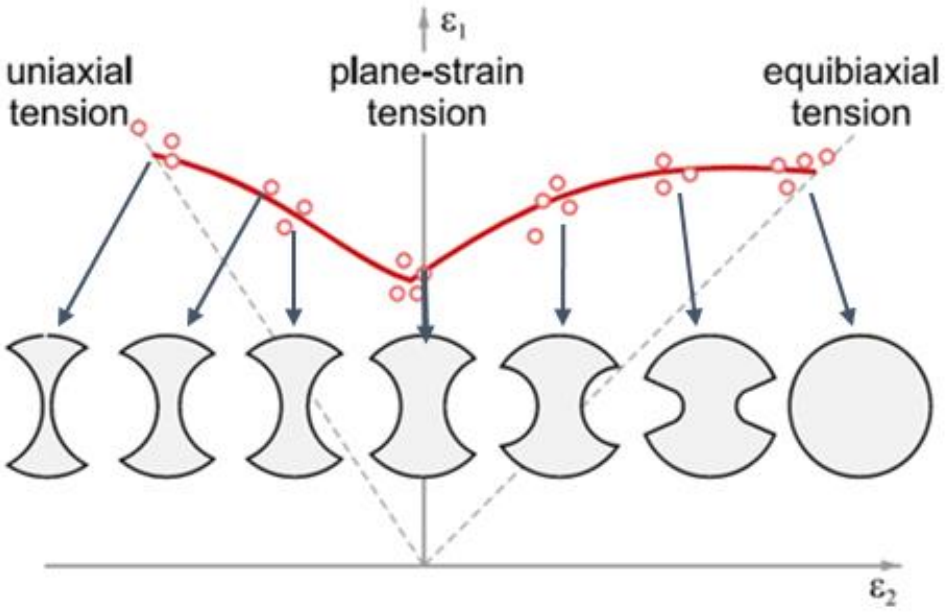

Figure 2.34 FLC defining samples [35]

2.5.4.2 Engineering-True Stress-Strain Curves

While shaping metal materials, a lot of engineering information is taken from true stress-strain curves. The most important of these graphs is the stress-strain graphs. In engineering and materials science, these graphs show the relationship between stress and strain. Using tensile samples cut in accordance with standards, tensile process is carried out at certain speeds and graphs are obtained. The sample continues to be extended until it breaks and stress-strain changes are recorded. Horizontal axis is defined as strain and vertical axis is defined as stress. The curve based on the original cross-section and length of the sample is called the engineering stress-strain curve, while the curve based on the instantaneous cross-section and length is called the true stress-strain curve.

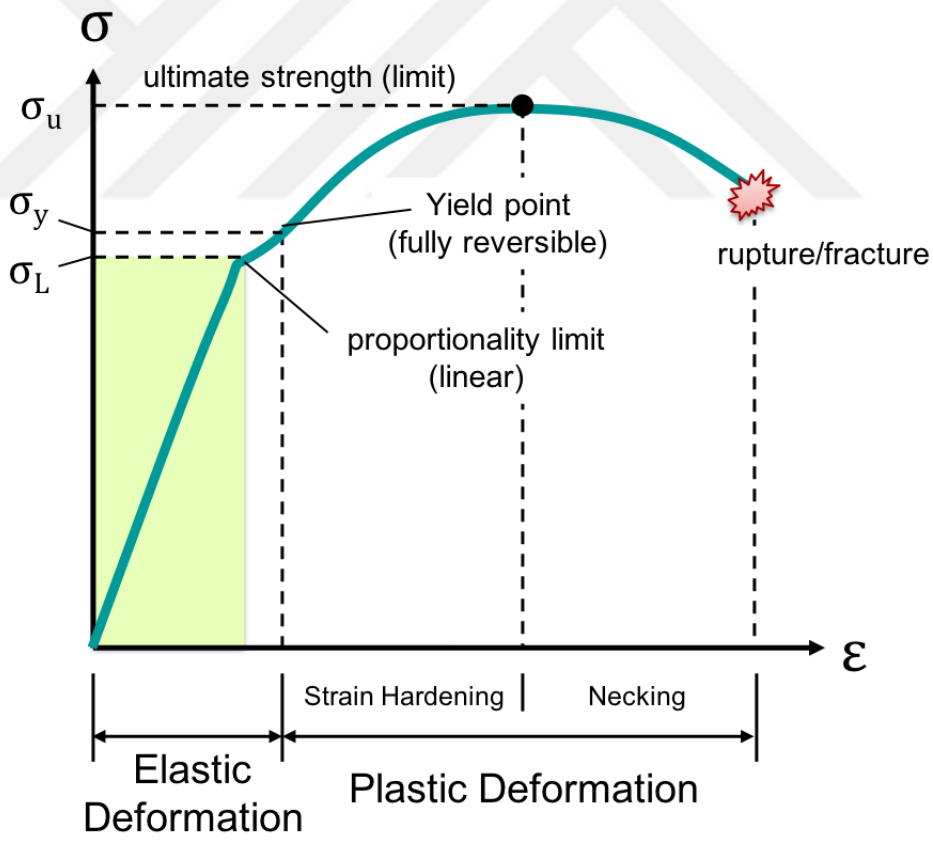

Figure 2.35 – Engineering stress-strain curve [37]

Basically, stress-strain graphs consist of two regions;

1- Elastic zone: In the elastic zone, the material can completely return to its original shape. There is no permanent deformation. Yield point $\sigma_y$is considered the end of this region. Yield point is determined using 0.2% offset.
2- Plastic region: The plastic region is examined in two separate areas. The first area is the hardening area. In this region, stress increases with strain. Stress and strain continue to increase until the UTS (Ultimate Tensile Strength) point. UTS is the region where the material is exposed to the highest stress. The necking region is the region where residual strain increases but stress decreases. Because rupture/fracture begins to occur in this region. The material becomes thinner and gives neck. In the fracture zone, the material breaks and the test is completed.

The behavior of each material is different. In some materials, the plastic zone does not form at all. Very hard materials show very little stretching behavior and break directly without passing into the plastic region. Glass is an example of this behavior.

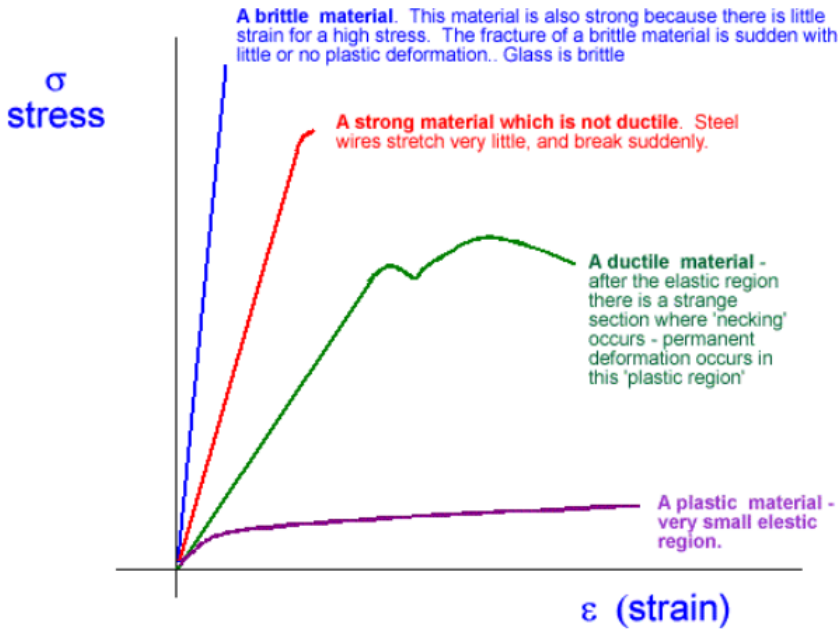

Figure 2.36 Stress-Strain graph of materials [38]

The sample named A below showed a ductile behavior in the tensile test (Figure 2.37). The reason for this is that when the fracture area was examined, it first necked and then broke. According to the stress-strain graph given above (Figure 2.36), it showed a behavior consistent with the ductile material graph. However, the material numbered B is a brittle material. It was broken directly without giving a necking area. Therefore, it can be considered in the brittle or strong material category.

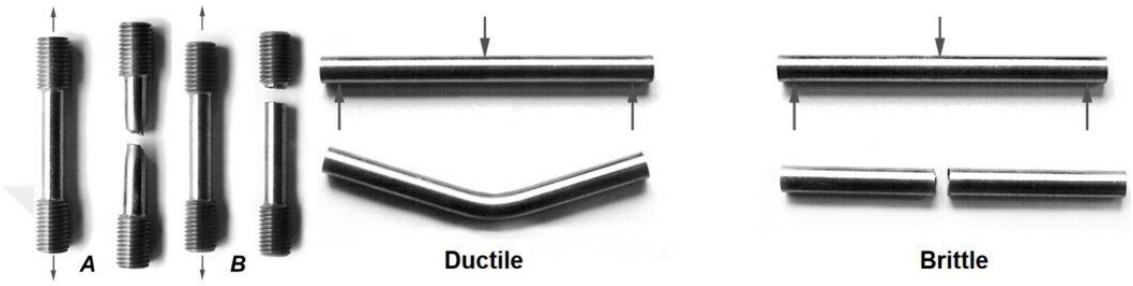

Figure 2.37 Example of ductile and brittle materials [38]

When calculating engineering stress, it is assumed that the sample diameter remains constant throughout the entire experiment.

$$\sigma = \frac{F}{A_0}$$

Engineering strain calculation is done by subtracting the first length from the final length and dividing by the first length.

$$\varepsilon = \frac{L - L_0}{L_0}$$

True stress is calculated using the instantaneous real cross-sectional area of the applied load.

$$\sigma_t = \frac{F}{A}$$

True Strain is a logarithmic value. However, due to the small values in Taylor expansion, it gives very similar results to engineering strain at small strain values.

$$\varepsilon_t = \int \frac{\delta L}{L}$$

For true stress;

$$\sigma = \frac{F}{A} = \frac{F}{A_0}\frac{A_0}{A} = \frac{F}{A_0}\frac{L}{L_0} = \sigma(1+\varepsilon)$$

For True Strain;

$$\delta\varepsilon_t = \frac{\delta L}{L}$$

$$\varepsilon_t = \ln\left(\frac{L}{L_0}\right) = \ln(1+\varepsilon)$$

The stress-strain in the neck region is expressed as follows.

$$\sigma_t = \frac{F}{A_{neck}} \qquad \varepsilon_t = \ln(\frac{A_0}{A_{neck}})$$

CHAPTER 3

3. EXPERIMENTAL ANALYSIS of MATERIAL

3.1 Introduction

Determining material properties with test methods is a very important step for simulation. An incorrectly created material card will cause differences with the results obtained from the simulation during the experiment phase.

3.2 Mechanical Characterization and Friction Tests

In this section, the friction test and mechanical characterization tests will be examined. These results are crucial to get better simulation results.

3.2.1 Mechanical Characterization tests

Devices at the Metal Forming Center of Excellence were used to examine the mechanical behavior of the material. TAI shared the tensile test results for Titanium CP2 material. In the flex-forming method, the strain rate is generally slow. So, test result which was provided by TAI, the slowest strain rate is taken as reference strain rate graph. The test performed at 0 degrees and 5mm/min strain rate was accepted as reference. According to the values obtained from the graph (Figure 3.1);

- Yield Point: 481,317 MPa
- UTS: 707,4486 MP

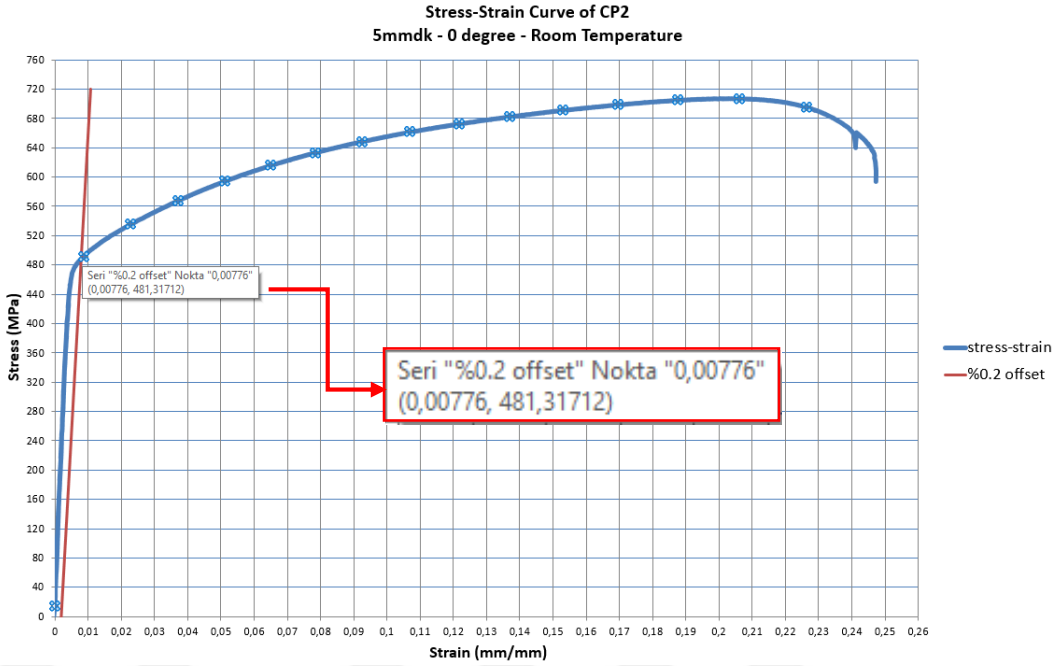

Figure 3.1 5mm min – 0° and Room Temperature Tensile Test Results

3.2.2 Elastic Modulus Determination Tests of the Material

Elasticity Modulus (E) is the modulus of elasticity describes the tensile elasticity of an object, or its tendency to deform along an axis to which forces are applied in opposite directions. Its unit is the stress unit. In special cases, the Elasticity modulus of the material can be considered as a measure of the stiffness of the material.

To determine the modulus of elasticity, impact excitation equipment measures the vibration frequency. It calculates Young's modulus using the mass and dimensions of the sample according to different measurements and standards. (ASTM E1876-15, ISO 12680-1, EN 843-2).

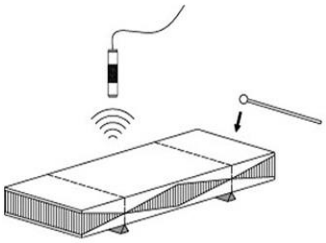

$$E = 0.9465 \left(\frac{m f_f^2}{w}\right)\left(\frac{L^3}{t^3}\right)T$$

with ***E*** *the Young's modulus*
f_f *the flexular frequency*
m *the mass*
L *the length*
w *the width*
t *the thickness*
T *the correction factor*

Figure 3.2 Basic Summary of System [39]

The purpose of this test is to determine the elasticity modulus (E) of the material by performing resonance frequency and damping analysis at room temperature with the

IMCE RFDA Device of 9 samples prepared in accordance with the ASTM E1876-15 standard. The pulse excitation technique is a non-destructive material characterization method to determine the elastic properties of the material. The samples delivered to us were rough and fine sanded with sandpaper. The elasticity modulus (E) measurements were made by defining the length, width, thickness and weight values of the samples on the IMCE RFDA Device (Figure 3.3).

Figure 3.3 IMCE RFDA-HTVP 1600 Device

The non-destructive impact excitation technique is based on recording the vibration signal induced by a microphone by hitting the sample with a small hammer. The resulting vibration signal is converted to the frequency domain by Fourier transform. The software determines the resonance frequency with high accuracy to calculate elastic properties.

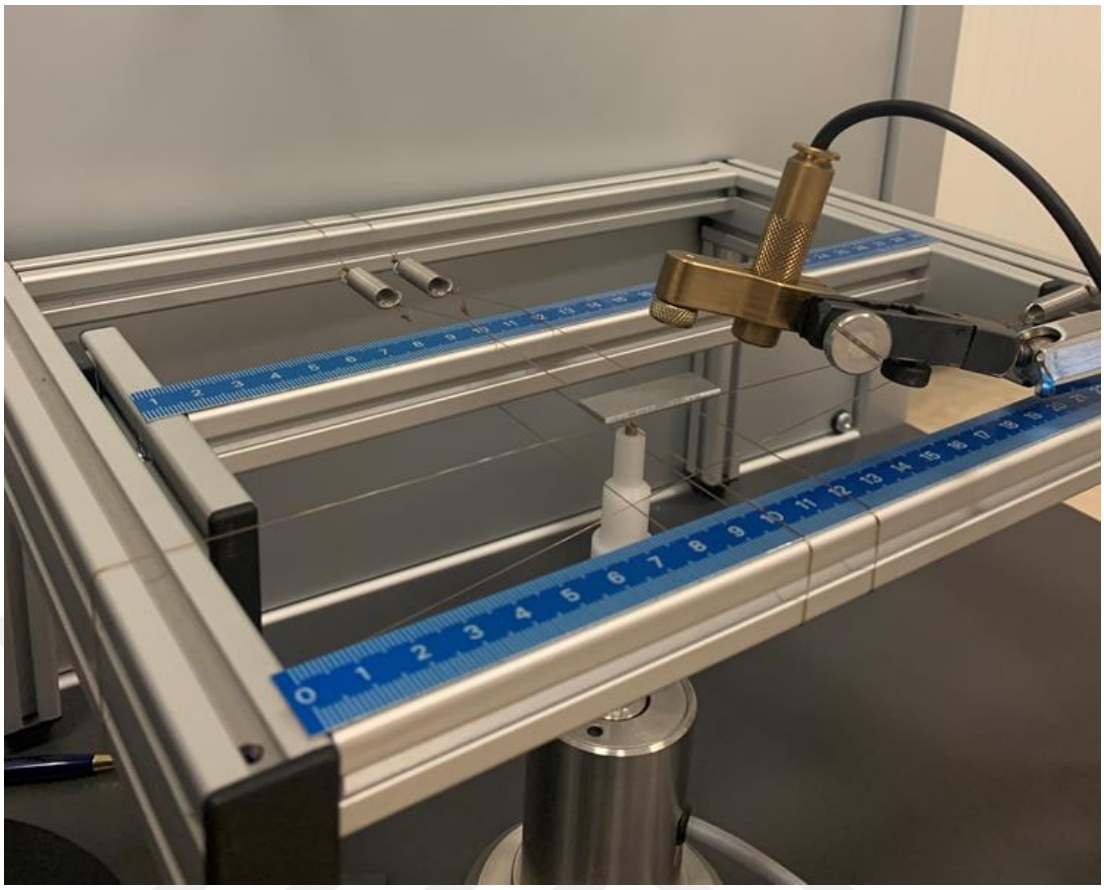

Figure 3.4 Experimental Setup General View

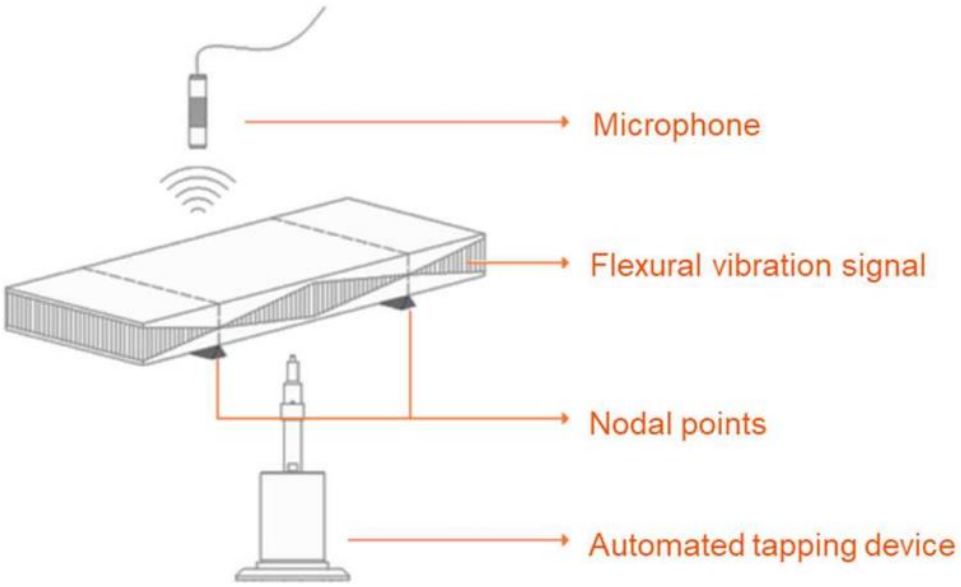

Figure 3.5 - Experimental setup diagram

3.2.2.1 Results of Elastic Modulus Determination Test

Parallel to Rolling Direction (0°) – Repeat 1.

Results: The results obtained from the resonance frequency and damping test performed at room temperature on the sample measuring 39.99 mm x 11.96 mm x 1.01 mm and weighing 2.24 g are given below. Accordingly, the Elasticity modulus (E) of the material was found to be 117.42 GPa.

Table 3.1 Parallel to Rolling Direction (0°) – Repeat 1.

Test Results			
Parallel to Rolling Direction (0°) – Repeat 1.			
Measurement Mode:	Flexural		
Sample Shape:	Rectangular Bar		
Dimentions		Elastic Properties	
Length (mm)	39.99	E-mod (GPa)	117.42
Width (mm)	11.96		
Thickness (mm)	1.01	ΔE-mod (GPa)	4.20
Mass (g)	2.24		
Flex. Freq. (Hz):	3259.24		

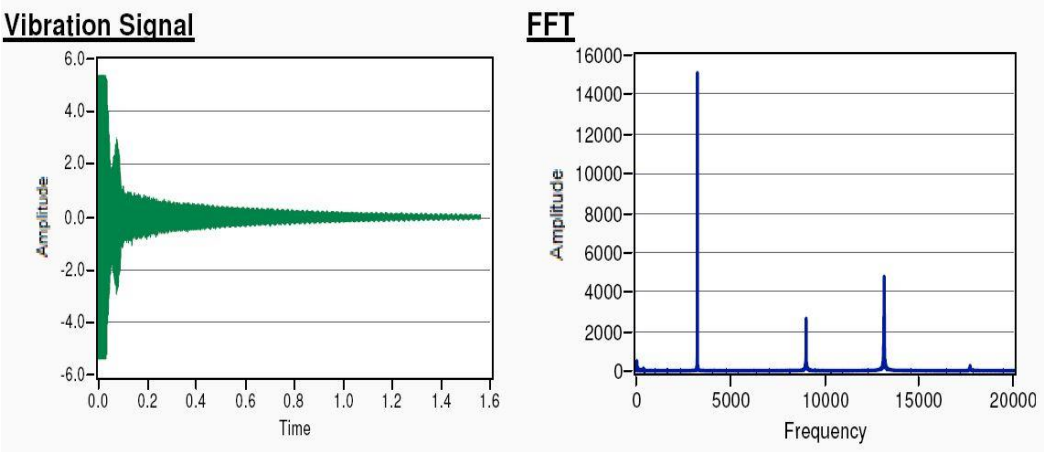

Figure 3.6 Vibration Signal and FFT Graphs

Parallel to Rolling Direction (0°) – Repeat 2

Results: The results obtained from the resonance frequency and damping test performed at room temperature on the sample measuring 40.00 mm x 11.98 mm x 1.01 mm and weighing 2.25 g are given below. Accordingly, the Elasticity modulus (E) of the material was found to be 118.4 GPa.

Table 3.2 Parallel to Rolling Direction (0°) – Repeat 2

Test Results			
Parallel to Rolling Direction (0°) – Repeat 2			
Measurement Mode:	Flexural		
Sample Shape:	Rectangular Bar		
Dimentions		Elastic Properties	
Length (mm)	40.00	E-mod (GPa)	118.40
Width (mm)	11.98		
Thickness (mm)	1.01	ΔE-mod (GPa)	4.23
Mass (g)	2.25		
Flex. Freq. (Hz):	3267.03		

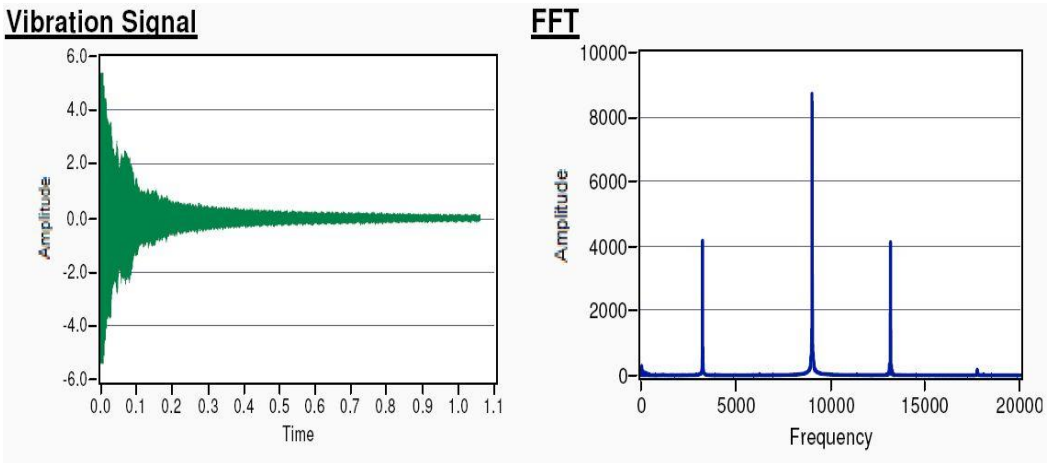

Figure 3.7 Vibration Signal and FFT Graphs

Parallel to Rolling Direction (0°) – Repeat 3

Results: The results obtained from the resonance frequency and damping test performed at room temperature on the sample measuring 40.00 mm x 11.98 mm x 1.82 mm and weighing 2.25 g are given below. Accordingly, the Elastic modulus (E) of the the material was found to be 115.28 GPa.

Table 3.3 Parallel to Rolling Direction (0°) – Repeat 3

Test Results			
Parallel to Rolling Direction (0°) – Repeat 3			
Measurement Mode:	Flexural		
Sample Shape:	Rectangular Bar		
Dimentions		Elastic Properties	
Length (mm)	40.00	E-mod (GPa)	115.28
Width (mm)	11.98		
Thickness (mm)	1.01	ΔE-mod (GPa)	4.09
Mass (g)	2.25		
Flex. Freq. (Hz):	3291.55		

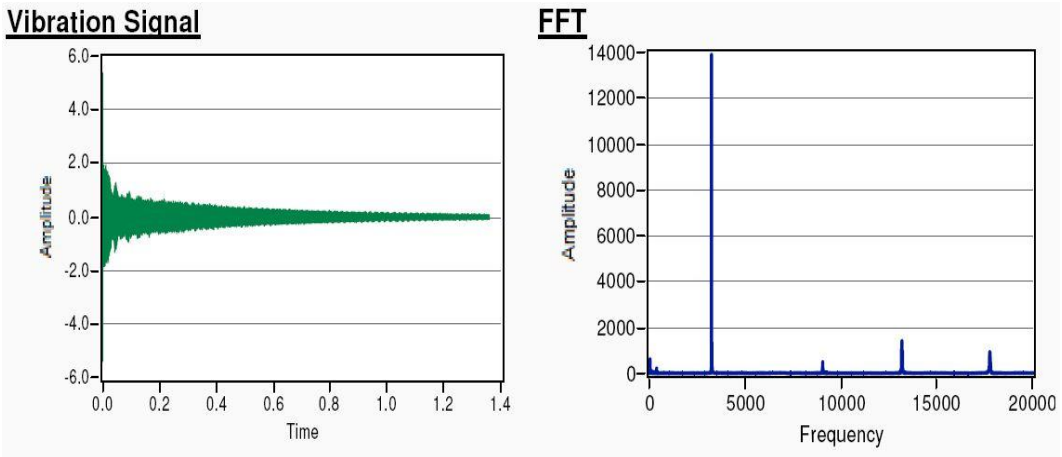

Figure 3.8 Vibration Signal and FFT Graphs

Rolling Direction (45°) – Repeat 1

Results: The results obtained from the resonance frequency and damping test performed at room temperature on the sample measuring 39.98 mm x 11.97 mm x 1.01 mm and weighing 2.23 g are given below. Accordingly, the Elasticity modulus (E) of the material was found to be 117.9 GPa.

Table 3.4 Rolling Direction (45°) – Repeat 1

Test Results			
Rolling Direction (45°) – Repeat 1			
Measurement Mode:	Flexural		
Sample Shape:	Rectangular Bar		
Dimentions		Elastic Properties	
Length (mm)	39.98	E-mod (GPa)	117.90
Width (mm)	11.97		
Thickness (mm)	1.01	ΔE-mod (GPa)	4.22
Mass (g)	2.23		
Flex. Freq. (Hz):	3275.87		

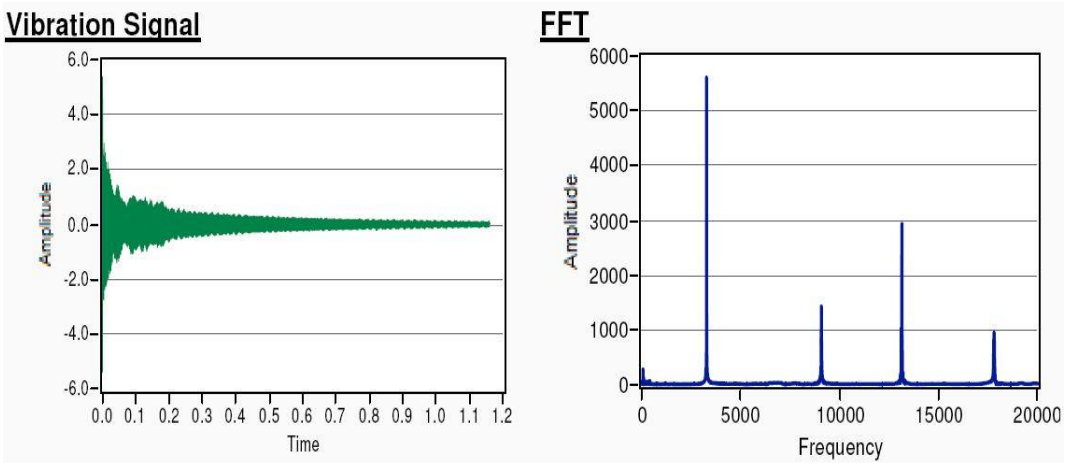

Figure 3.9 Vibration Signal and FFT Graphs

Rolling Direction (45°) – Repeat 2

Results: The results obtained from the resonance frequency and damping test performed at room temperature on the sample measuring 39.98 mm x 11.99 mm x 1.01 mm and weighing 2.24 g are given below. Accordingly, the Elasticity modulus (E) of the material was found to be 118.96 GPa.

Table 3.5 Rolling Direction (45°) – Repeat 2

Test Results			
Rolling Direction (45°) – Repeat 2			
Measurement Mode:	Flexural		
Sample Shape:	Rectangular Bar		
Dimentions		Elastic Properties	
Length (mm)	39.98	E-mod (GPa)	118.96
Width (mm)	11.99		
Thickness (mm)	1.01	ΔE-mod (GPa)	4.25
Mass (g)	2.24		
Flex. Freq. (Hz):	3285.91		

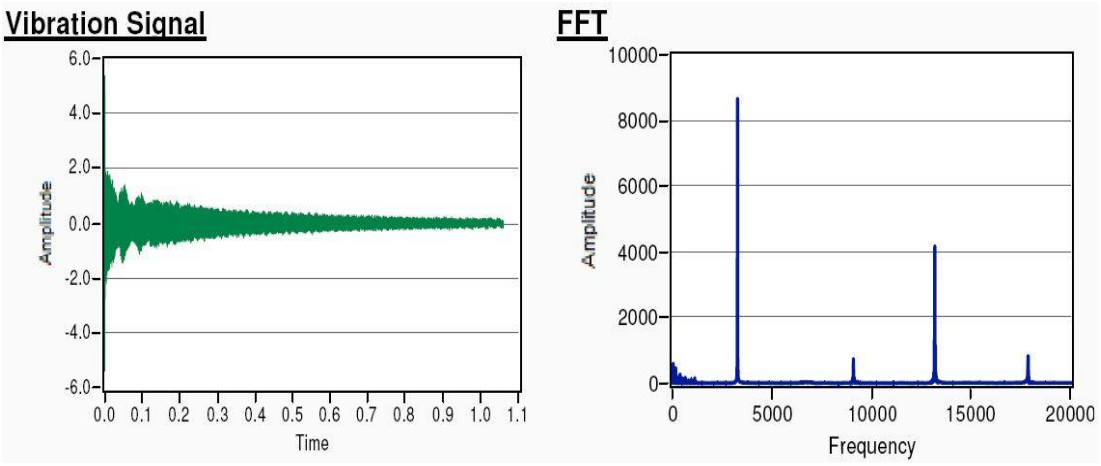

Figure 3.10 Vibration Signal and FFT Graphs

Rolling Direction (45°) – Repeat 3

Results: The results obtained from the resonance frequency and damping test performed at room temperature on the sample measuring 39.96 mm x 11.97 mm x 1.01 mm and weighing 2.25 g are given below. Accordingly, the Elasticity modulus (E) of the material was found to be 120.32 GPa.

Table 3.6 Rolling Direction (45°) – Repeat 3

Test Results			
Rolling Direction (45°) – Repeat 3			
Measurement Mode:	Flexural		
Sample Shape:	Rectangular Bar		
Dimentions		Elastic Properties	
Length (mm)	39.97	E-mod (GPa)	120.32
Width (mm)	11.97		
Thickness (mm)	1.01	ΔE-mod (GPa)	4.30
Mass (g)	2.25		
Flex. Freq. (Hz):	3295.81		

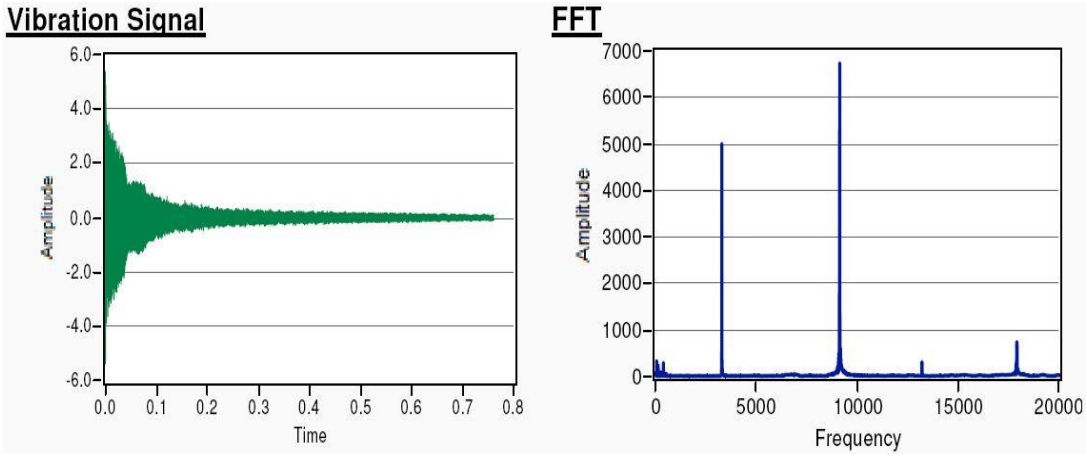

Figure 3.11 Vibration Signal and FFT Graphs

Rolling Direction (90°) – Repeat 1

Results: The results obtained from the resonance frequency and damping test performed at room temperature on the sample measuring 39.97 mm x 11.98 mm x 1.01 mm and weighing 2.25 g are given below. Accordingly, the Elasticity modulus (E) of the material was found to be 122.49 GPa.

Table 3.7 Rolling Direction (90°) – Repeat 1

Test Results			
Rolling Direction (90°) – Repeat 1			
Measurement Mode:	Flexural		
Sample Shape:	Rectangular Bar		
Dimentions		Elastic Properties	
Length (mm)	39.97	E-mod (GPa)	122.49
Width (mm)	11.98		
Thickness (mm)	1.01	ΔE-mod (GPa)	4.38
Mass (g)	2.25		
Flex. Freq. (Hz):	3326.71		

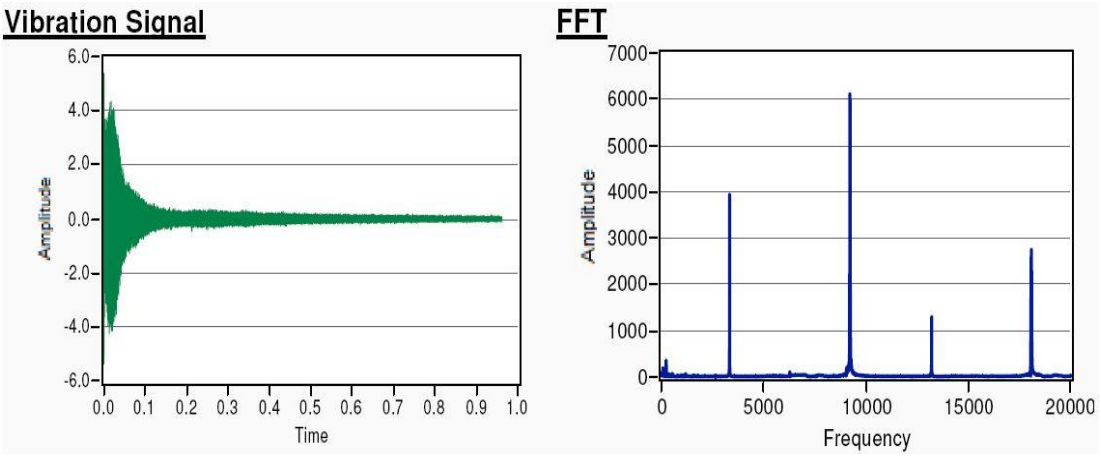

Figure 3.12 Vibration Signal and FFT Graphs

Rolling Direction (90°) – Repeat 2

Results: The results obtained from the resonance frequency and damping test performed at room temperature on the sample measuring 39.99 mm x 11.99 mm x 1.01 mm and weighing 2.25 g are given below. Accordingly, the Elasticity modulus (E) of the material was found to be 122.16 GPa.

Table 3.8 Rolling Direction (90°) – Repeat 2

Test Results			
Rolling Direction (90°) – Repeat 2			
Measurement Mode:	Flexural		
Sample Shape:	Rectangular Bar		
Dimentions		Elastic Properties	
Length (mm)	39.97	E-mod (GPa)	122.16
Width (mm)	11.98		
Thickness (mm)	1.01	ΔE-mod (GPa)	4.37
Mass (g)	2.25		
Flex. Freq. (Hz):	3322.32		

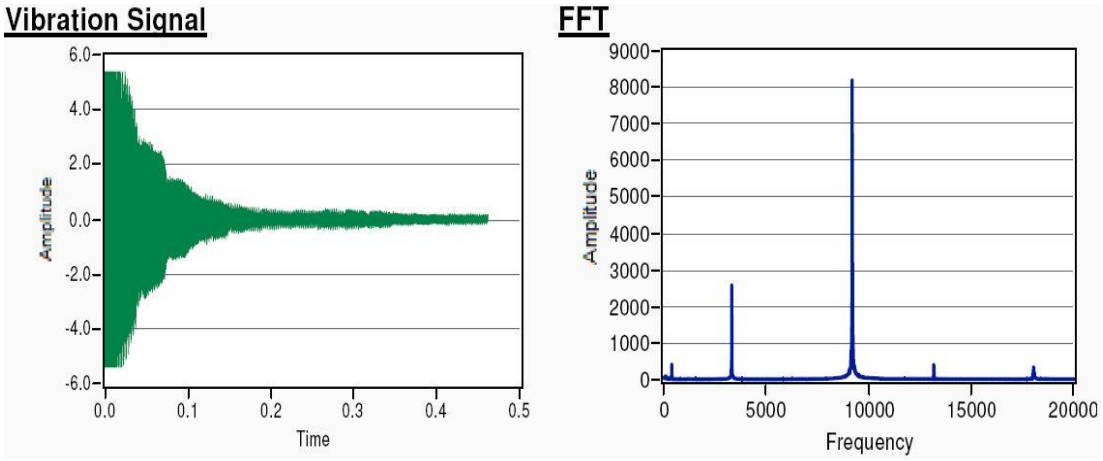

Figure 3.13 Vibration Signal and FFT Graphs

Rolling Direction (90°) – Repeat 3

Results: The results obtained from the resonance frequency and damping test performed at room temperature on the sample measuring 39.99 mm x 11.98 mm x 1.01 mm and weighing 2.24 g are given below. Accordingly, the Elasticity modulus (E) of the material was found to be 121.42 GPa.

Table 3.9 Rolling Direction (90°) – Repeat 3

Test Results			
Rolling Direction (90°) – Repeat 3			
Measurement Mode:	Flexural		
Sample Shape:	Rectangular Bar		
Dimentions		Elastic Properties	
Length (mm)	39.97	E-mod (GPa)	121.42
Width (mm)	11.98		
Thickness (mm)	1.01	ΔE-mod (GPa)	4.34
Mass (g)	2.25		
Flex. Freq. (Hz):	3312.21		

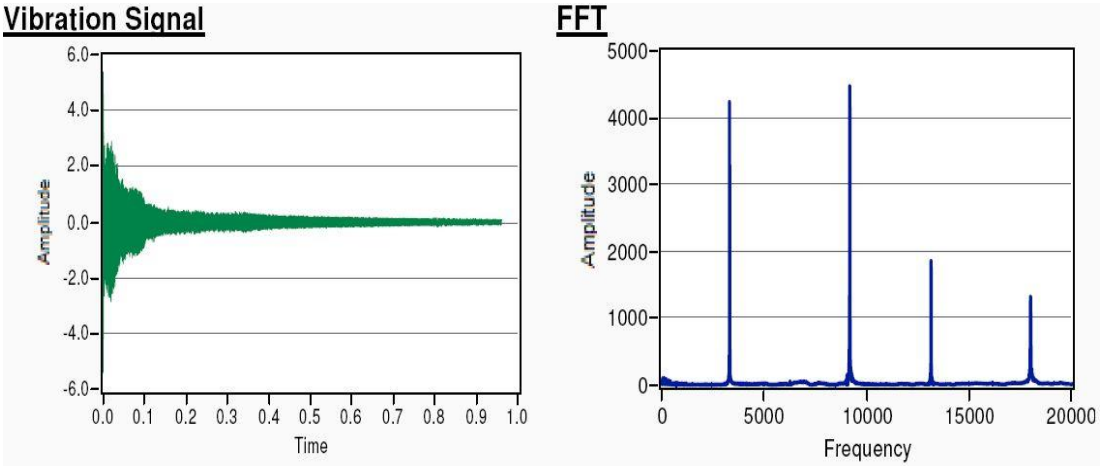

Figure 3.14 Vibration Signal and FFT Graphs

Conclusion and comments:

Table 3.10 Elastic Modulus Test Average

Cutting Angle	Repeat	E-mod (GPa)
0°	1	117.42
	2	118.4
	3	115.25
	Average	**117.02**
45°	1	117.9
	2	118.96
	3	120.32
	Average	**119,06**
90°	1	122.49
	2	122.16
	3	121.42
	Average	**122,02**

Elastic modulus results for pure titanium will be used in elastic and plastic deformation calculations of titanium sheets using the finite element method. If it is possible to use direction-dependent elastic values in finite element programs, according to the table above:

- 117 GPa for 0° direction
- 119 GPa for 45° direction
- 122 GPa for 90° direction

receivable. However, if the average value is used, 119.3 GPa can be used.

3.2.3 Coefficient of Friction Measurements

Tribometer was used to determine the friction coefficient of the material. Experiments were carried out in 2 stages.

Dry surface;

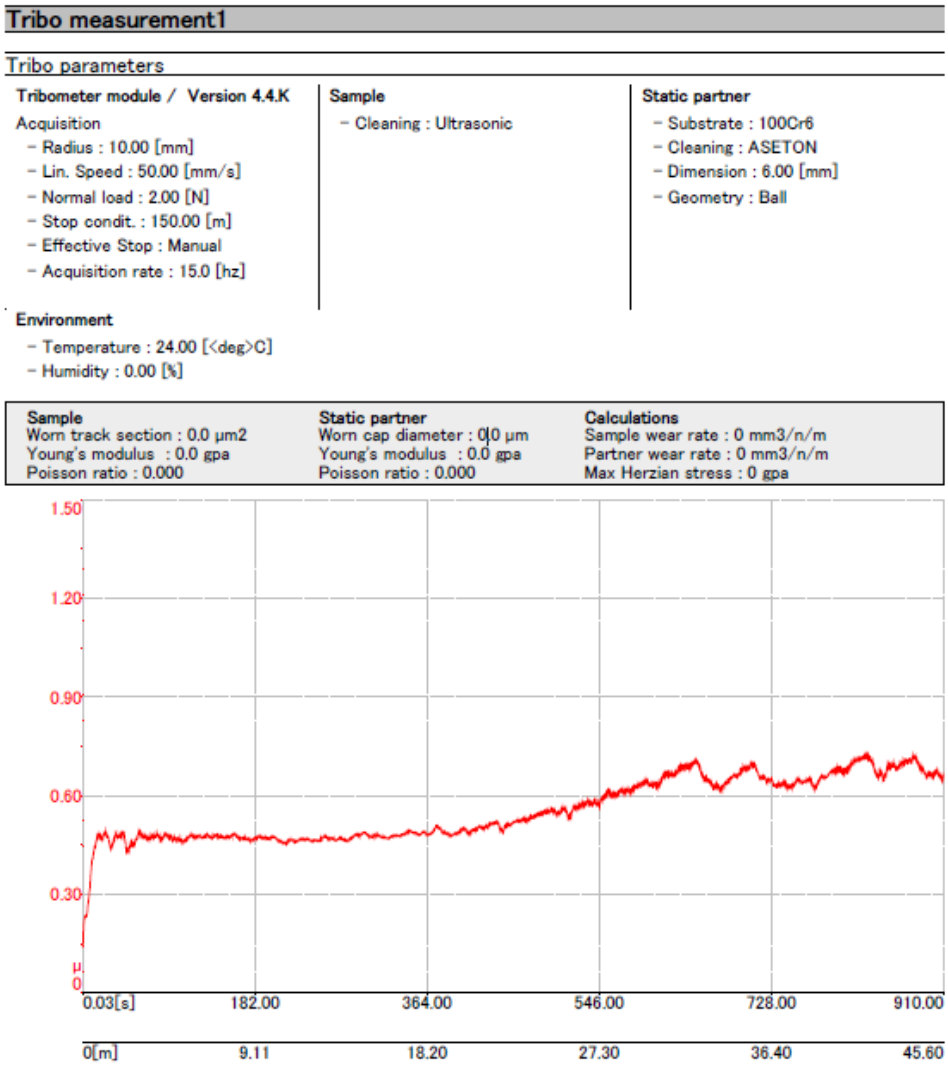

Figure 3.15 Friction measurement

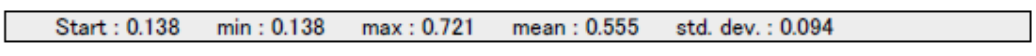

Figure 3.16 Friction measurement results

Lubricated with machine oil;

Tribo measurement1

Tribo parameters

Tribometer module / Version 4.4.K

Acquisition
- Radius : 8.00 [mm]
- Lin. Speed : 50.00 [mm/s]
- Normal load : 2.00 [N]
- Stop condit. : 150.00 [m]
- Effective Stop : Manual
- Acquisition rate : 15.0 [hz]

Sample
- Cleaning : Ultrasonic

Static partner
- Substrate : 100Cr6
- Cleaning : ASETON
- Dimension : 6.00 [mm]
- Geometry : Ball

Environment
- Temperature : 24.00 [<deg>C]
- Humidity : 0.00 [%]

Sample	Static partner	Calculations
Worn track section : 0.0 µm2	Worn cap diameter : 0.0 µm	Sample wear rate : 0 mm3/n/m
Young's modulus : 0.0 gpa	Young's modulus : 0.0 gpa	Partner wear rate : 0 mm3/n/m
Poisson ratio : 0.000	Poisson ratio : 0.000	Max Herzian stress : 0 gpa

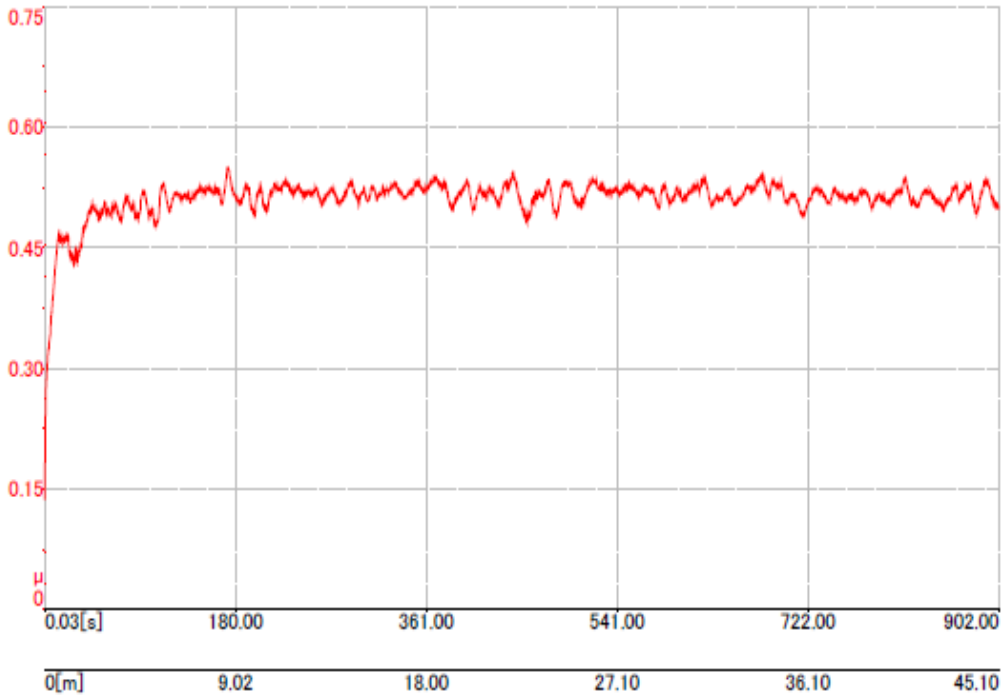

Figure 3.17 Friction measurement

Start : 0.136 min : 0.136 max : 0.548 mean : 0.511 std. dev. : 0.025

Figure 3.18 Friction measurement results

All these tests were performed in triplicate. The friction value to be used in the analysis was decided to be 0.5.

Table 3.10 The results of friction tests

Test number	Dry Surface	Machine Oiled
1	0,5-0,7	0,5
2	0,45-0,7	0,5
3	0,45-0,7	0,5

Table 3.11 The tribometer test results

Test number	**Steps**	**Dry Surface**	**Machine Oiled**
1	Min	0,136	0,136
	Max	0,721	0,548
	Mean	0,555	0,511
	Std,Dev,	0,094	0,025
2	Min	0,203	0,138
	Max	0,713	0,558
	Mean	0,539	0,510
	Std,Dev,	0,092	0,042
3	Min	0,196	0,139
	Max	0,711	0,548
	Mean	0,542	0,510
	Std,Dev,	0,096	0,037

CHAPTER 4

4. DESIGN AND SIMULATION STAGES

4.1 Design of Forming Pattern

The shaping pattern to be used is aimed to provide the highest rigidity and lowest distortion. The most important design criterion for the highest rigidity was determined as second moment of inertia. To increase the second moment of inertia, maximum depth will be applied. Additionally, the determined geometry will be designed in both positive and negative directions. Thus, the second moment of inertia will double. The design criteria to be applied within the scope of this thesis are as follows;

1- Maximum rigidity
2- Minimum distortion and springback
3- Maximum 10% thinning

Depth criteria will be taken into consideration for maximum rigidity in the forming pattern to be created. For criteria such as warping, springback and thinning, depth, draft angles, distance between two shaping patterns and radius measurements will be optimized.

It was decided that the forming pattern would be in the form of a plus (+) to ensure equal rigidity in all directions. Elastic analysis - plastic analysis - design sections will be carried out in parallel. The most rigid design will be determined by the results obtained from elastic analysis. Plastic analyzes will then be carried out. In the plastic analysis part, the thinning-warping and springback stages will be optimized by design.

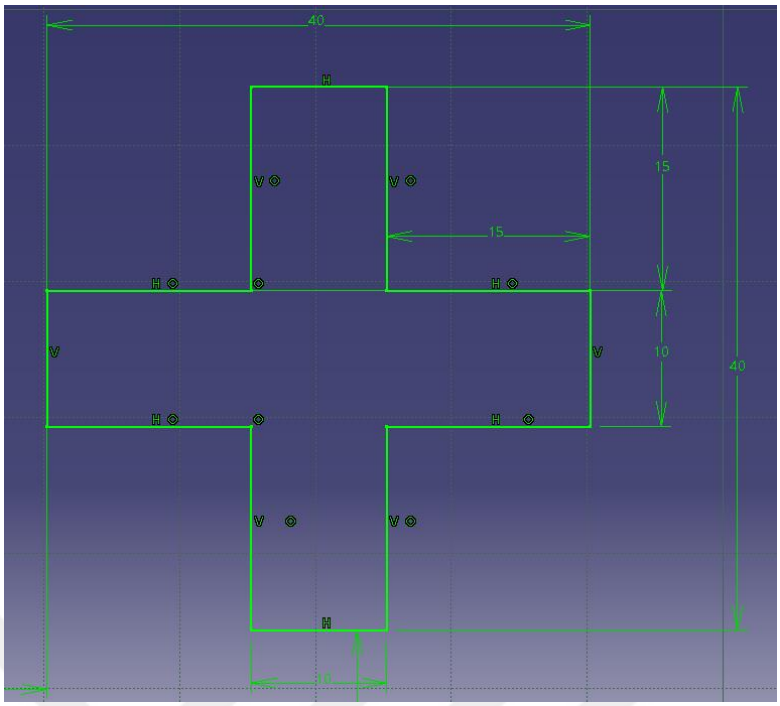

Figure 4.1 General dimension of forming pattern

4.2 Elastic Analysis

At this stage, before perform forming analysis, the Ansys-Mechanical module is used. Elastic analysis will be used to decide among the designs that have the least deflection. The design that gives the least deflection under 5N load will be selected for mold manufacturing. The purpose of this section is to find the right design approach. Detailed elastic analyzes will be carried out after plastic analyses. The reason for this is that, with the results obtained from plastic analyses, thinning, distortion and springback events will be optimized by design.

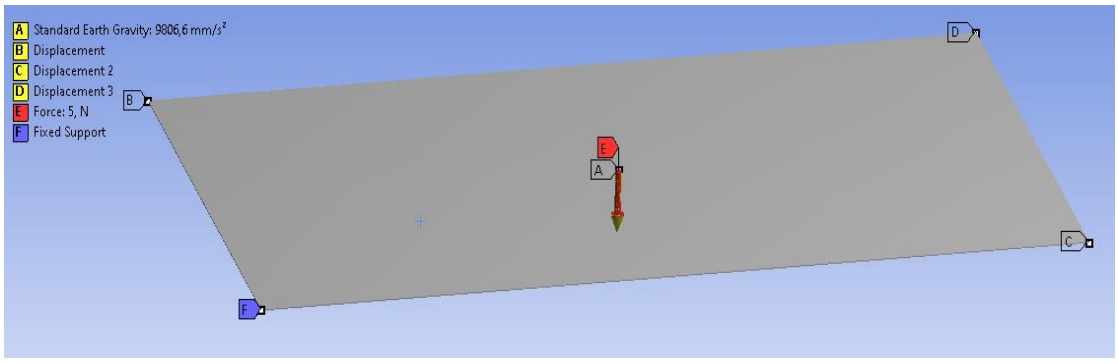

Figure 4.2 System Overview

The material parameter as below. These data was taken from TAI library.

Properties of Outline Row 3: Titanium

	A	B	C	D	E
1	Property	Value	Unit		
2	Density	4,51	g cm^-3		
3	Isotropic Secant Coefficient of Thermal Expansion				
4	Coefficient of Thermal Expansion	8,89E-06	C^-1		
5	Isotropic Elasticity				
6	Derive from	Young's Modulus and Poisson's...			
7	Young's Modulus	1,19E+05	MPa		
8	Poisson's Ratio	0,34			
9	Bulk Modulus	1,2396E+11	Pa		
10	Shear Modulus	4,4403E+10	Pa		
11	Tensile Yield Strength	475	MPa		
12	Tensile Ultimate Strength	707	MPa		

Figure 4.3 Material Parameters

Structural

Isotropic Elasticity

Derive from	Young's Modulus and Poisson's Ratio
Young's Modulus	1,19e+05 MPa
Poisson's Ratio	0,34000
Bulk Modulus	1,2396e+05 MPa
Shear Modulus	44403 MPa
Isotropic Secant Coefficient of Thermal Expansion	8,89e-06 1/°C
Tensile Ultimate Strength	707,00 MPa
Tensile Yield Strength	475,00 MPa

Figure 4.4 Material Parameters

For elastic analysis, the supporting 4 points method is used. One corner is fixed, one corner is constrained only in Z and X directions, the other two corners are constrained only in Z axis. The gravitational force on the material is defined and the load is defined as a point from the middle point. Thus, the simulation of the study to be carried out in the experimental study is carried out.

In elastic analysis, some mess structure criteria are determined from the literature. Mesh are created by taking reference as quality Table 4.1.

Table 4.1 Mesh criterias

	Bad
	Acceptable
	Perfect

Mesh structure Quality Criteria			
Element Quality	0	-	1
Aspect Ratio	0	5-10	20
Jacobian Ratio	0	10	30
Warping Factor	0	0.1	1
Parallel Deviation	0		170
Skewness	0	0.80-94	1
Orthagonal Quality	0	0.1-0.15	1

490 mm x 266 mm Sheet Elastic Simulations					
Pattern	**Design**	**Design Name**	**Load (N)**	**Deflection (mm)**	**Improvement (mm)**
		Blank (490x264)	5	32,1	-
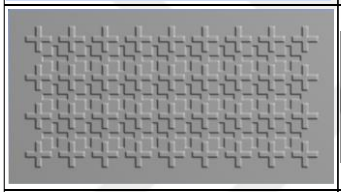		Design 1.1	5	7,9318	24,2
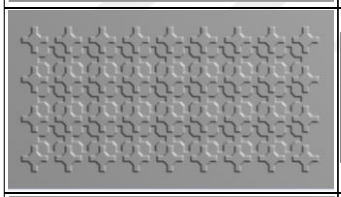		Design 2.1	5	7,9087	24,2
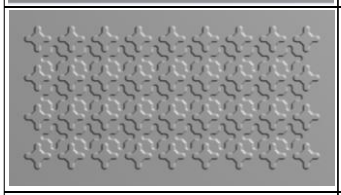		Design 2.2	5	9,2334	22,9
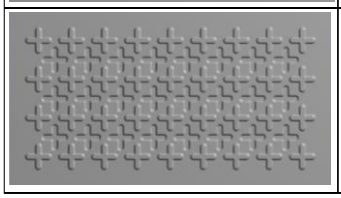		Design 3.1	5	9,3899	22,7

Figure 4.5 Design Comparison

Improvement was calculated according to the data obtained from all designs made. The formula used for recovery calculation is as follows;

$$\text{Blank Deflection(mm)} - \text{Design Deflection (mm)} = \text{Improvement (mm)}$$

As a result of the study, design 2.1 was taken as reference. In the following stages, this pattern will be optimized according to manufacturability, thinning, distortion and springback conditions (Figure 4.5).

4.3 Plastic Finite Element Methods

4.3.1 Introduction

In this study, Finite Element Method is used to examine the behavior of sheet metal during forming. Finite element method has been used for many years to solve complex engineering problems. Within the scope of this thesis, the thinning rate on the material after shaping will be examined using the Finite element method. After the analysis outputs obtained from each analysis, design optimizations will be carried out and a new analysis will be made. The biggest advantage of the Finite Element Method is saving time and cost. In this optimization study, many experimental steps were reduced and the mold geometry closest to the correct geometry was created.

In this section, the studies carried out in each analysis step will be mentioned. Simulation steps such as settings made while creating the simulation file, simulation steps, parameters, optimizations, network structure will be explained.

4.3.2 Material Modelling

In this section, the defining of sheet metal and rubber material modeling to the PAM-STAMP program will be examined.

4.3.2.1 Sheet Metal Material Modelling

Within the scope of this thesis, CP2-Titanium material is used. Some mechanical tests were carried out to create the pure titanium material model. Within the scope of these tests, the stress strain graphs, elastic modulus (119.3 GPa) (E) and friction coefficient (0.5) of the material mentioned in the experimental tests section were obtained and used. And additionally, Orthotropic Hill 48 isotropic law was used for these simulations.

Stress-strain graphs were created with the data obtained from the tensile test. A standard stress-strain graph consists of two regions: elastic and plastic regions. Since

the analysis is a plastic analysis, only the plastic region will be taken as reference in plastic simulation (Figure 4.6).

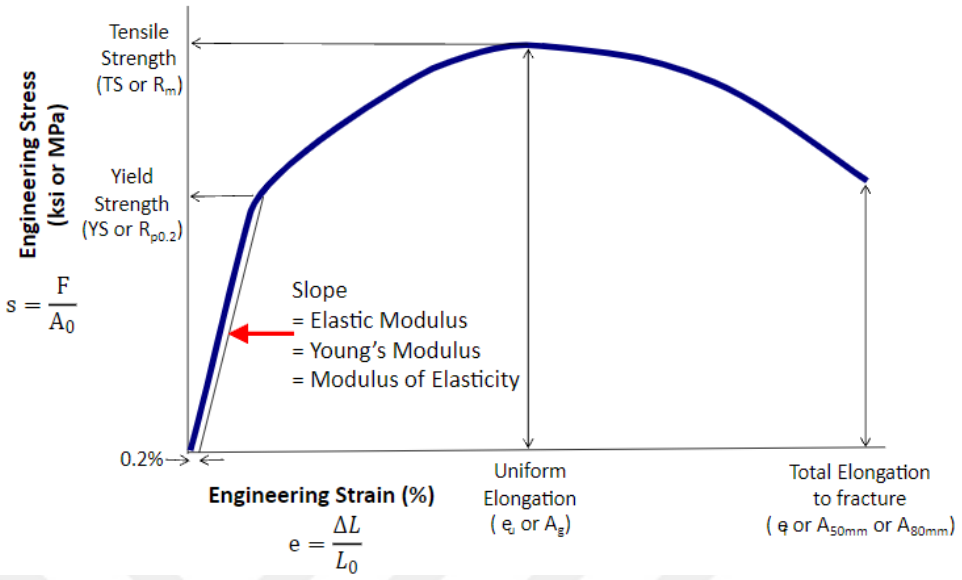

Figure 4.6 A general stress strain graph [40]

Experimental data was used to create the Hardening Curve. Test values performed at room temperature with a tensile test data of 5mm/min are taken as reference. Since a plastic analysis will be performed, a 0.2% offset value was calculated from the test data and the yield point was found.

To find the 0.2% offset value, first the young modulus of the experimental data was found (Figure 4.7).

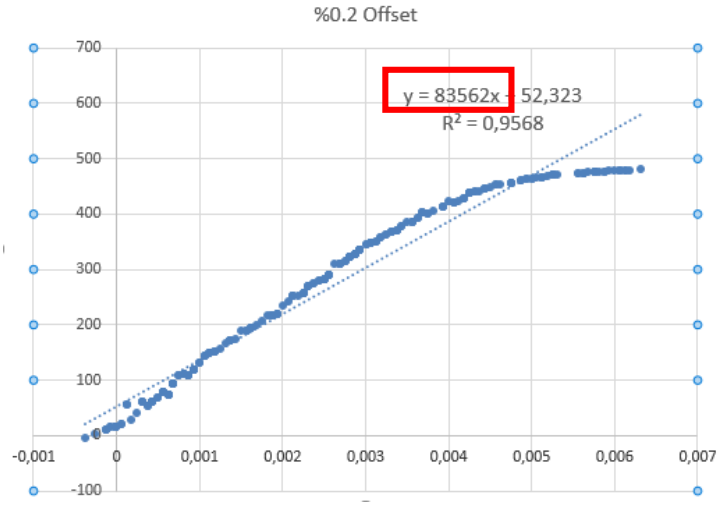

Figure 4.7 Young Modulus on graph

After Young's Modulus (E) calculation, a 0.2% offset line was drawn by increasing the strain value by 0.002 and multiplying the strain value by the Young's modulus. At this point, the yield point was determined as 481,317 MPa (Figure 4.8).

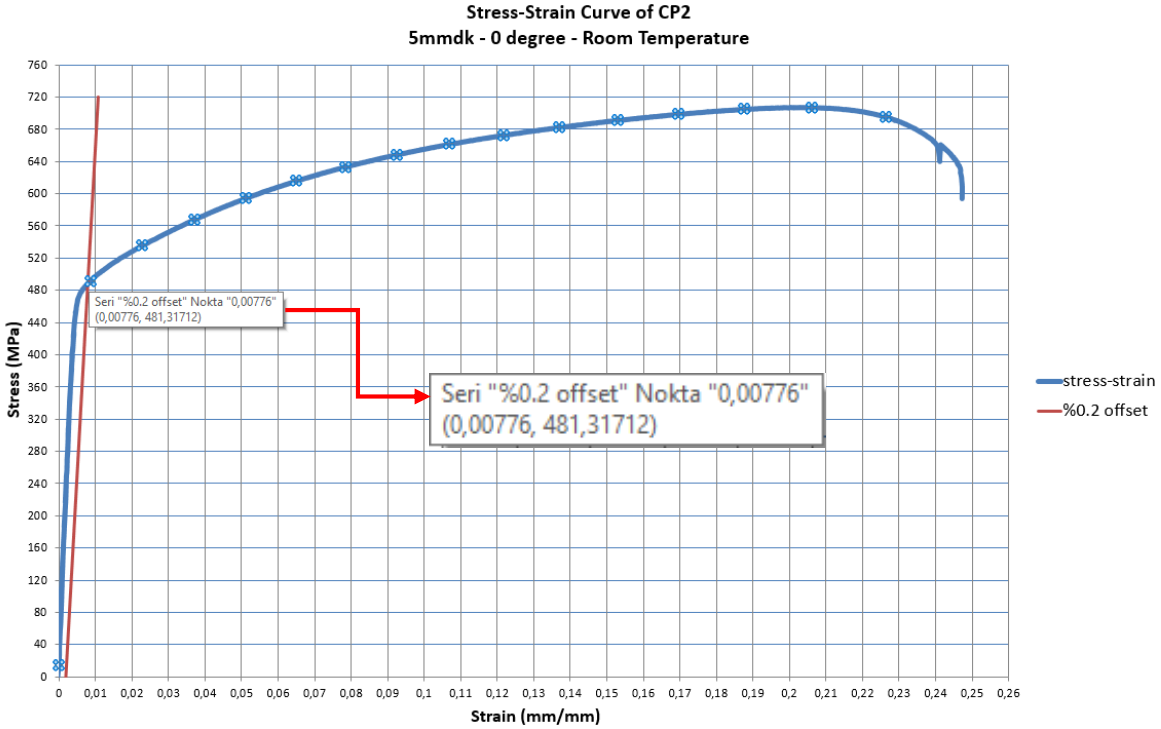

Figure 4.8 Yield point

After the yield point was defined, the engineering stress-strain curve was converted to True stress-strain curve to create the hardening curve (Figure 4.9).

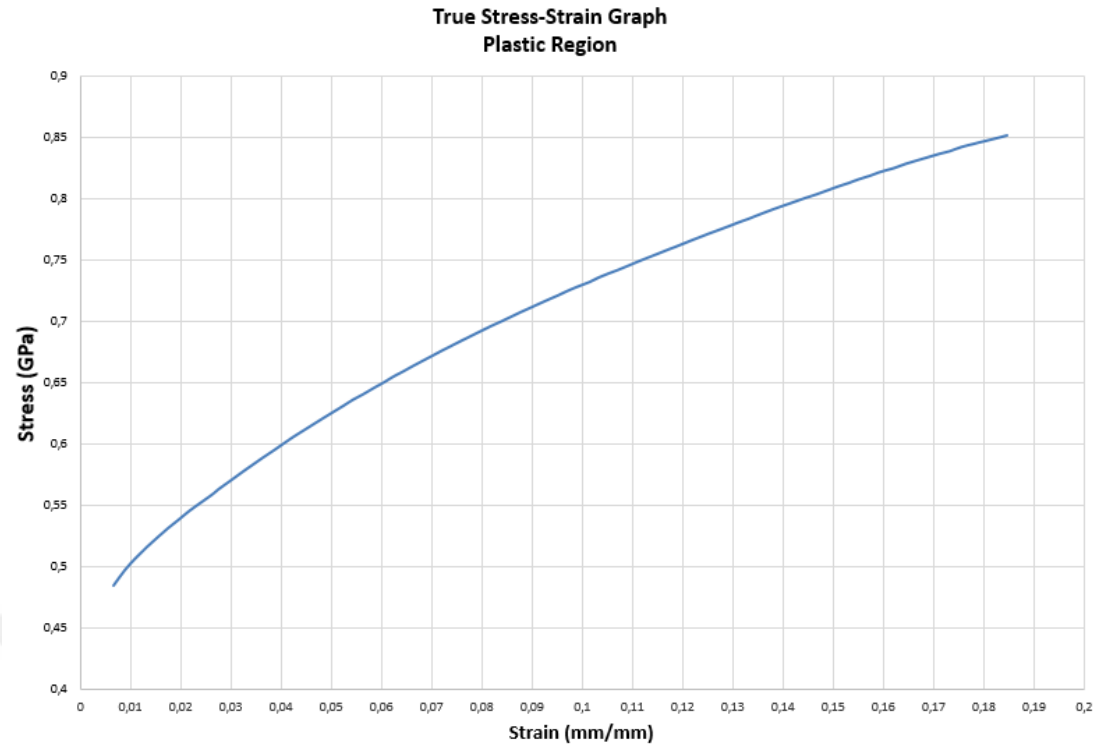

Figure 4.9 True Stress-Strain graph

These obtained data were entered into the PAM-STAMP calculation tool to determine the most accurate material model.

Information required for the calculation tool;

1- True Stress-Strain values (Plastic region)
2- Reference thickness
3- Young's modulus (Experimental)
4- Yield Stress
5- Uniform Deformation (until UTS)
6- Tensile stress
7- Total elongation

Ref. Thickness	E (Young)	Rp (Yield Stress)	Ag (Uniform Def.)	Rm (Tensile Stress)	A80(%) - Total Elong.
0,6	119,3	0,481317	20,28	0,70744867	24,72

Figure 4.10 Information which are used in calculation tool

Calculations were carried out assuming the material was isotropic. Calculations were compared with experimental data using Hollomon, Krupkowsky and Power law. Strain values in the plastic region have been shifted to 0.

Power Law: The strain hardening curve is defined from a Power Law (Ludwick equation). Explains the relationship between true stress and plastic strain (Figure 4.11).

$$\sigma = a + b.\varepsilon_p{}^n$$

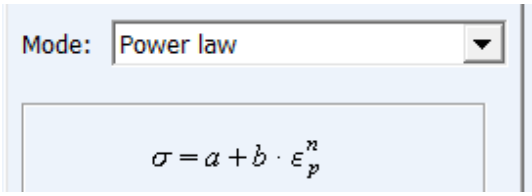

Figure 4.11 Power law equation

a: Initial yield stress

b: Strength coefficient (same definition as K coefficient in Hollomon Law

n: Strain Hardening Exponent

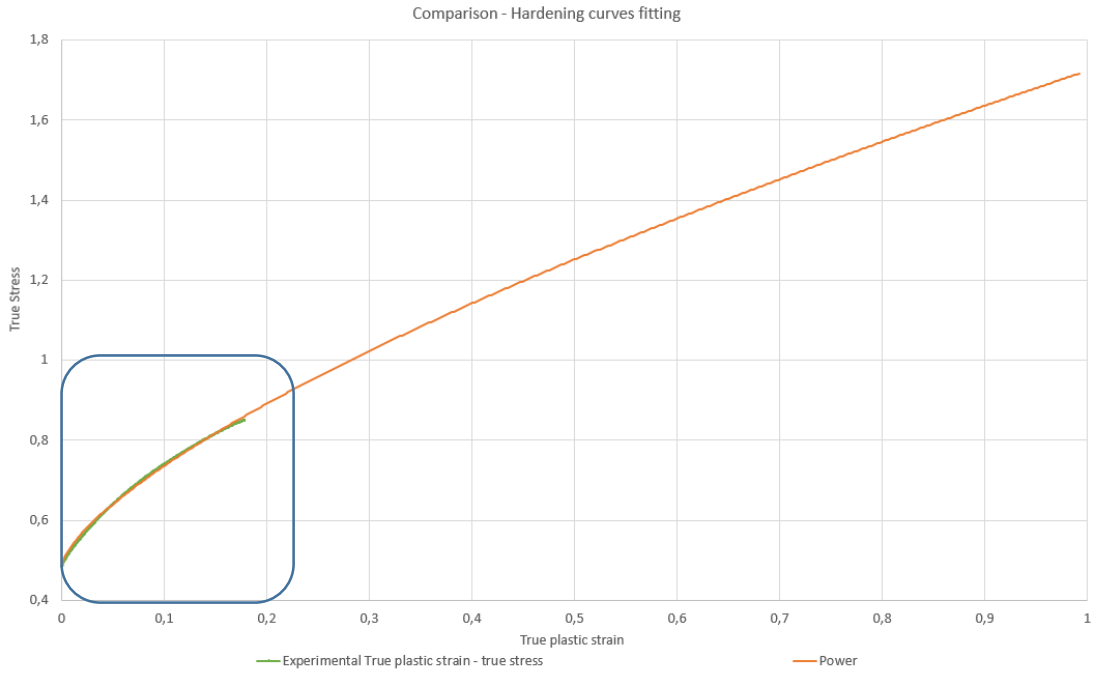

Figure 4.12 Power law accuracy by comparising experimental data

According to power law, accuracy was determined as 93.86%.

Hollomon Law; Hollomon's isotropic hardening law, which describes the true stress/true strain relationship (type of power law) of a material in uniaxial tensile testing, is defined as (Figure 4.13):

$$\sigma = K\varepsilon_p{}^n$$

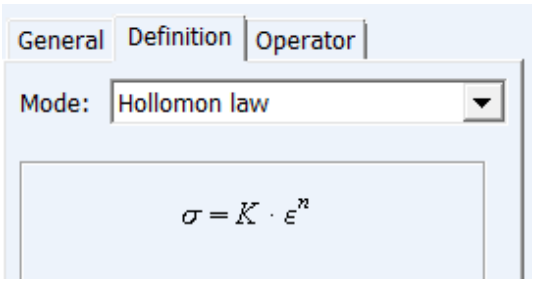

Figure 4.13 Hollomon law equation

- K: Strength coefficient of material
- n: Strain hardening exponent
- Re: Yield stress

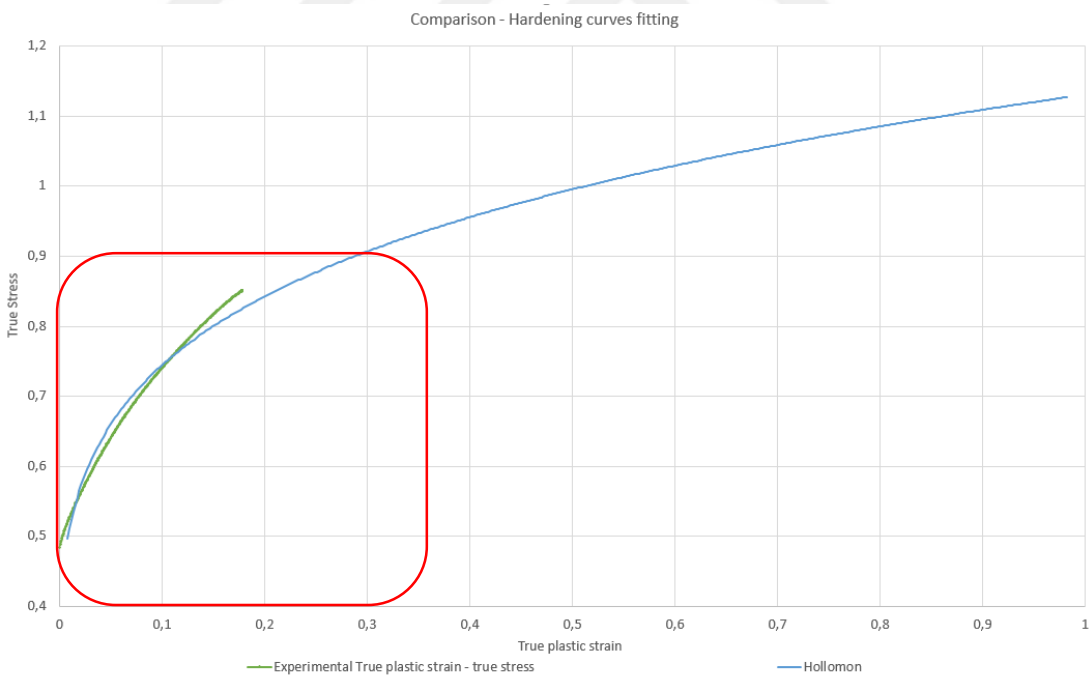

Figure 4.14 Hollomon law accuracy by comparing experimental data

According to Hollomon law, accuracy was determined as 79.31%.

Krupkowsky (Swift) law; The strain hardening curve is described by Krupkowsky (Swift) law. It is the most used in isotropic hardening law (Figure 4.15).

$$\sigma = K(\varepsilon_0 + \varepsilon_p)^n$$

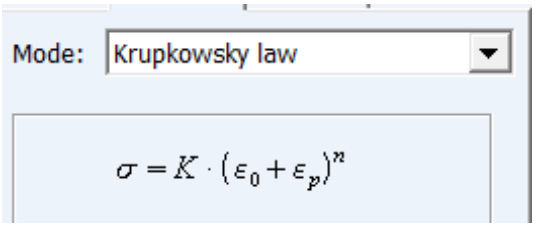

Figure 4.15 Krupkowsky law equation

- K: Strength coefficient
- n: Strain hardening exponent
- Eps0: Initial plastic strain (pre-strain)

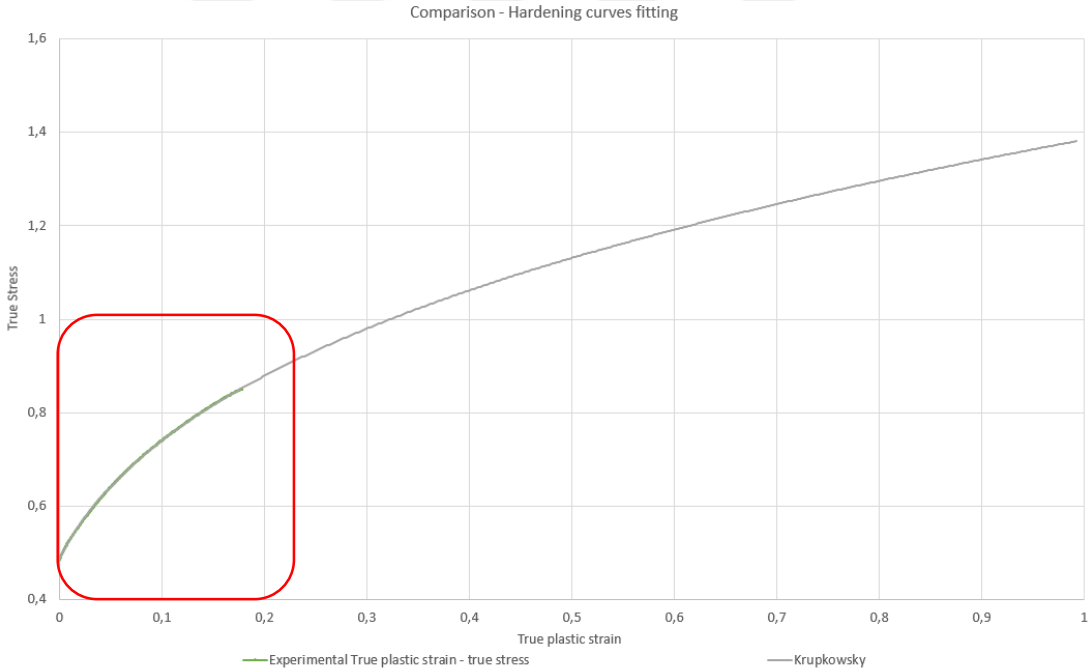

Figure 4.16 Krupkowsky law accuracy by comparing experimental data

According to Krupkowsky, the accuracy was determined as 98.47%.

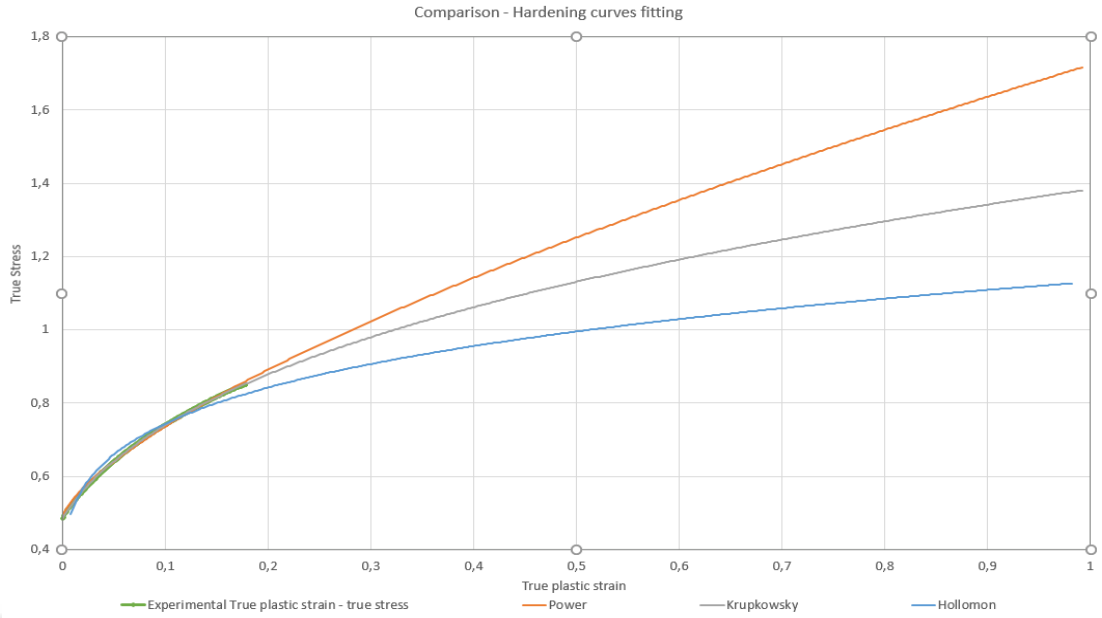

Figure 4.17 All equation comparison with experimental data

Since all these results converge when evaluated according to the graph above, the law that gives the most accurate result is Krupkowsky's law. That's why this law is taken as reference in material modeling.

Table 4.2 The accuracy of laws

STANDARD MATERIAL PARAMETERS	
Young Modulus	119,3
Yield Stress (0.2%)	0,48451
Eng UE (Ag%)	20,28
UTS	0,70745
Poission Ratio	0,35 (Literature)
Density	4.5E-6 (Literature)
ACCURACY (%)	
Hollomon	79,30982
Power	93,86609
Krupkowsky	98,47447

The parameters obtained according to Krupkowsky's law are as follows;

Table 4.3 Krupkowsky law's values to draw graph

Krupkowsky (Swift)	
K	**1,3704**
n	**0,30505**
Eps0	**0,0331**

The obtained values should be plotted graphically and compared with experimental results. The x-y coordinates of the graph drawn by the program according to the formula were taken from the program and a stress-strain graph was drawn. This graph is superimposed with the stress-strain graph created with experimental data.

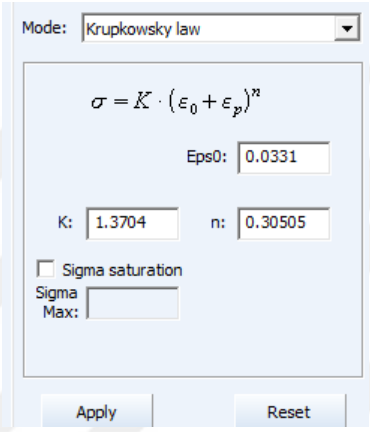

Figure 4.18 Inputs for Krupkowsky law

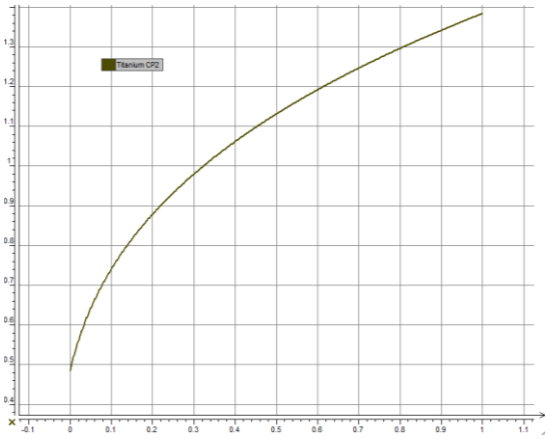

Figure 4.19 An image titanium-CP2 material graph after the graph are defined to program

With this process, Titanium-CP2 material card was created and defined in the program.

4.3.2.2 Rubber Material Modelling

Rubber material is an elastomer material produced naturally or synthetically. It is produced synthetically using polymeric components. It has a wide range of uses in engineering problems due to its mechanical properties. The feature observed within the scope of this thesis is its flexibility. Rubber material can stretch under a certain load and return to its original shape without deformation. It shows a different behavior than other materials in the stress-strain curve. In the Flex-forming method, this mechanical feature serves to show the function of a mold.

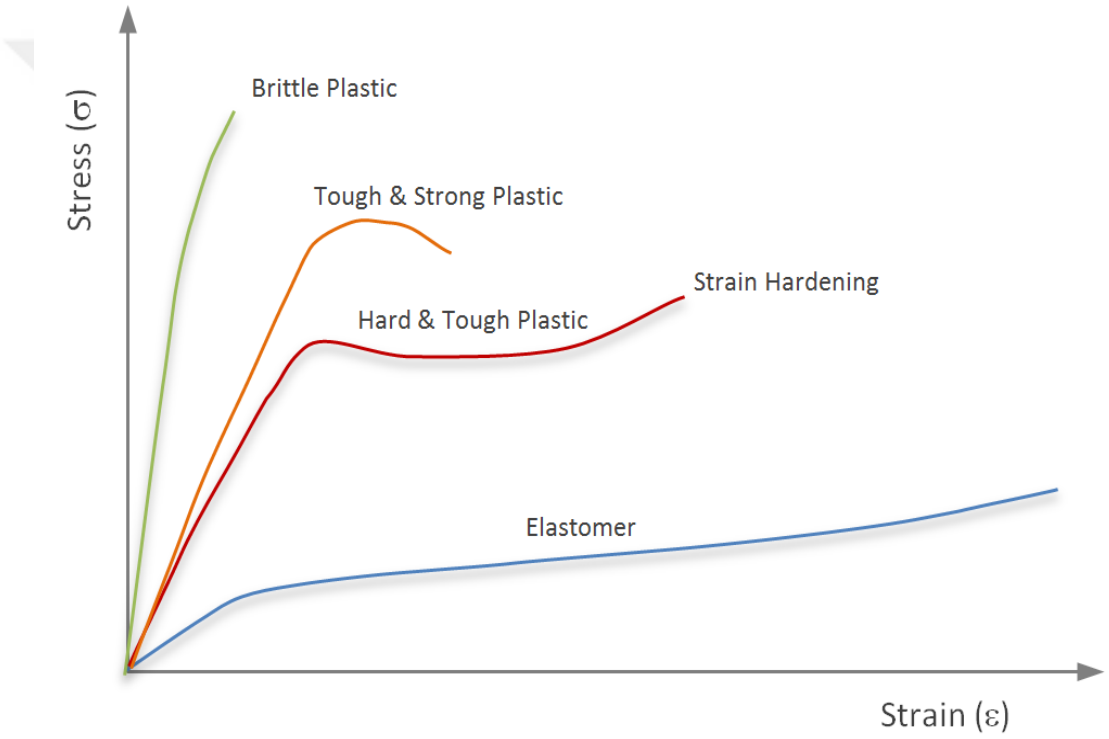

Figure 4.20 Stress-Strain graph of different material [41]

The Mooney-Rivlin law is an extremely widely used method in the rubber material board forming process. The constants C1 and C2 are estimated using the following equations. To obtain these constants, tests such as uniaxial tension, equibiaxial compression, equibiaxial tension, uniaxial compression are used. The Mooney Rivlin model, which includes constants C1 and C2, is generally valid for strains below 100%.

$$W = W(I_1, I_2, I_3) = A(I_1 - 3) + B(I_2 - 3) + W(I_3)$$

Where A and B are material properties and ($W(I_3)$) is an incompressibility penalty function.

$I_1 = 3 + 2J_1$

$I_2 = 3 + 4J_1 - 4J_2$ Right Cauchy-green Strain Invariants

$I_1 = 1 + 2J_1 - 4J_2 + 8J_3$

$J_1 = Tr(\varepsilon_{ij})$

$J_2 = \frac{1}{2}.\varepsilon_{ij}.\varepsilon_{ij} - \frac{1}{2}.J_1$ Green-Lanfrange Strain Invariants

$J_3 = dET(\varepsilon_{ij})$

$S_{ij} = \frac{\partial W}{\partial E_{ij}} - p\delta_{ij}$ S_{ij} is the 2^{nd} Pialo-Kirchhoff stress tensor.

Where;

S_{ij} The elements of the Pialo-Kirchhoff stress tensor, where i and j are indices representing the directional components. (e.g., S_{11}, S_{22} $S_{33}S_{12}$for different components).

W: Strain energy density.

E_{ij}: Green-Lagrange strain tensor components.

p: Hydrostatic pressure.

δ_{ij}: Kronecker delta function.

In a previous study conducted by TAI, which provided theoretical support to this thesis study, a uniaxial tensile test was performed for the rubber used. According to these test results, the constants C1=A=0.4 MPa, C2=B=0.1 MPa were used. The mechanical and geometric properties of the rubber used are as follows;

- Mooney Rivlin Law
- Multiple type material
- Rolling Direction = X direction
- Density; 1.24E-6
- C1=A=0,0004 GPa
- C2=B=0,0001 GPa
- Thickness = 40 mm

4.3.3 Defining Possible Geometries Based On Simulation Results

Finite element modeling analyzes are processes that take a long time and require computers with high processing power. In line with elastic analysis, studies have been carried out on the geometries with the least deflection. During the elastic analysis phase, Design 2.1 was designed without sharp corners and draft angles. This design has been optimized in terms of draft angles and radius through preliminary plastic analysis [Table 4.5] [Figure 4.21]. When choosing the most accurate geometry, not only deflection but also manufacturability was taken into consideration. The design criteria are depicted with the pictures and table below;

Table 4.4 Numbers of geometric features

Geometric Features	
Picture Number	Geometric Features
1	Geometry
2	Depth
3	Draft Angle 1
4	Draft Angle 2
5	Inner Radius
6	Full Inner Radius
7	Corner Radius
8	Upper Radius
9	Bottom Radius
10	X Number of Patterns (Top-Bottom)
11	Y Number of Patterns (Top-Bottom)
12	Draw-Bead

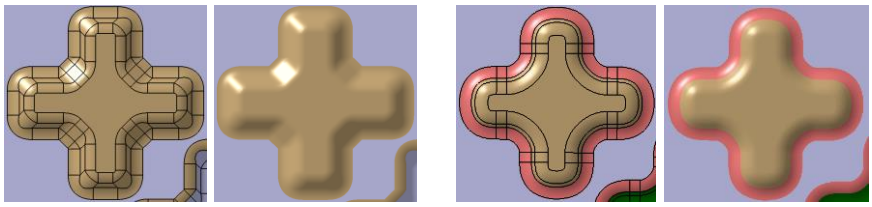

1- Figure

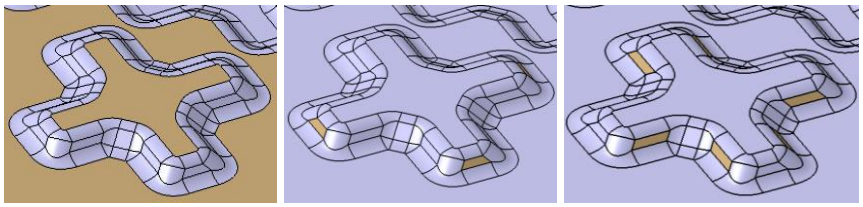

2 – Depth 3 - Draft Angle 1 4 - Draft Angle 2

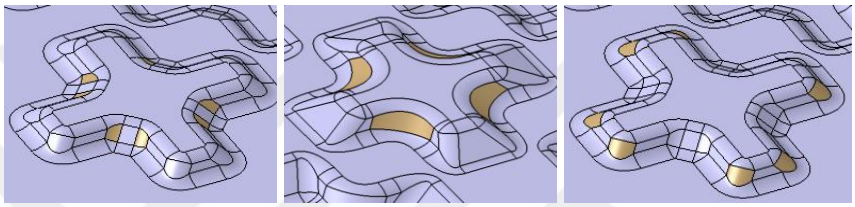

5 – Inner Radius 6 - Full Inner Radius 7 – Corner Radius

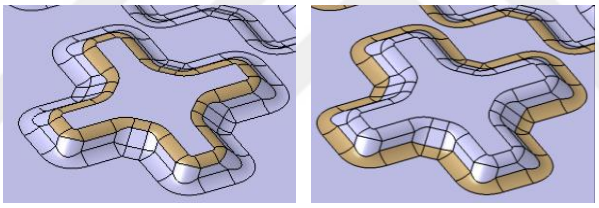

8 – Upper Radius 9–Bottom Radius

Figure 4.21 Design locations

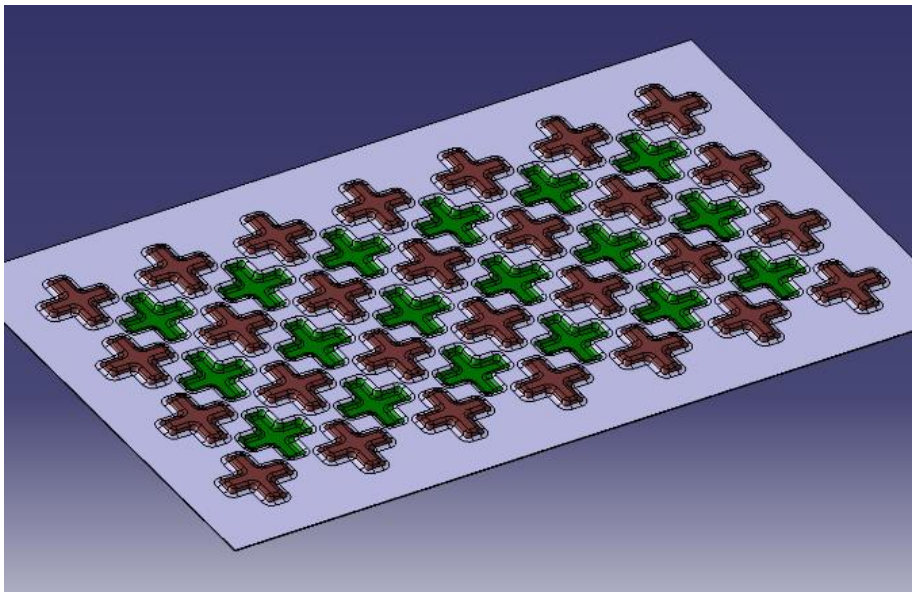

10-11- X-Y Number of Patterns

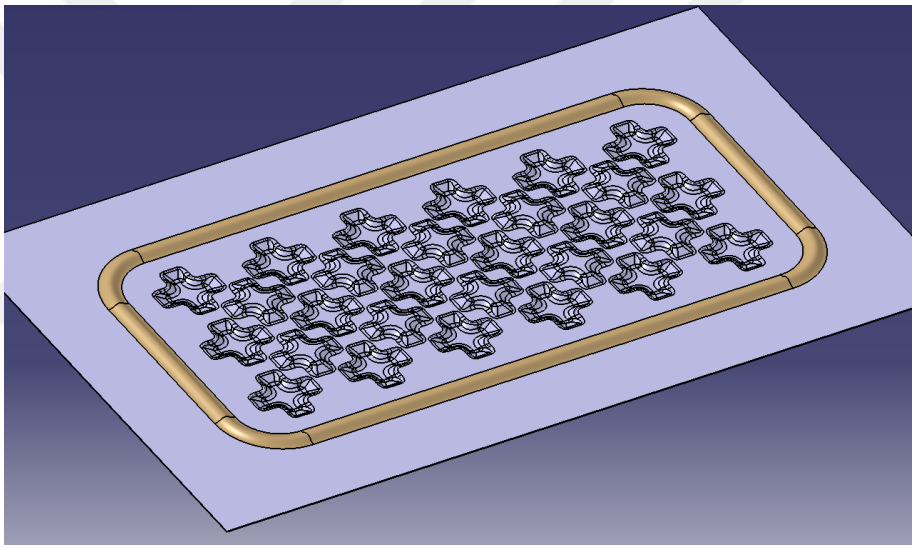

12 - Draw-Bead

Figure 4.22 Design Locations

The results and geometric properties of all analyzes are as in the table below (Table 4.5). The analysis that gave the best results was determined as Designs 19, 22, 23 and 24.

Table 4.5 The simulation result to select best geometry

	Geometric Features												Plastic Simulation			
	1	2		3	4	5	6	7	8	9	10	11	12	13	14	15
Design Number	Geometry Name	Depth (mm)	DrawBead Depth	Draft Angle 1	Draft Angle 2	Inner Radius (mm)	Inner Full Radius (mm)	Corner Radius (mm)	Upper Radius (mm)	Bottom Radius (mm)	X Number of Patterns (Top-Bottom)	Y Number of Patterns (Top-Bottom)	Minimum Thickness (mm)	Mold Closing Gap (mm)	Thickness After springback (mm)	Springback (mm)
1. Design	With Corner	2,0	2,0	70°	60°	5	-	5	Chordal (2,5)	4,6	7-6	4-3	0,562	0,137	0,557	15,208
2. Design	Corner-Drawbead	2,0	2,0	70°	60°	5	-	5	Chordal (2,5)	4,6	5-6	2-3	0,560	0,14	0,557	9,63
3. Design	Spline	2,0	2,0	65°	-	Spline	-	Spline	5	4,6	7-6	4-3	0,56	0,13	0,559	19,074
4. Design	With Corner	2,0	2,0	70°	-	5	-	5	Chordal (3)	4,6	7-6	4-3	0,567	0,075	0,566	13,384
5. Design	With Corner	2,0	2,0	70°	-	10	-	10	11,5	6	7-6	4-3	0,569	0,044	0,568	14,055
6. Design	With Corner	2,5	2,5	70°	60°	5	-	5	Chordal (2,5)	4,6	7-6	4-3	0,557	0,149	0,554	14,507
8. Design	Spline	2,7	2,7	50°	-	Spline	-	Spline	5	4,6	7-6	4-3	0,54	0,333	0,54	15,85
10. Design	With Corner	3,0	3,0	50°	-	5	5	5	4	4,6	7-6	4-3	0,531	0,518	0,53	14,356
11. Design	With Corner	3,0	3,0	50°	-	5	-	5	4	4,6	7-6	4-3	0,531	0,444	0,531	14,405
12. Design	Spline	3,0	3,0	50°	-	Spline	-	Spline	5	4,6	7-6	4-3	0,532	0,394	0,531	15,089
13. Design	With Corner	3,0	3,0	50°	-	5	-	5	Chordal (4)	4,6	7-6	4-3	0,534	0,359	0,534	14,814
14. Design	With Corner	3,0	3,0	55°	-	5	-	5	Chordal (4)	4,6	7-6	4-3	0,535	0,262	0,535	15,468
15. Design	With Corner	3,0	3,0	58°	-	5	-	5	Chordal (4)	4,6	7-6	4-3	0,536	0,212	0,536	15,752
16. Design	With Corner	3,0	3,0	70°	50°	5	-	5	Chordal (3)	4,6	7-6	4-3	0,535	0,237	0,531	15,555
17. Design	With Corner	3,0	3,0	70°	50°	8	-	5	Chordal (3)	4,6	7-6	4-3	0,537	0,231	0,539	15,615
18. Design	With Corner	3,0	3,0	70°	50°	8	-	5	Chordal (3)	5,5	7-6	4-3	0,542	0,227	0,541	15,84
19. Design	With Corner	3,0	3,0	70°	55°		13	5	Chordal (3)	5,5	7-6	4-3	0,553	0,167	0,553	17,638
20. Design	Corner-Drawbead	3,0	3,0	70°	50°	8	-	5	Chordal (3)	5,5	5-6	2-3	0,538	0,226	0,538	17,515
21. Design	Corner-Drawbead	3,0	3,0	70°	50°	9	-	5	Chordal (3)	6	5-6	2-3	0,541	0,223	0,539	16,96
22. Design	Corner-Drawbead	3,0	3,0	70°	55°	-	13	5	Chordal (3)	5,5	5-6	2-3	0,549	0,172	0,55	15,314
23. Design	Drawbead-Cage	3,0	3,0										0,557	0,232	0,557	24,857
24. Design	Drawbead-Frame	3,0	3,0										0,538	0,088	0,532	20,213

4.3.4 Evaluation of Results

At the beginning of the project, constraints such as thinning and springback deflection were determined as the objectives of the study. The maximum acceptable thinning was decided to be 10% (up to 0.54 mm). In addition, minimum springback and maximum rigidity are expected.

The rigidity ratio of the material is directly related to the depth of the forming pattern. Since the degree of second moment of inertia increases in proportion to the square of the depth, the main goal in these designs is to increase the rigidity of the material by increasing the depth to maximum levels. Therefore, even though designs with a depth of 2.0 mm give the least thinning and the best mold closing values, designs with a depth of 3.00 mm will show better rigid behavior.

These are designs where at least springback level drawbead is applied after being shaped according to the analysis results. By comparing the elastic behavior of the shaped material with a load applied from the midpoint, it will be decided which mold to manufacture.

A total of 24 designs were analyzed and some results were obtained in these analyses (Table 4.5). The most important factors affecting thinning, which is one of our limitations, have been determined.

2- Depth; It is the parameter that has the most impact on thinning. This is an expected result, as stretching increases as depth increases.

3-4- Draft Angle; It has very important effects not only on thinning but also on formability. Even if the thinning is at sufficient levels, when the press pressure is increased, the mold closing will decrease and the thinning will increase as it approaches 0. Therefore, draft angle has a direct effect on both thinning and mold closing.

5-6 Inner Radius; It has a significant effect on thinning as it looks like a protrusion when shaping in the negative direction. Small radii have a negative effect as depth increases. Because these regions behave close to sharp corners. Inner Radius is directly

related to draft angle-depth. Inappropriate draft angle and depth can directly negatively increase the effect of the inner radius on thinning.

7- Corner Radius; It is directly effective in thinning. Sharp corners have a negative effect on thinning. Therefore, the highest radii should be given to optimize these areas. Thus, thinning can be optimized by softening sharp corners.

8- Upper Radius; It is effective in mold closing and thinning. Sharp corners should be softened whenever possible.

9- Bottom Radius; In the 17th and 18th Designs, only the bottom Radius was increased from 4.6 mm to 5.5 mm in order to enter the thinning limits. It slightly reduced the stretching effect and gave a positive result.

10-11-X-Y Number of patterns; The distance between the forming geometries is very critical. In order to increase the rigidity of the material, it is necessary to place as many forming patterns as possible on the sheet metal. Therefore, the distance between two forming patterns should be at minimum levels. However, the two patterns should not affect each other during shaping. In design numbers 7 and 9, the distance of the patterns on the X and Y axes has been increased. According to the analysis results (Figure 4.23, the space between the two patterns was determined as 19.5 mm on the X axis and 10 mm on the Y axis, and Radius and depth optimizations were made by keeping these distances constant.

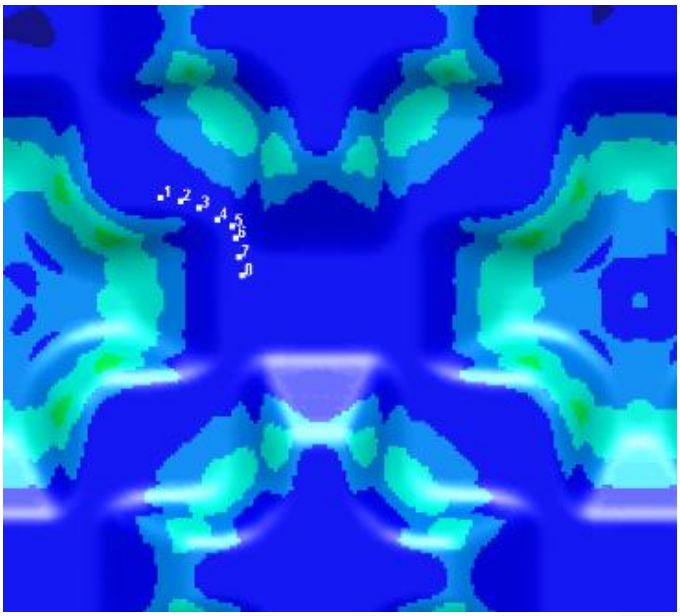

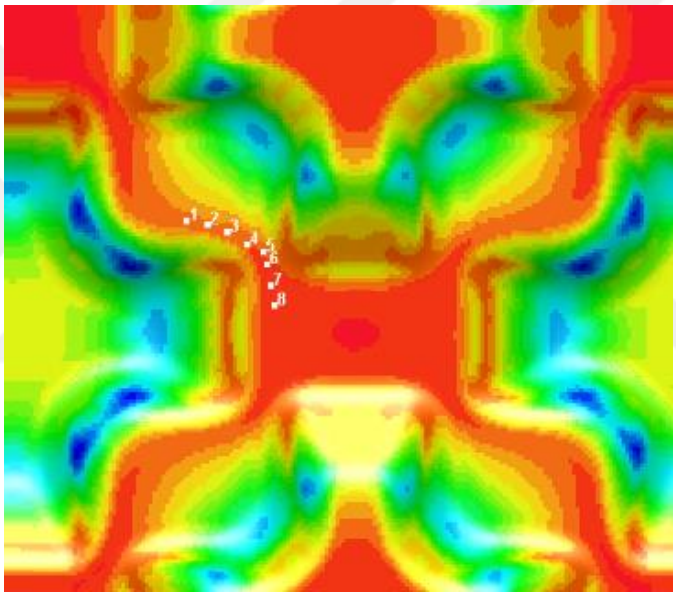

Location	Thickness	Thinning
1	0.593641	0.0105987
2	0.593704	0.0104932
3	0.594302	0.00949663
4	0.595475	0.00754166
5	0.595596	0.00734079
6	0.597341	0.00443208
7	0.598003	0.00332785
8	0.598187	0.00302154

Figure 4.23 Thickness distribution in between two forming pattern

12-The drawbead design has been shown to be very effective in reducing springback and distortion. However, the use of drawbead throughout the design increases springback and distortion. A drawbead design that surrounds the applied forming geometry has been found to be most suitable. As long as the design is created by defining a certain space in the shaping patterns, it does not have a big effect on thinning. In drawbead designs that surround the geometry, the radius of the X and the region should be given appropriately. 20.design due to the Radius size in the design, the pattern shown in the picture has more thinning than other patterns.

Therefore, by reducing the radius, the measurement between the pattern and the drawbead was increased and some improvement was achieved.

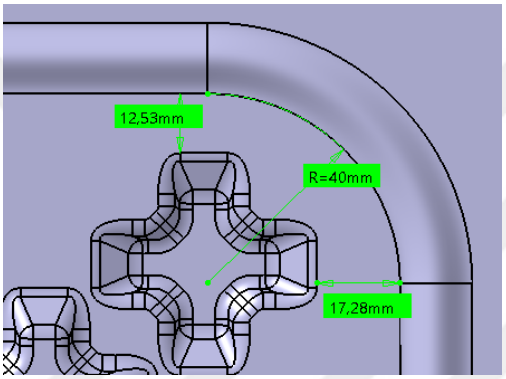

Figure 4.24 20. Design

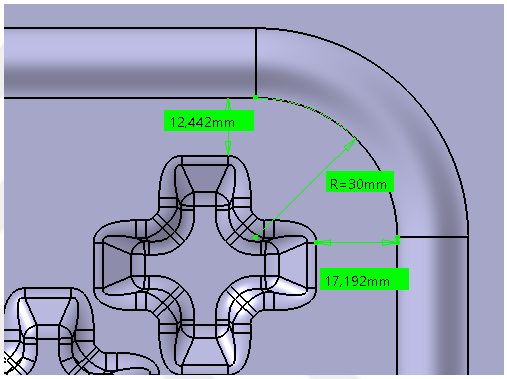

Figure 4.25 21. Design

According to these results, designs 19, 22, 23 and 24 will be put into elastic analysis. According to the elastic analysis results, the design that gives minimum deflection will be selected as the most optimum design.

Although the thinning and shaping parameters of the two designs are the same, the springback of design 22 is less. Which mold will be produced will be decided with the data obtained from elastic analysis. However, since the most successful design according to current conditions is the 22nd design, the simulation results of design 22 will be examined in detail in this section.

The thickness distribution is suitable for design restrictions. Minimum thickness should be 0.54mm. In design 22, minimum thickness is 0.549 (Figure 4.26).

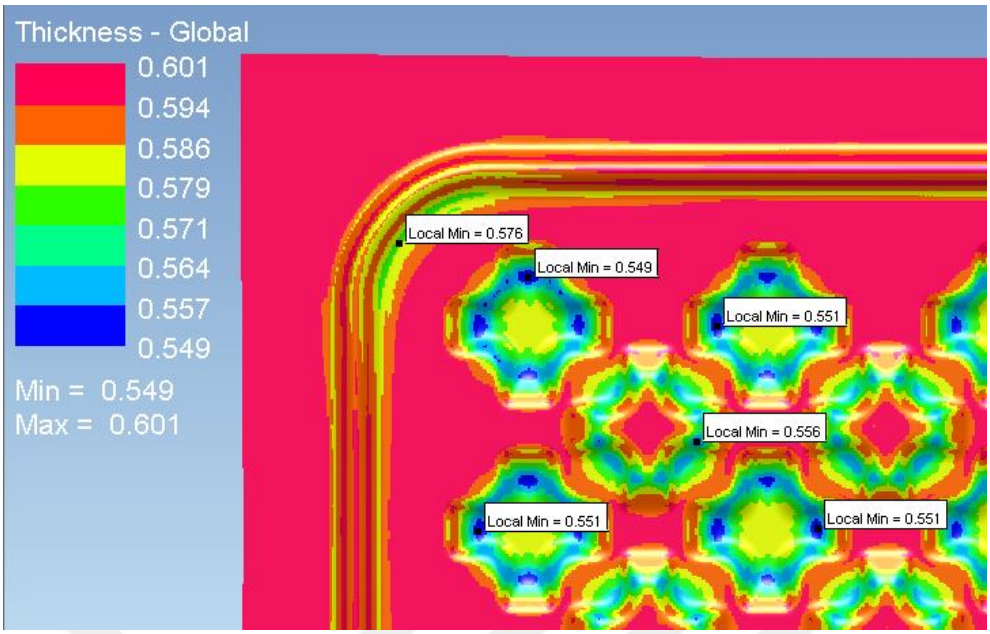

Figure 4.26 Local minimum thickness

The major strains on the geometry are as shown in the picture below.

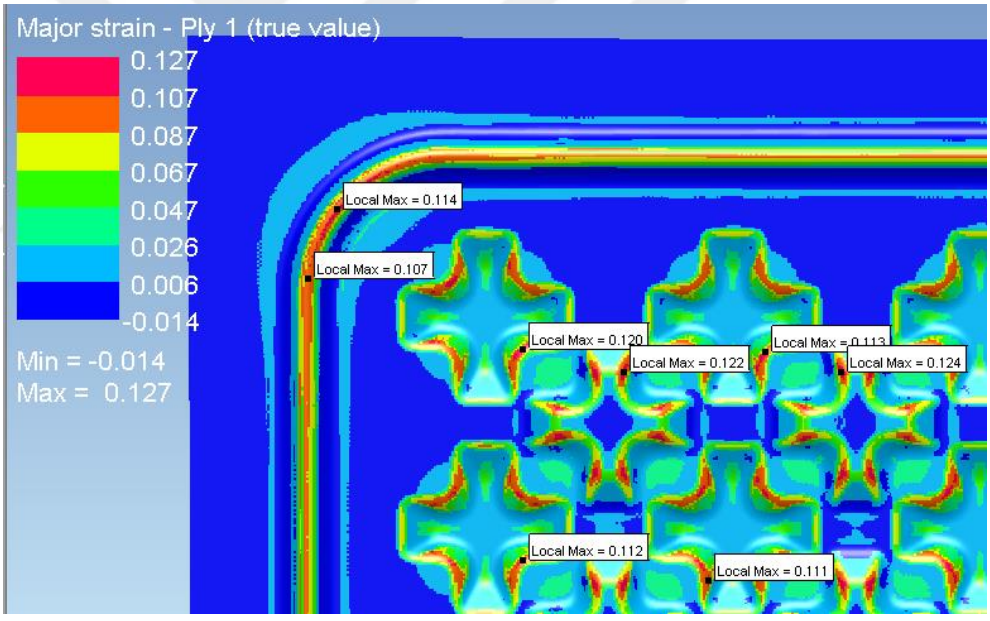

Figure 4.27 Local maximum strain values

Forming Limiting Diagram depicts the formability of the material. When we examine the FLD graph of the geometry we shaped, we see that there are no problems such as cracking, breaking or excessive thinning. There is no risk in shaping since it remains below the range of approximately 0.25-0.26, which is considered the safe zone (Figure 4.28).

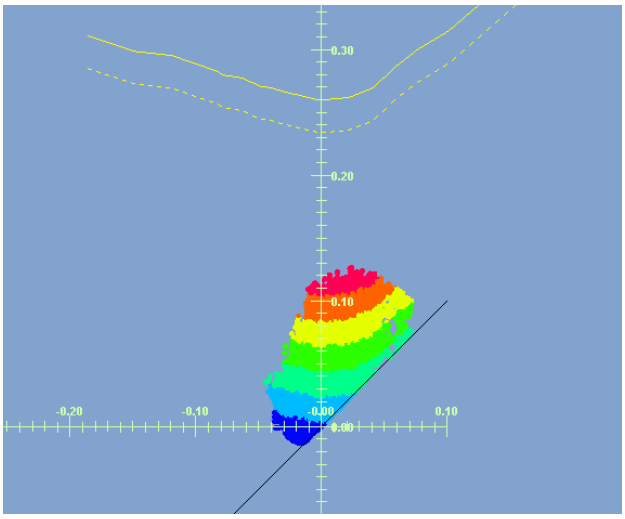

Figure 4.28 FLD graph of design

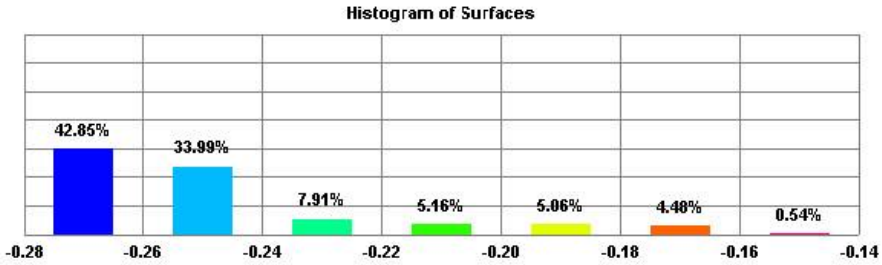

Figure 4.29 The histogram of surfaces

The highest strain regions are seen in the inner corners in the negative direction.

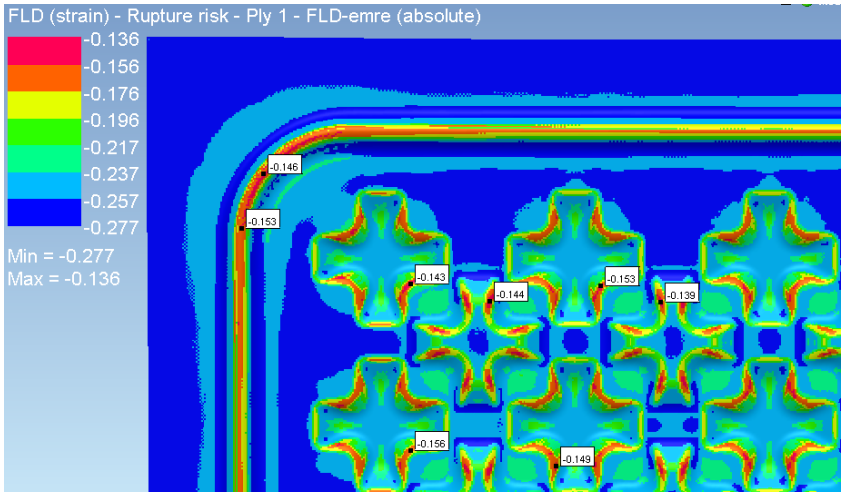

Figure 4.30 The strain values of design

In the FLD by quality chart, we examined wrinkling trends depending on strain regions. Strong wrinkling trend zones were detected in the corners and bottom areas of the pattern. The strain occurring in these regions affects the springback. It is within acceptable limits (Figure 4.31).

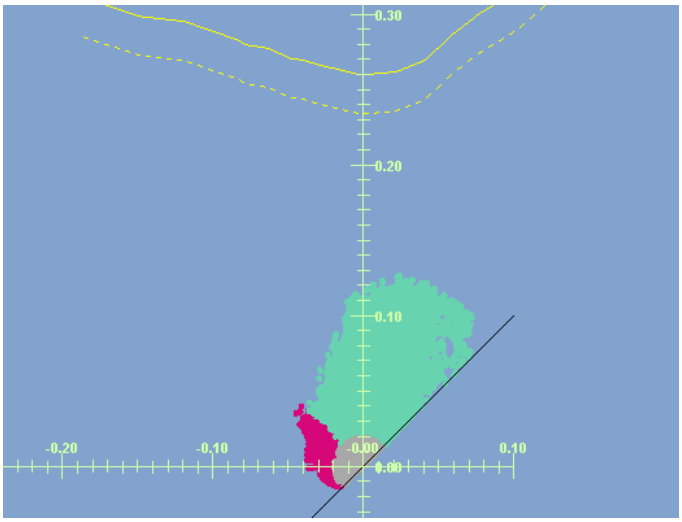

Figure 4.31 FLD graph of design

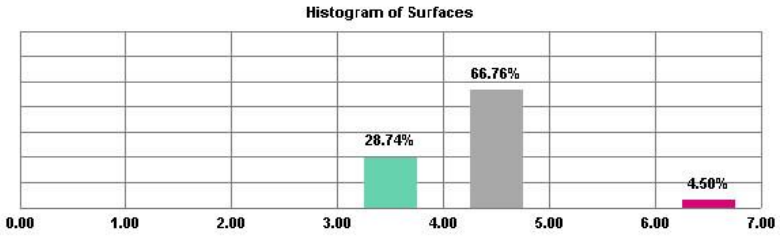

Figure 4.32 Histogram of surfaces

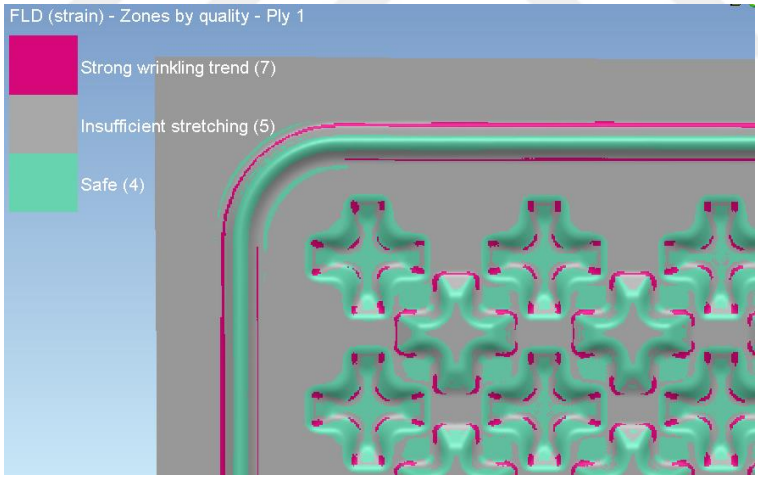

Figure 4.33 Wrinkling trend of design

It is expected that a distortion in the material will be seen when the mold is opened after shaping. It has been observed that the part has a springback, especially in unformed areas (Figure 4.34).

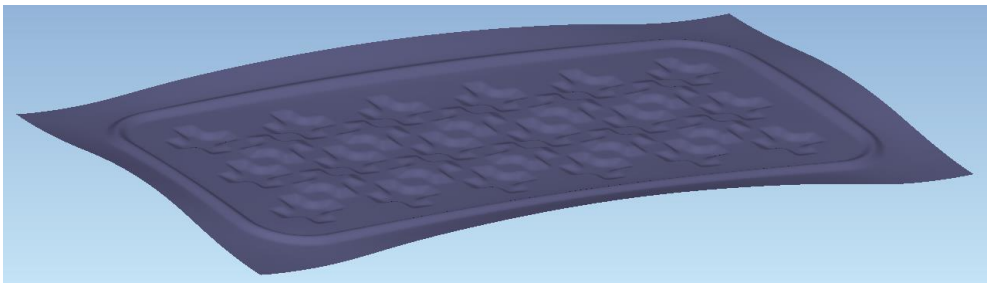

Figure 4.34 the simulation result of design 22

In the experimental phase, a maximum 15,314 mm distortion is expected on the part (Figure 4.35).

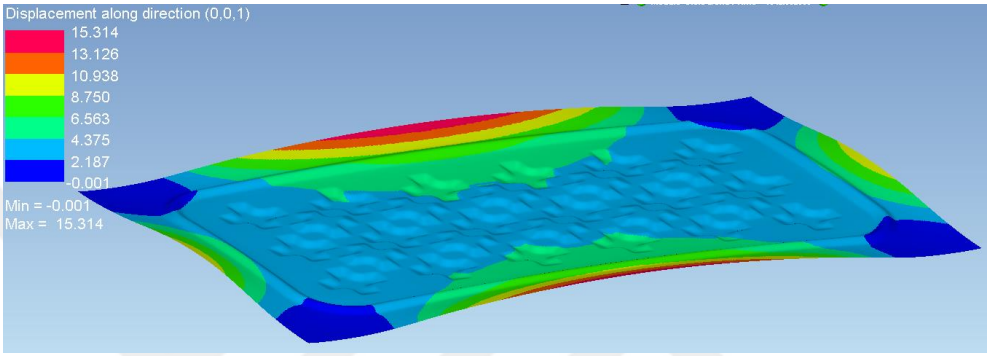

Figure 4.35 the simulation result of design 22

The last issue examined is the distance between the mold and the sheet material in the final stage of forming. As can be seen, although the corner areas are softened, there is an unshaped area of 0.172 mm between the negative forming pattern and the mold.

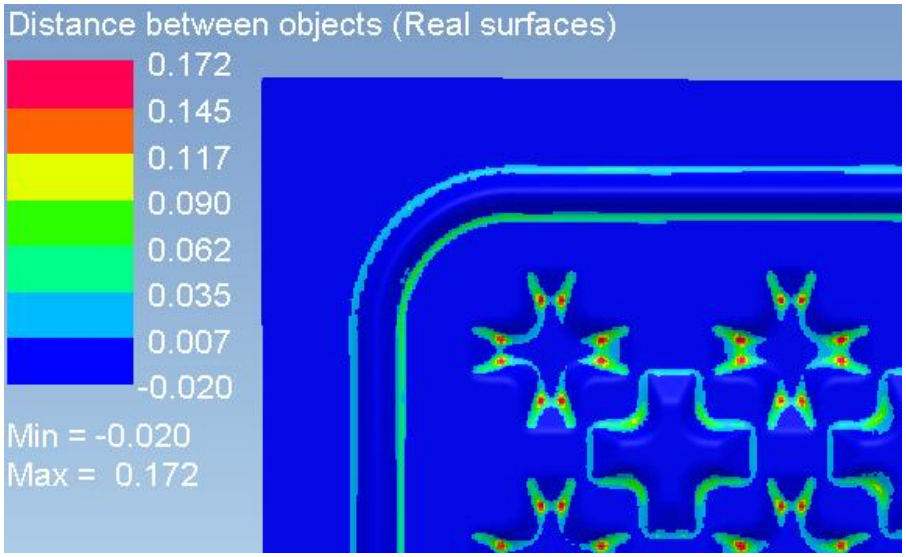

Figure 4.36 The distance in between design 22 and die

4.4 Second Stage Elastic Simulations

As a result of the plastic analysis, four designs were decided. As a result of the analysis, each geometry exhibited a different distortion behavior. Therefore, while making the comparison, the distorted version of each geometry and its elastic behavior after applying a 5N load from the midpoint were examined. These elastic simulations are carried out in PAM-STAMP.

The establishment and physics of the system are as follows.

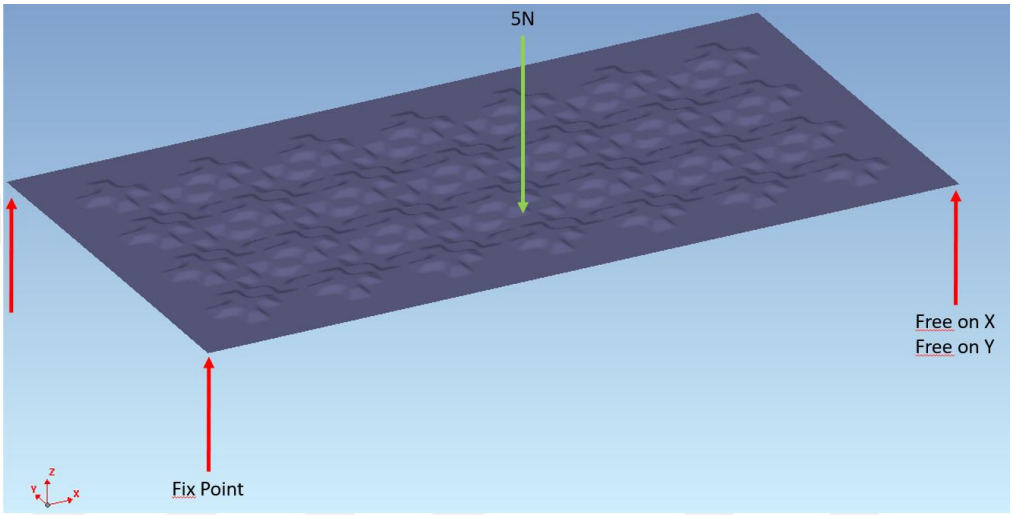

Figure 4.37 An overview of elastic deformation simulation and test rig

The simulation is setup as supporting 4 point (Figure 4.37). In experimental stage, the same conditions will be applied to produced part.

According to the simulation result, the deflection of the unformed sheet metal part was found as 14.273 mm (Figure 4.38).

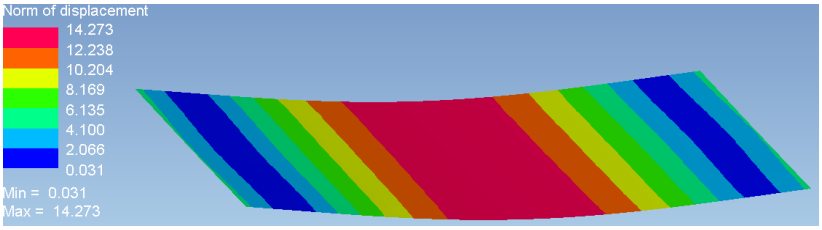

Figure 4.38 The unformed part deflection under 5N

22nd design, maximum deflection was observed as 1,645 mm in the middle region. Keeping the shaping pattern, the same, one row from the corners was canceled and replaced with a drawbead design. The deflection and springback results according to the drawbead design result are as follows.

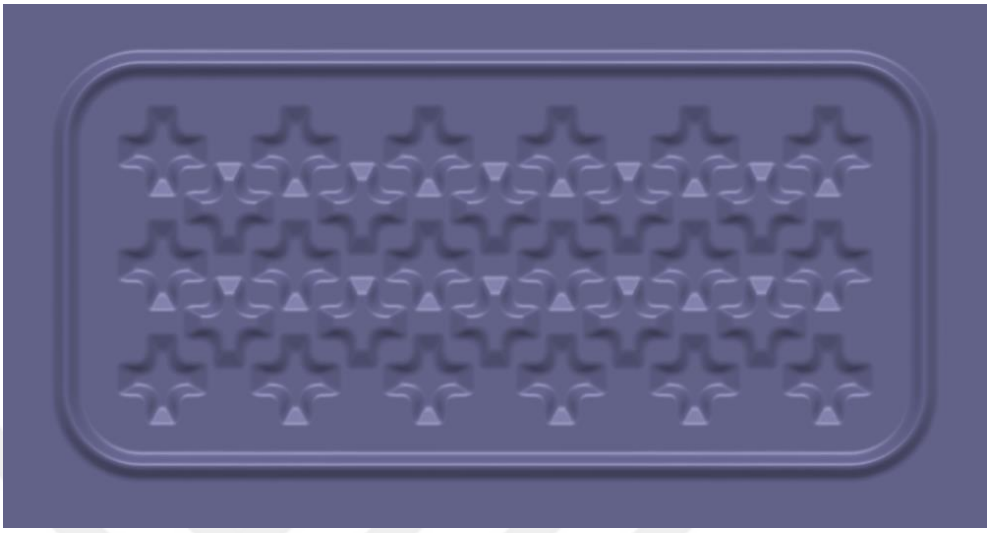

Figure 4.39 22nd Design

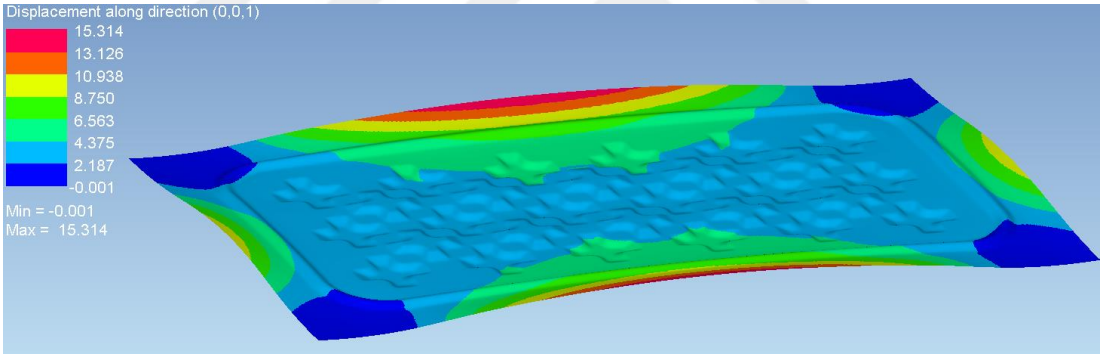

Figure 4.40 22nd Design springback

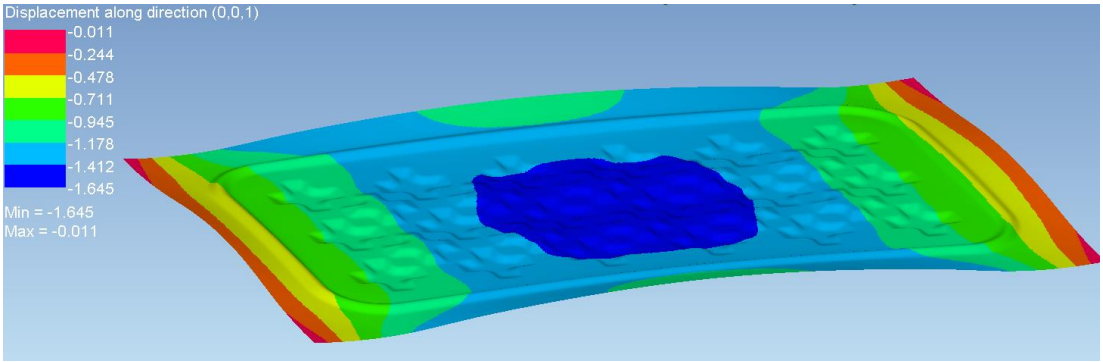

Figure 4.41 The deflection of 22nd design under 5N load

19. Design, the maximum deflection was observed in the middle region as 5,043 mm. Results are as follows.

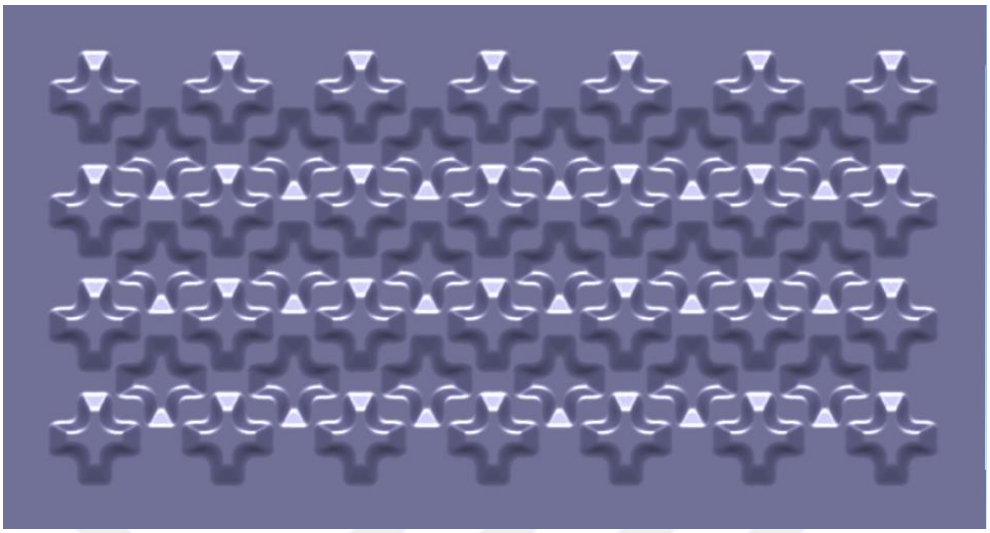

Figure 4.42 19nd Design

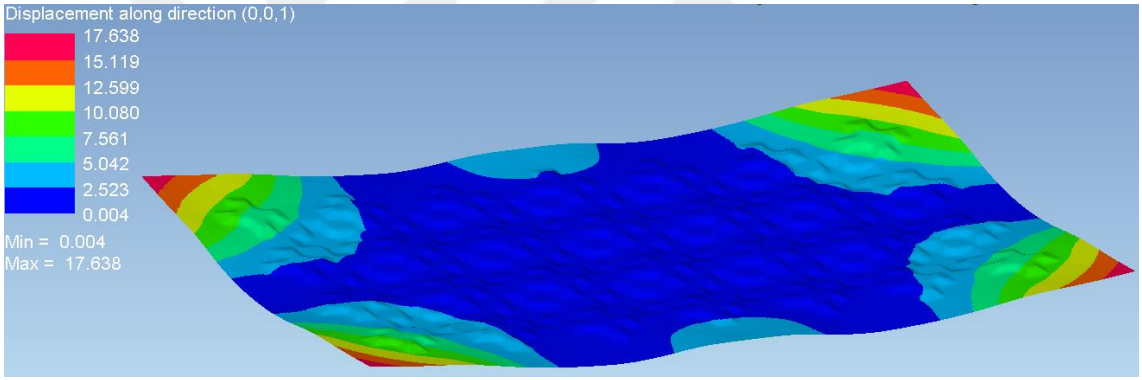

Figure 4.43 19nd Design springback

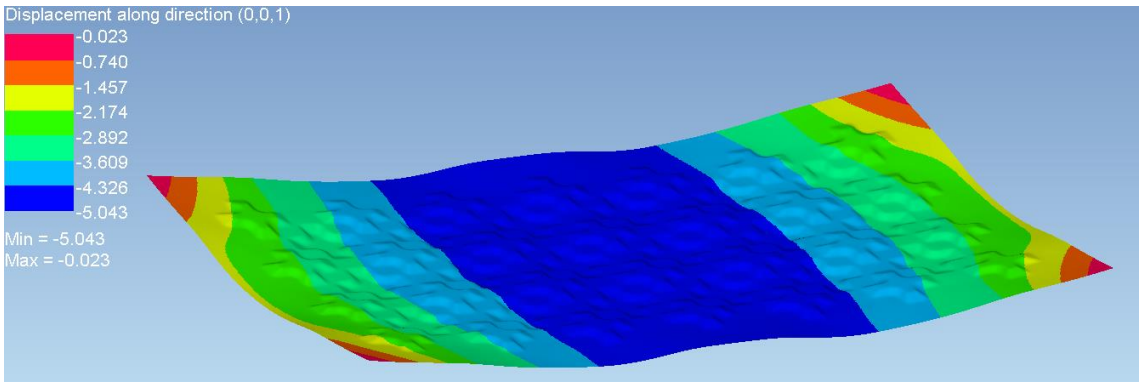

Figure 4.44 19nd Design Deflection under 5N Load

23. Design the draw bead design has been shown to be beneficial. Therefore, the full drawbead pattern was applied in the form of a cage and the result was examined elastically.

The maximum deflection was observed in the middle region as 2,446 mm.

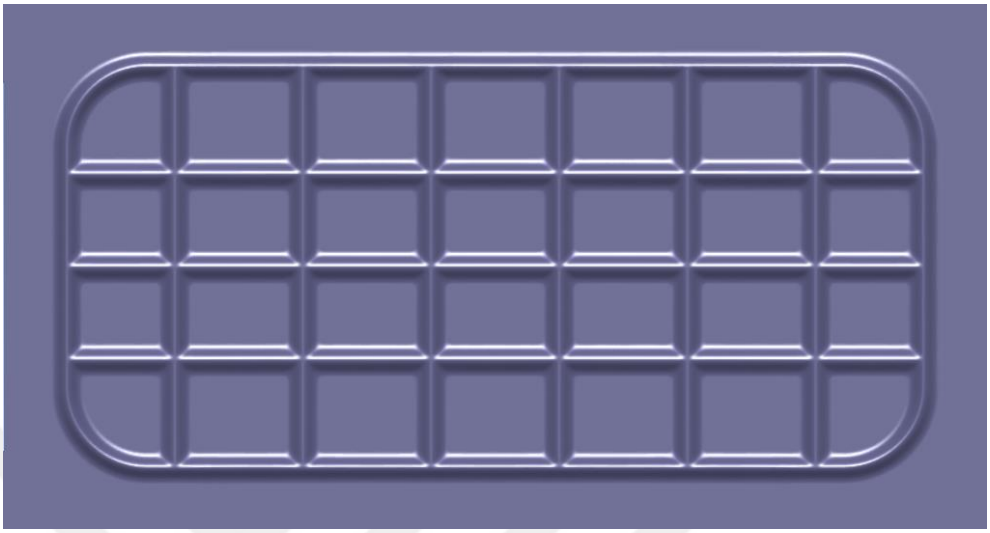

Figure 4.45 23nd Desgin

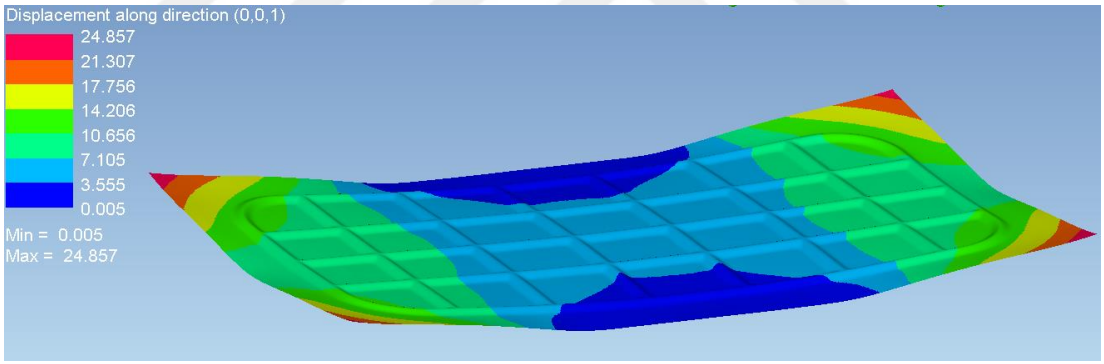

Figure 4.46 23nd Design Springback

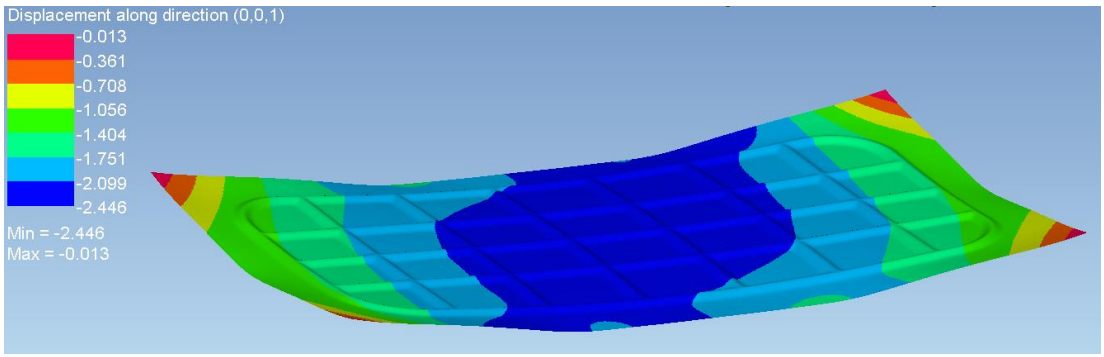

Figure 4.47 23. Design deflection under 5N load

The 24nd design was defined like a frame. The maximum deflection was observed in the middle region as 1,199 mm. Results are as follows;

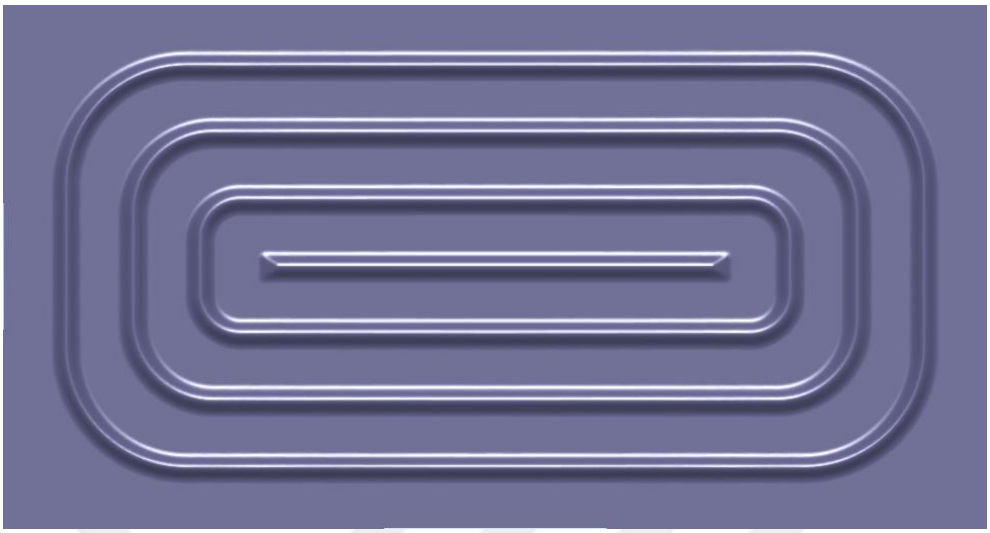

Figure 4.48 24nd design

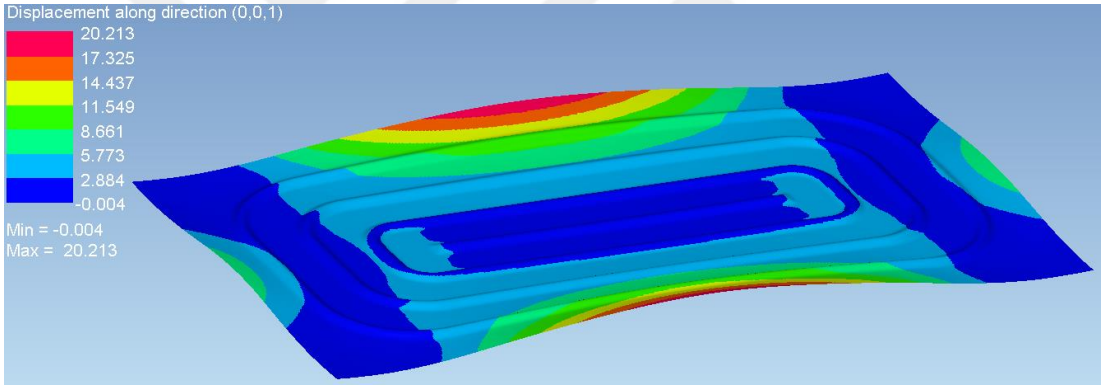

Figure 4.49 24nd Design Springback

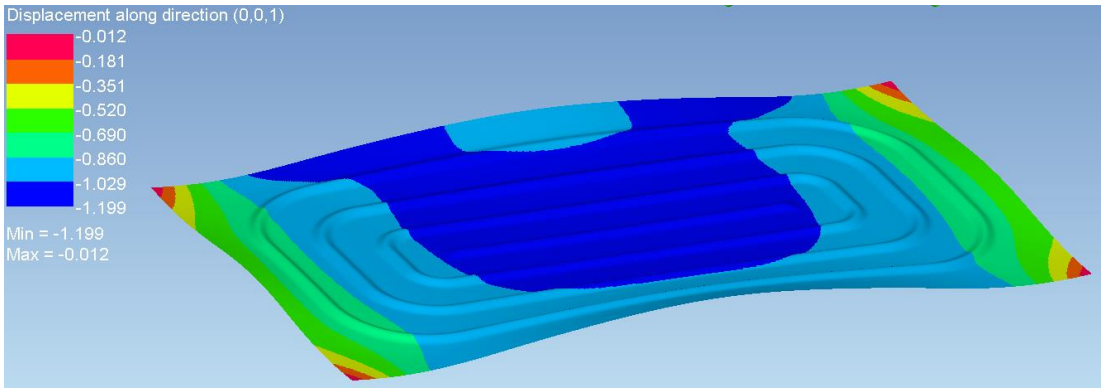

Figure 4.50 24nd Design deflection under 5N load

4.4.1 Elastic Finite Element Methods Results

As a result of all simulations, many criteria were examined. Designs 22 and 24 gave the two best results. However, since the springback values of the 24th Design were very high, it was decided to continue with the 22nd Design (Table 4.6).

Table 4.6 Thickness, gap, springback and deflection simulation result of selected design

	Geometric Features	**Simulation Results**			
	1	**12**	**13**	**14**	**15**
Design Number	Geometry	Thikness After Forming	Mold Closing Gap (mm)	Springback (mm)	Deflection (mm)
19. Design	With Corner	0,553	0,167	17,638	5,043
22. Design	With Corner-Drawbead	0,549	0,172	15,314	1,645
23. Design	Full Drawbead-Cage	0,557	0,232	24,857	2,446
24. Design	Full Drawbead-Frame	0,538	0,088	20,213	1,199

4.5 Production and Experimental Stage

4.5.1 Die Manufacturing

Molds of the decided geometry were produced using 3-axis CNC and first sandblasting and then polishing were performed as a surface improvement operation.

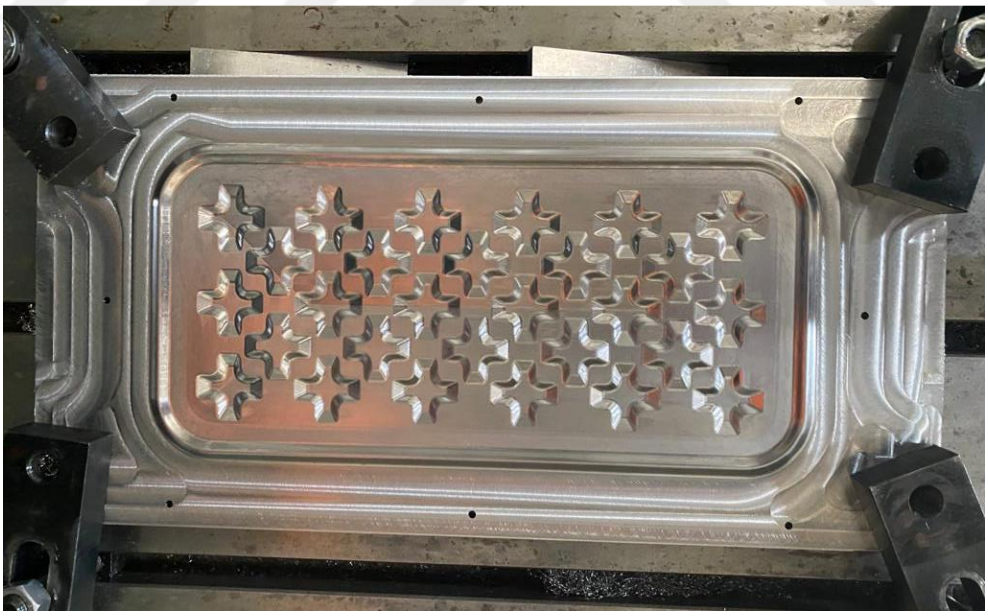

Figure 4.51 Die manufacturing

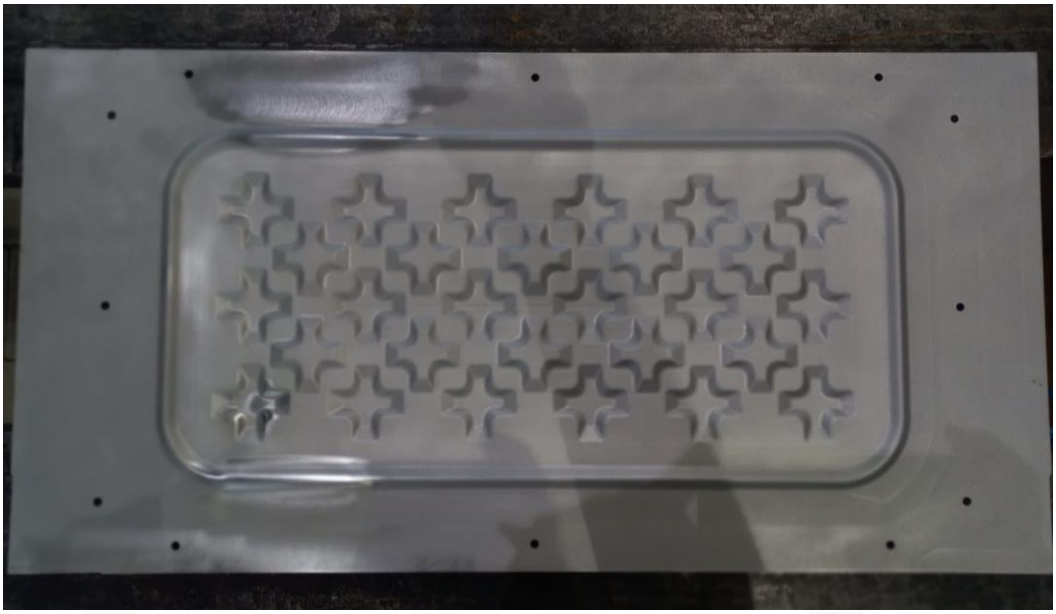

Figure 4.52 Sandblasting operation

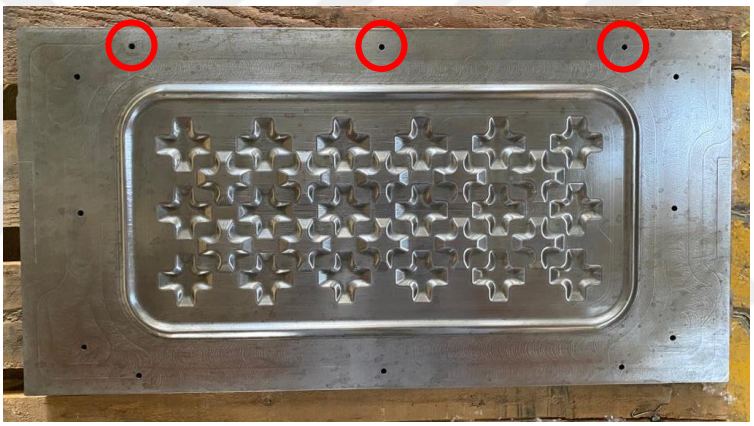

Figure 4.53 Polished die and pin locations

Three pin holes are placed on each edge of the mold to prevent the cut sheet metal part from moving during shaping (Figure 4.53). By inserting pins into these holes, it will prevent the part from slipping during shaping.

4.5.2 Sheet forming Stage

Before the sheet forming stage, the mold manufacturing process was completed and the sheets were cut to appropriate sizes using guillotine shears. Subsequently, tests were carried out at TAI, which provided equipment and experimental equipment support for this thesis.

In the hydroforming device with a pressure capacity of 1200 bar, the 800 bar pressure reported to us as safe limits are set on the device screen (Figure 4.54).

Figure 4.54 The flex-forming machine screen

Then, pins were placed in the mold, which was processed and finalized at Atilim University Metal Forming Center of Excellence. Then the mold was lubricated with machine oil.

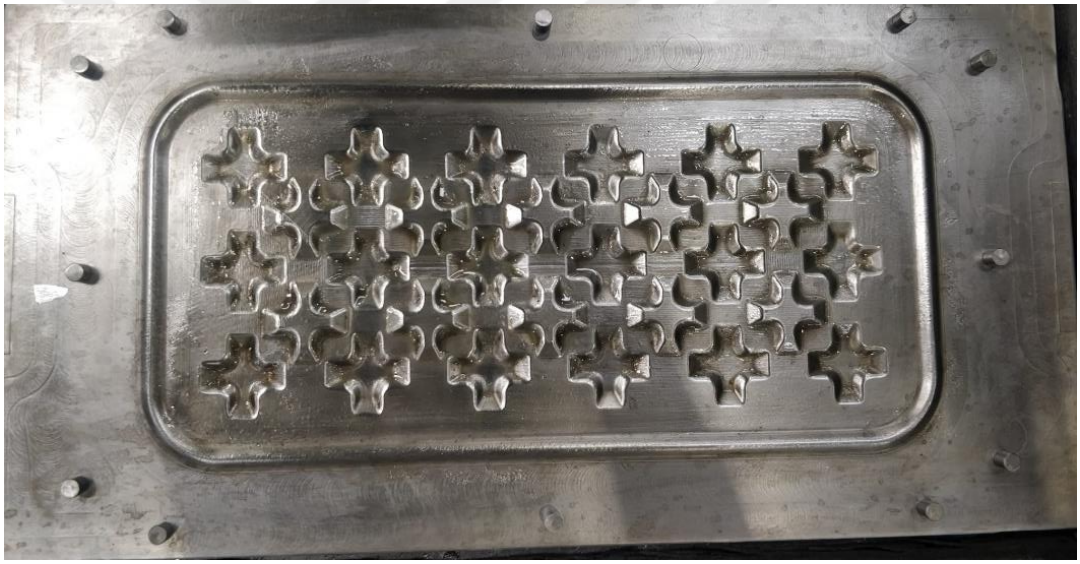

Figure 4.55 Lubricated die

Sheet metal parts cut using guillotine shears were placed in the mold, which was lubricated and all operations were completed. Thanks to the pins, the sheet metal part will not be able to change its location during forming (Figure 4.56).

Figure 4.56 placing the part in the mold

Pressure-Holding pressure parameters were adjusted, and after the mold was lubricated with machine oil, the hydroforming machine was started and the shaping process was carried out.

Figure 4.57 Deformed sheet

The holding pressure is automatically defined in the simulation. According to the results, a minimum holding pressure of 50 ms will be sufficient. A holding pressure set above 50 ms has no significant effect on shaping. In the experimental stage, the holding pressure was adjusted for 3 seconds and shaping took place. Experiments were

conducted on 2 different devices under the same conditions. Visually, the forming results were the same for both hydroforming devices.

Compared to the simulation results, the part was not fully formed. The sheet metal part could not fully take the shape of the mold. The reasons for this will be examined in the evaluation section.

Figure 4.58 Deformed sheet-shaping patterns

4.5.3 Measurement Stage

The measurement stages for the parts previously shaped in the TAI production area were carried out in the Atilim University Manufacturing Engineering Laboratory.

When the shaped piece was examined for elastic measurements, it was decided that a reliable measurement could not be taken due to springback. When the simulation and shaped parts were examined, it was understood that the distortion was not in the shaped area, but outside the shaped area. Since one of the aims of the project was to achieve minimum springback, it was decided to cut the unformed areas. Taking the Drawbead design as a reference, the part was trimmed by drawing a 2mm offset line. This trimming operation will be done in simulation, too (Figure 4.59). The cut version of the piece, when viewed under atmospheric pressure and supported at 4 corners, is as follows (Figure 4.60).

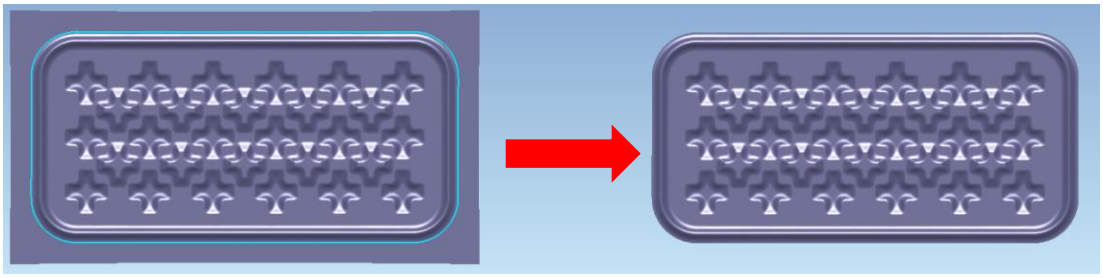

Figure 4.59 The trimming operation in simulation

Figure 4.60 Test rig

Elastic measurements will be carried out in 2 stages;

1- Elastic measurements of the deformed part
2- Elastic measurements of the unformed part

4.5.3.1 Deformed part elastic measurement

The previously designed experimental setup for elastic measurements of the shaped part was produced at MFCE.

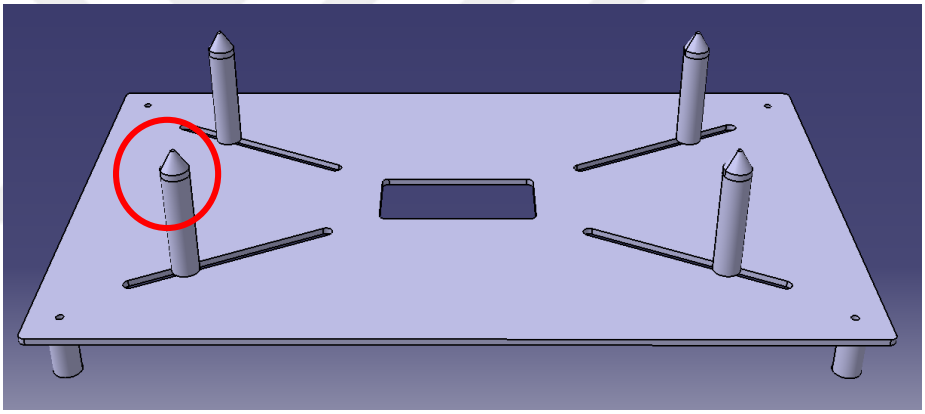

Figure 4.61 Test rig

The regions of the established experimental setup marked with red circles are designed to touch the middle of the drawbead channel (Figure 4.61). Thus, it is aimed to minimize experimental errors.

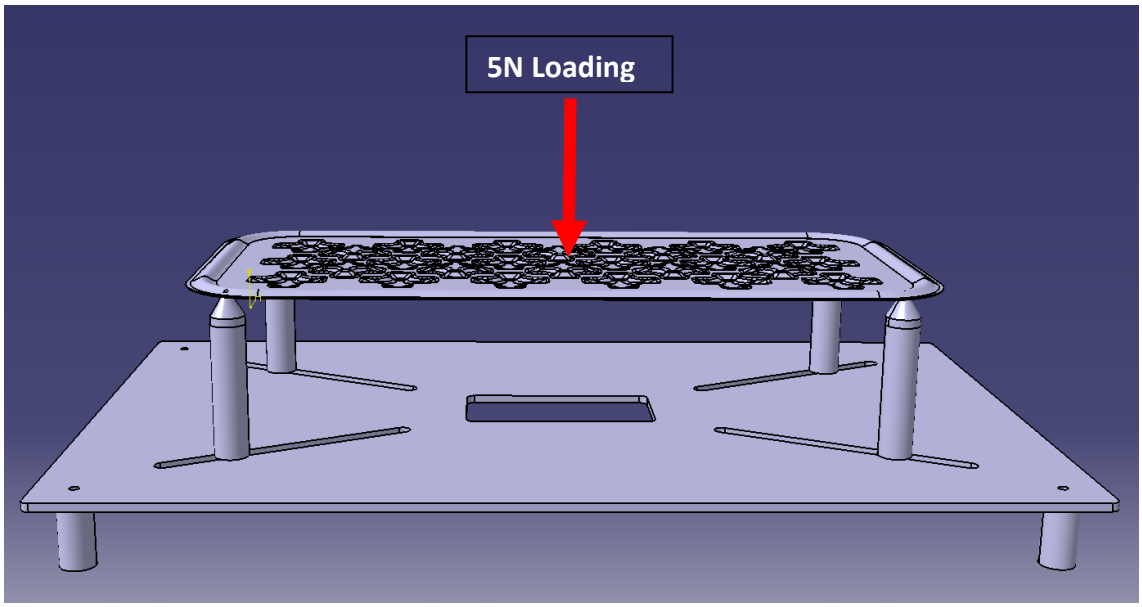

Figure 4.62 Test rig

System layout will be done as shown in figure 81. A 5N load equals approximately 500 gram-force(gf). And One newton equals about 100 g on Earth. So it is aimed to reach to nearly 500 grams. The aim was to achieve a weight of 500 grams by placing previously cut circular sheet metal pieces on top of each other. An metric 4 nut was glued to the middle point of the cut circular piece at the bottom. The purpose of this is to apply a point load as in the simulation, rather than a distributed load.

As a result of the measurement, a weight of approximately 490 grams was obtained. (Figure 4.63)

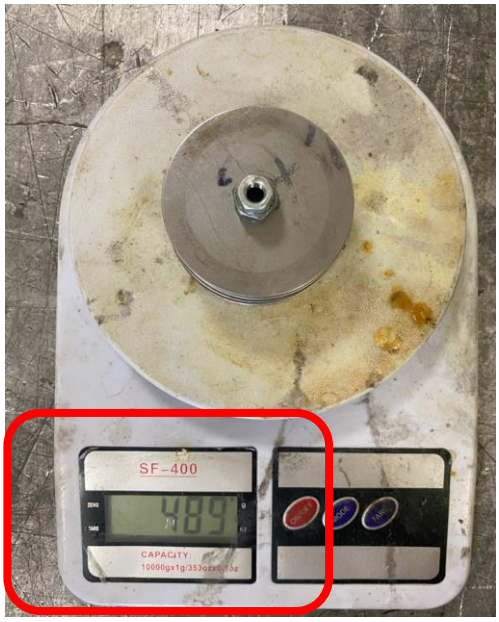

Figure 4.63 Weight measurement

Measurement points were determined in the experimental setup. The lower-middle point of the geometry was taken as the measurement point. The dial indicator is fixed to metal plates as seen in the picture. The system is placed on a flat table and the dial gage is fixed (Figure 4.64).

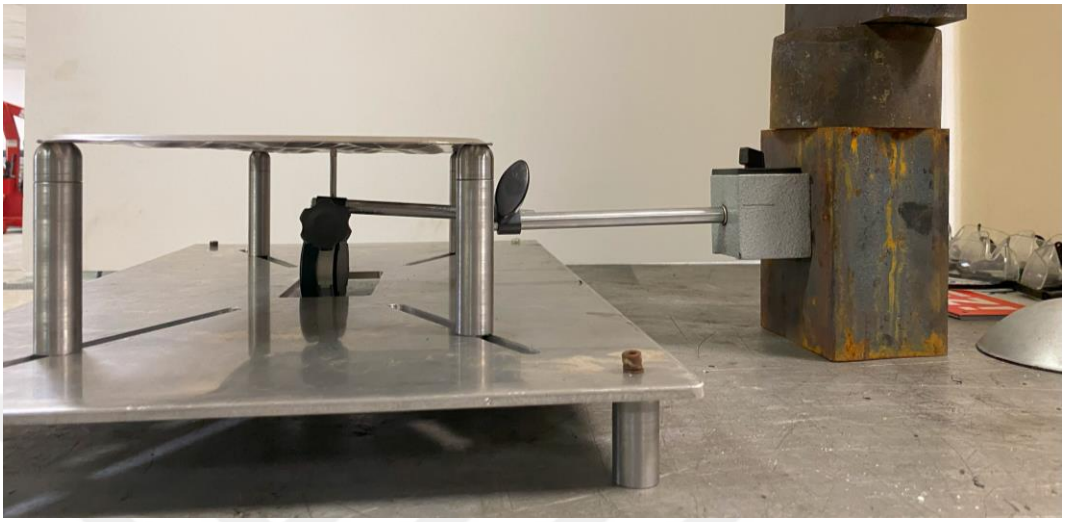

Figure 4.64 Locating the dial gage

After the system was completely ready, the dial gage was reset and the load started to be loaded.

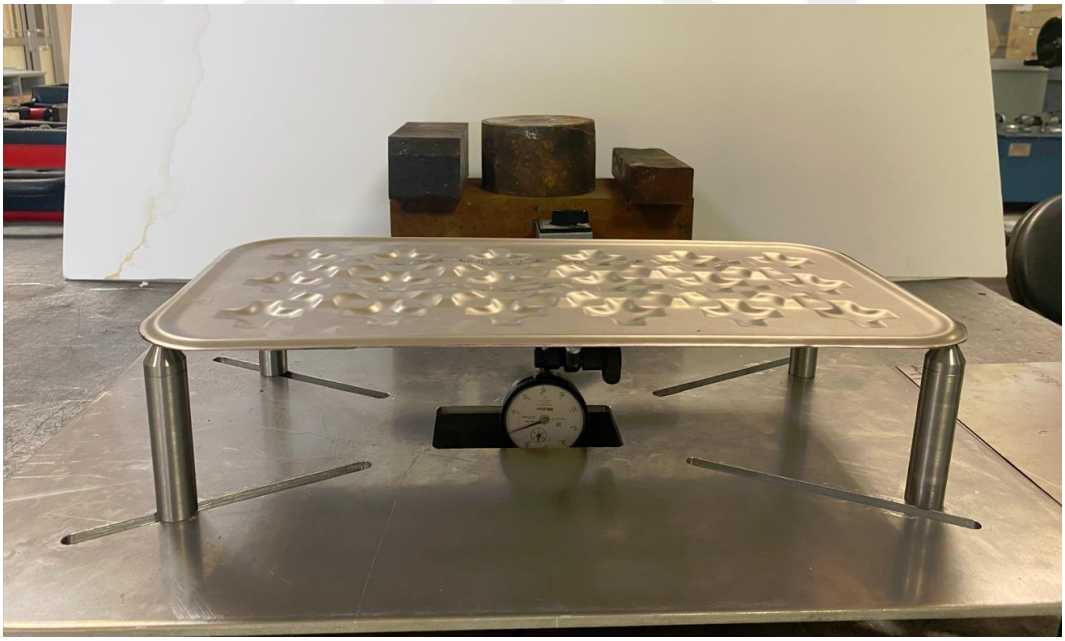

Figure 4.65 Deflection measurements

Approximately 500 grams of load was loaded from the middle point of the system (Figure 4.66). This test was performed by lifting and reloading the load for 5 repetitions.

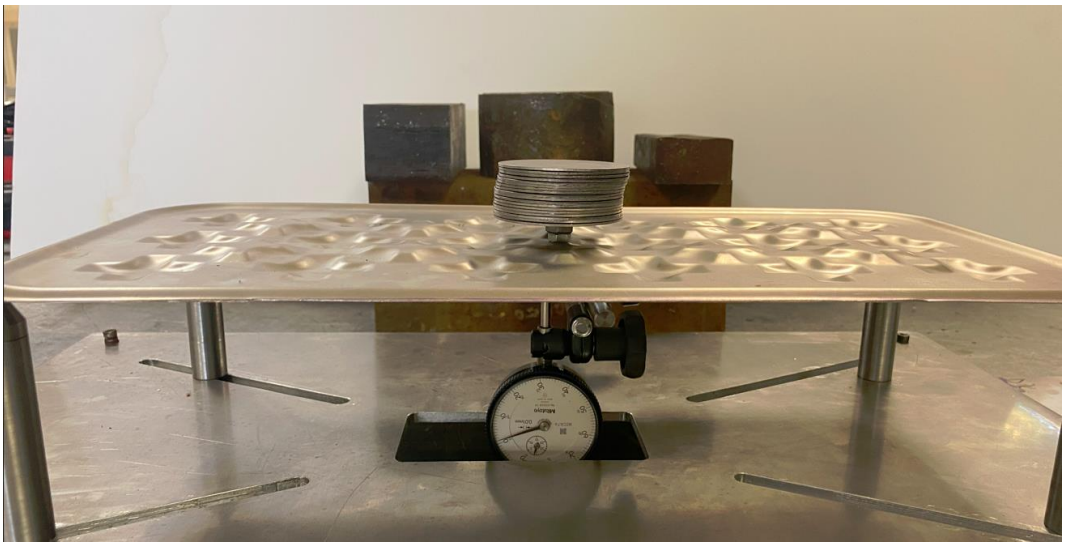

Figure 4.66 Weight Loading Step

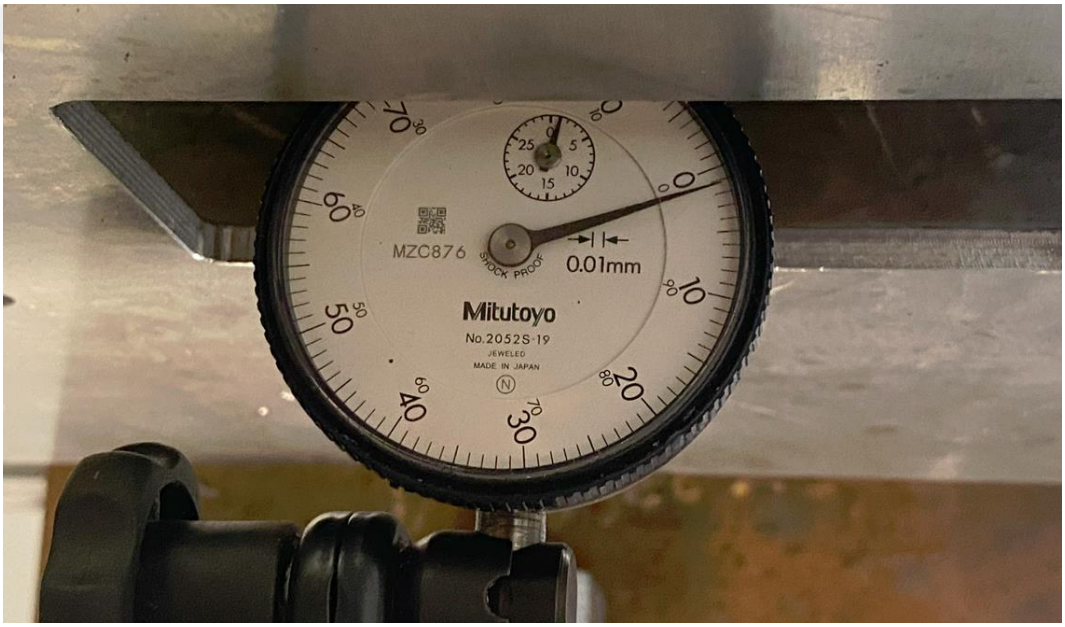

Figure 4.67 Dial Gage Result

Table 4.7 Deformed part deflection result (Experimental)

Deformed Part	
Experiment number	**Deflection (mm)**
1	1,02
2	1,05
3	1,02
4	0,99
5	1,02

4.5.3.2 Unformed part elastic measurement

As a second stage, elastic measurements of the unformed part were made. The measurement points of the shaped part were not changed in the experimental setup, and measurements were taken by touching the same points as much as possible (Figure 4.68).

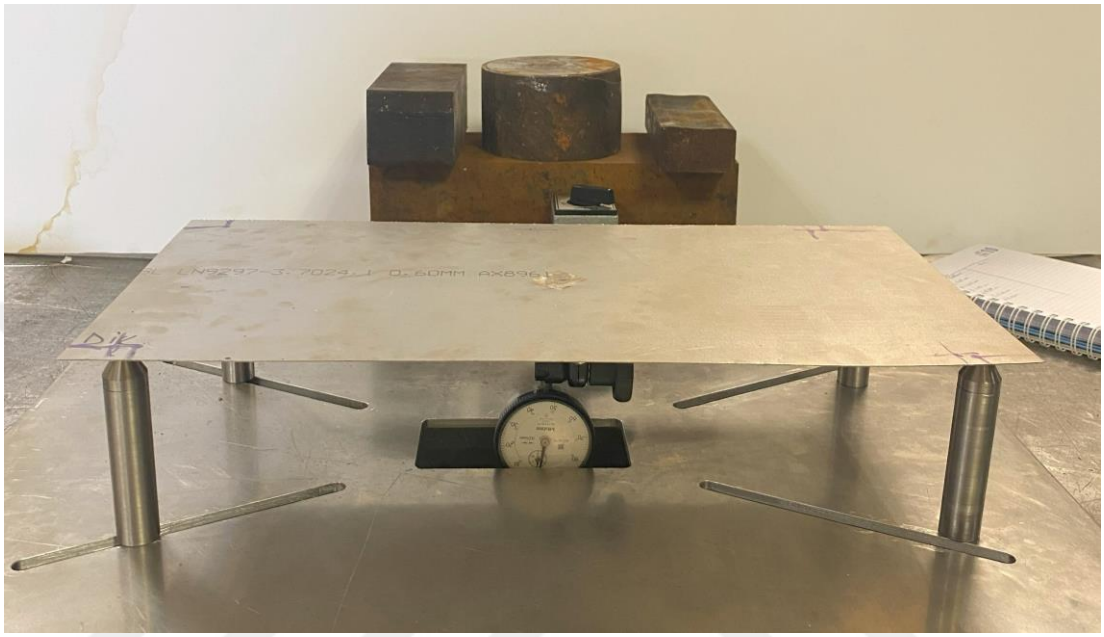

Figure 4.68 Test Setup

A total of 5 repeated measurements were made for the unshaped geometry. At each measurement, the weight was lifted and loaded again.

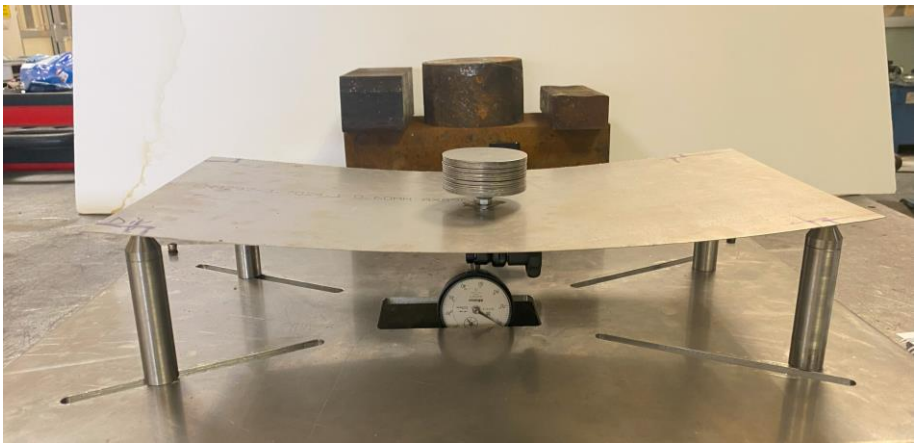

Figure 4.69 Weight Loading Step

The measurement result of the unshaped geometry was examined as 11.81 mm on average.

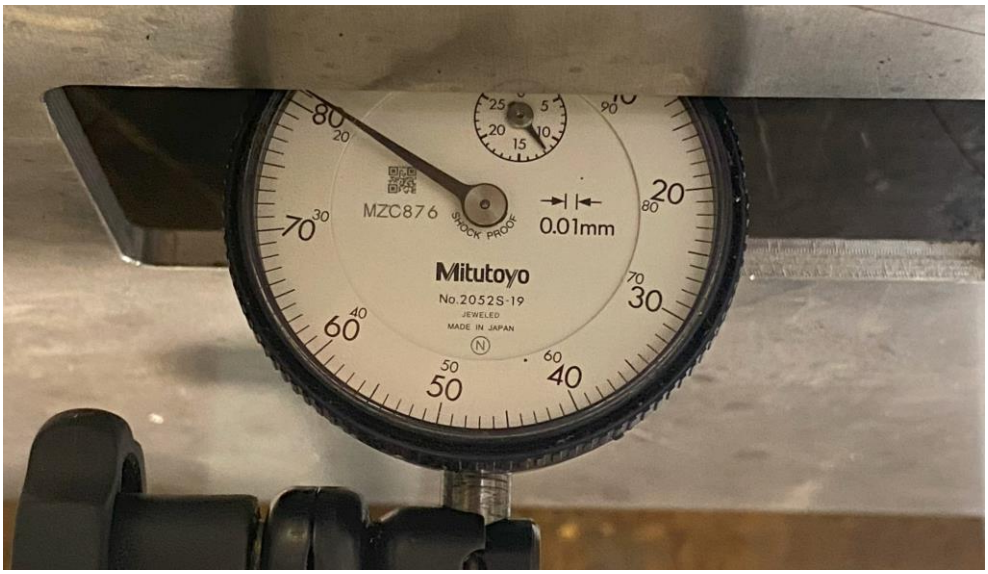

Figure 4.70 Dial Gage Result

Table 4.8 Unformed Part Experimental Results

Unformed Part	
Experiment number	**Deflection (mm)**
1	11,85
2	11,78
3	11,90
4	11,70
5	11,82

4.5.3.3 Deformation Measurements

GOM Argus measurement was made to examine the scanned data of the part in three dimensions. For this purpose, a part of the part is etching (Figure 4.71).

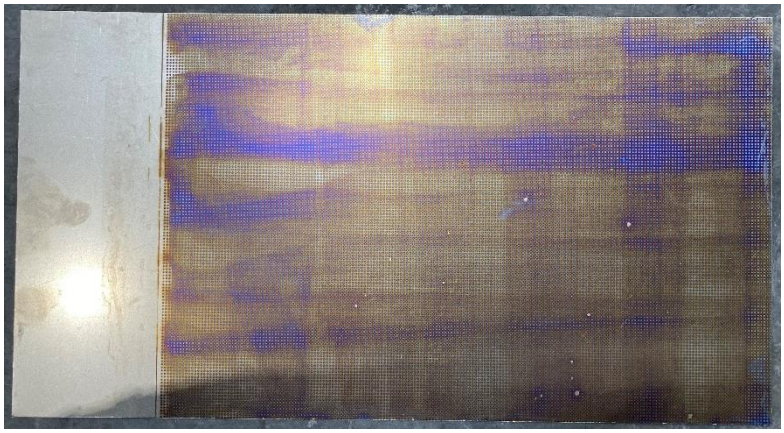

Figure 4.71 Etching

Figure 4.72 Placing the marked face into the mold

The marked area was chosen as the area that kisses the mold. Then, the shaping process was carried out with the same parameters. The scanning of the shaped part was carried out with GOM Argus.

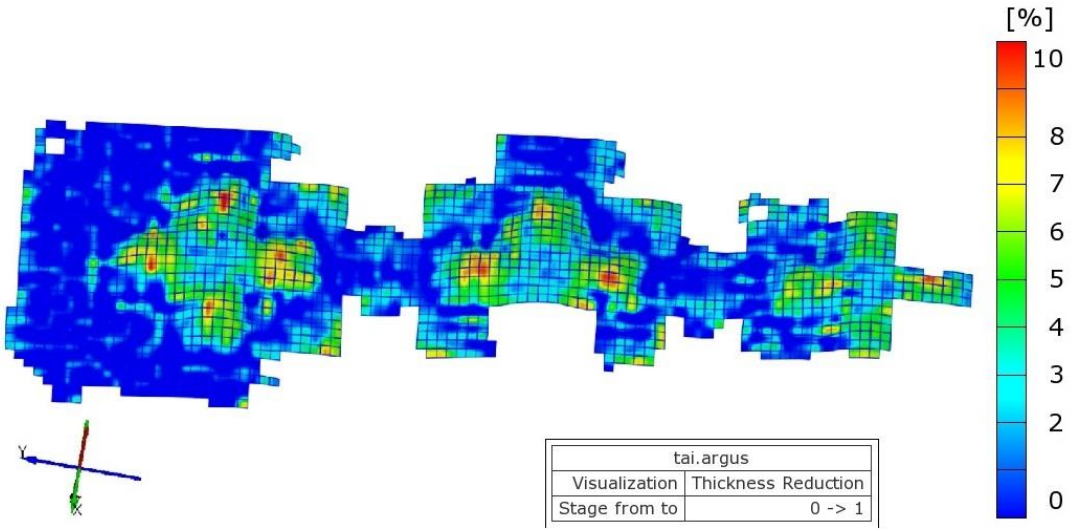

Figure 4.73 Thickness distribution of GOM Argus measurement

According to the thickness distribution, a decrease in thickness of around 10% was observed in the region where the thinning was highest (Figure 4.73).

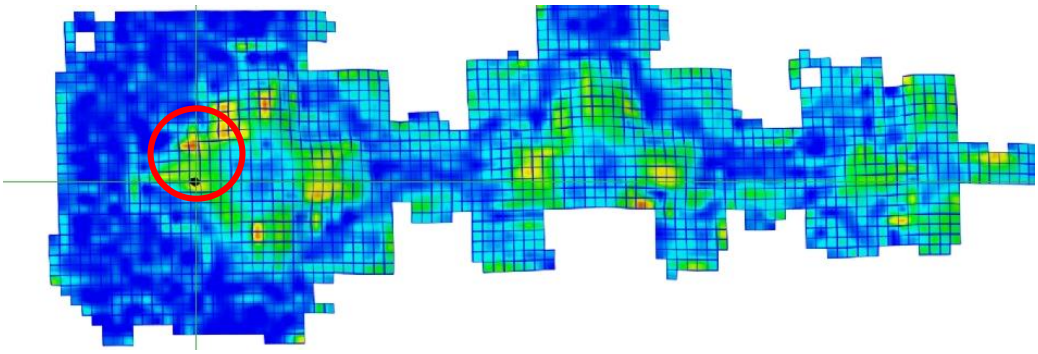

Figure 4.74 Marking the region with the highest thinning in GOM Argus measurement

Table 4.9 Results from GOM Argus measurement

Point name	Value	Unit
Coordinate X	1,6338	mm
Coordinate Y	139,1023	mm
Coordinate Z	15,9802	mm
Thinning	9,9157	%

According to the data obtained, the thinning is 9.91%. This shows that it is approximately 0.54 mm thick (Table 4.9).

4.5.3.4 Scanning the Deformed Part for Springback Investigation

After the deflection measurements and thickness scans of the deformed and trimmed part was completed, the part is scanned with 3D lasering technique. The best fitting method are applied with reference geometry. Measurements are taken in 2 separate ways. First of all, measurements are taken on the draw-bead (Figure 4.75). The short edges of the part are below nominal surfaces within the range of -1.2mm to -1.45mm. It has been observed that it approaches the nominal size as they approach the middle region from the long edges.

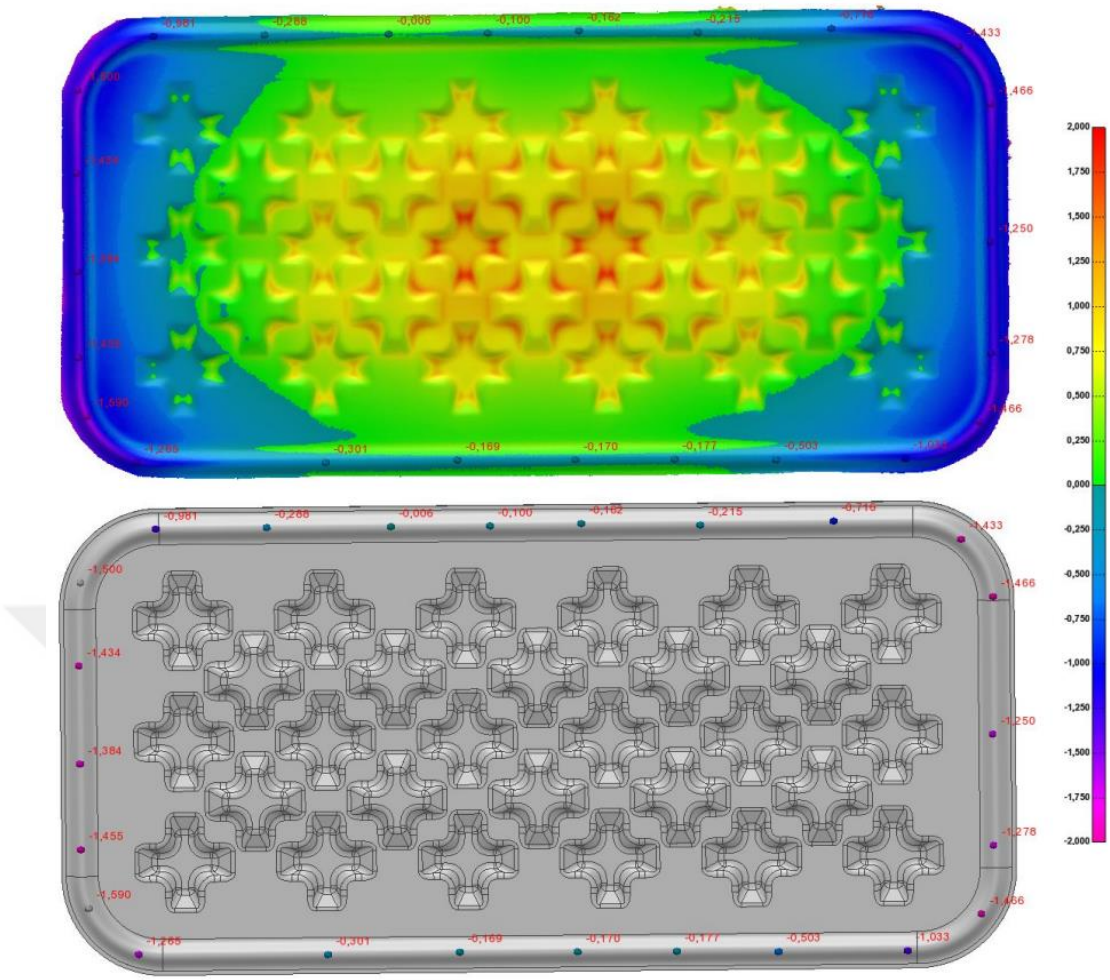

Figure 4.75 FARO laser scanner result of deformed sheet to investigate springback

The second measurement taken is from the inner areas of the part (Figure 4.76). It was observed that in these regions, especially the middle region of the part remained above the mold geometry. The areas near the short edges are close to the nominal surface, while the middle areas are approximately 1 mm above. This indicates that the part is springback from the middle regions or close to the short edge.

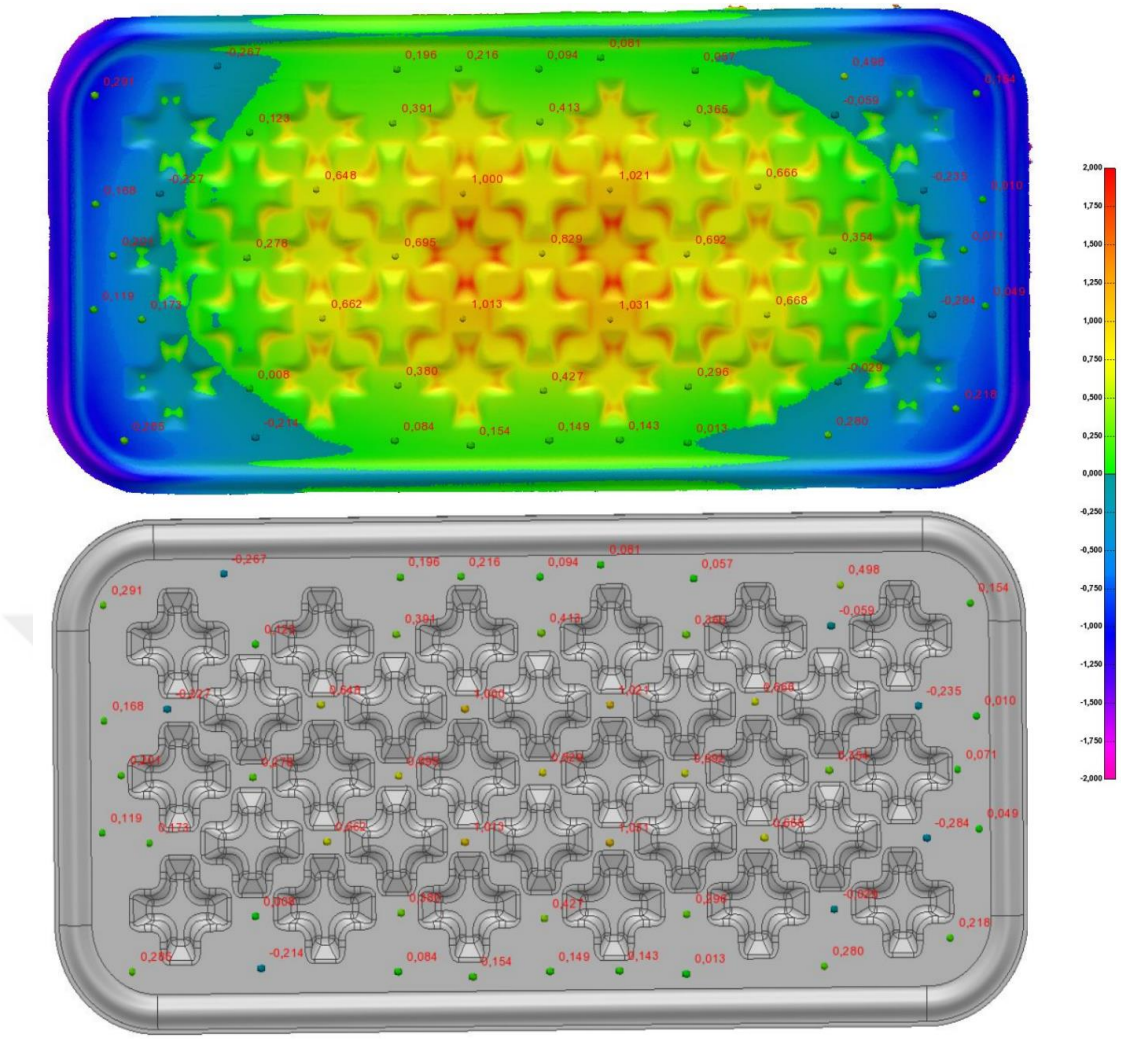

Figure 4.76 FARO laser scanner result of deformed sheet to investigate springback

4.6 Resimulation, Results and Comparing the Simulation Data with Scanned Data

4.6.1 Resimulation and Results

As a result of the experimental studies, it became necessary to update the simulation again. The reason for this is that the support points used in elastic analysis are determined as 4 corners in the simulation. The support points defined in the simulation conducted before the experimental study are as follows (Figure 4.77).

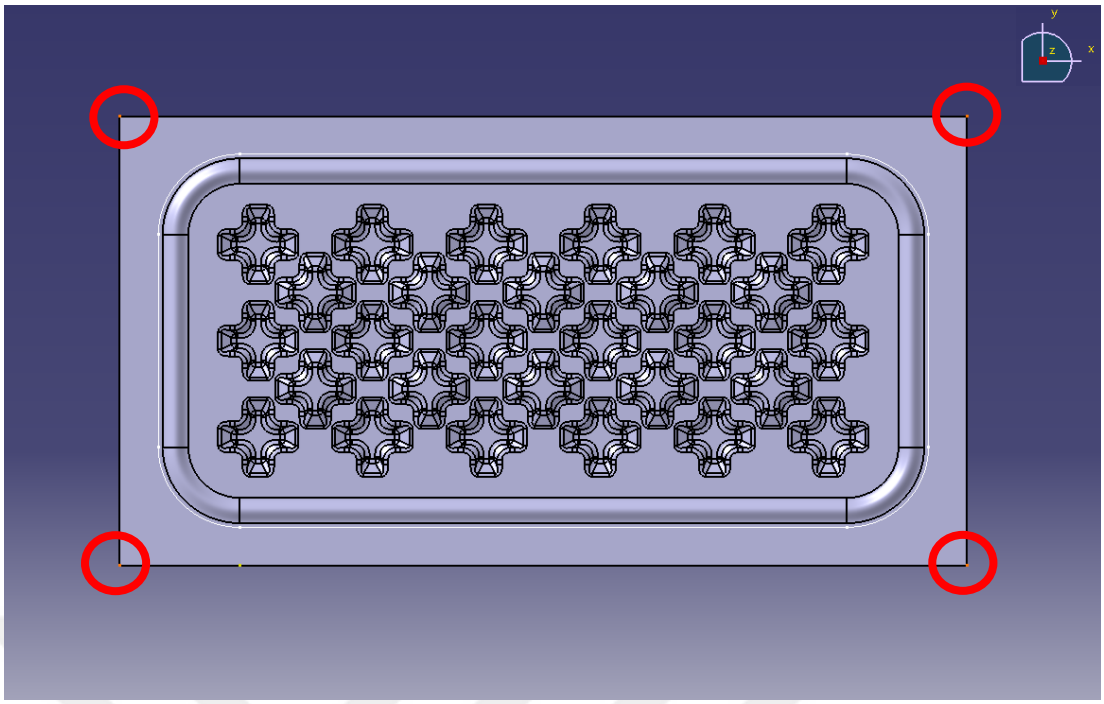

Figure 4.77 Previous support points

After the experimental stage, the part was cut by offsetting the drawbead outline by 2.5 mm. The purpose of this study is that the springback and distortion rates are high since the outer regions of the part are not shaped. New support points were determined and the simulation was updated under these conditions (Figure 4.78).

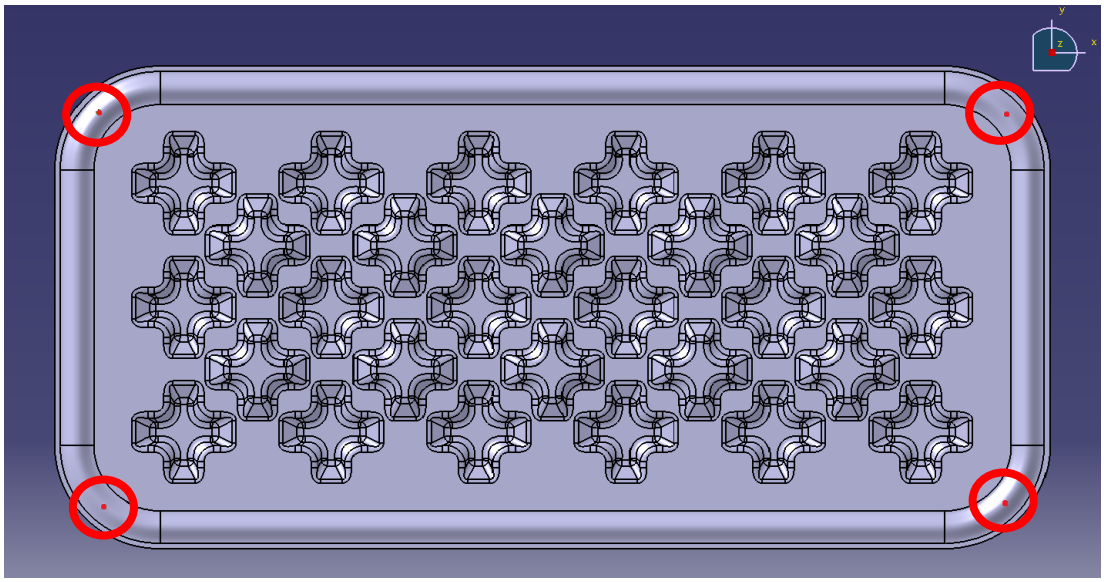

Figure 4.78 New support point

The updated trim lines were activated immediately after the shaping phase and springback was simulated relative to the new trimmed part.

In this case, the simulation was completed in 4 stages. The important parameters of the stages are as follows;

1- Forming
   - 0.08 GPa and 0.04 GPa forming pressure
   - Rubber Mooney Rivlin constant (A=0.004 GPa, B=0.001 GPa)
2- Springback
   - Trimming operation
   - Springback calculation of sheet metal
3- Elastic-1
   - Fixing the sheet metal part from the middle point
   - Gravitational acceleration
4- Elastic-2
   - Defining 4-point support
   - Defining 5N load to the midpoint

The first stage, Forming, is the stage in which the part is shaped using a mold and rubber membrane. In the second stage, springback, the shaped piece is trimmed using the trimming line. The springback simulation is then performed using the trimmed part (Figure 4.79). In the Elastic-1 stage, it is the final shape that the part takes under atmospheric pressure and own weight of the deformed part, without any external load, after being removed from the mold before being placed in the experimental setup. In the Elastic-2 stage, it is the stage where a 5N load is applied and simulated by selecting an area the size of a screw from the middle region, supported from 4 points.

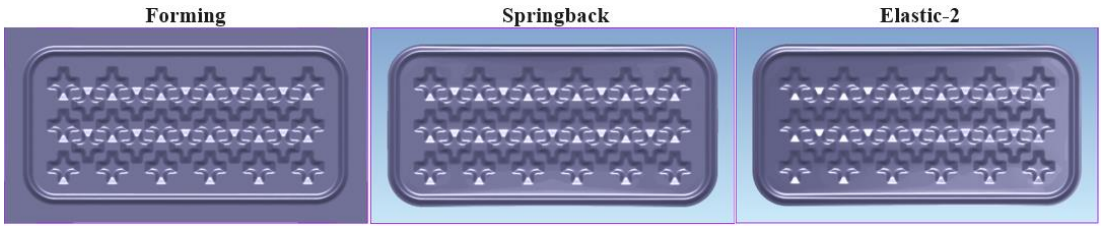

Figure 4.79 Updated simulation steps

As seen in the springback phase (Figure 4.80), a springback is observed in the z-axis on the long edges of the part. The new springback value was determined as 3.604 mm

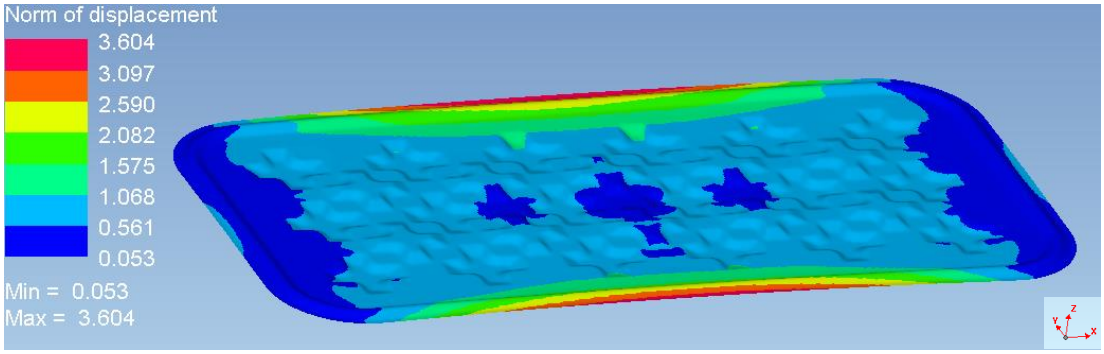

Figure 4.80 Updated simulation results-Springback stage

In the Elastic-1 stage (Figure 4.81), the part has changed some shape under atmospheric pressure and own weight of part.

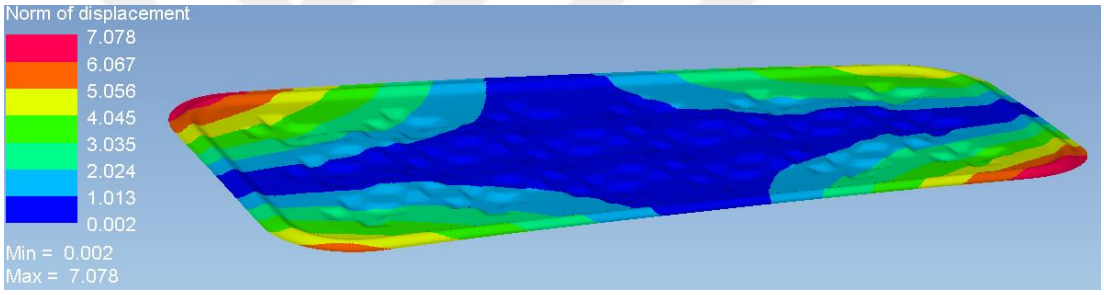

Figure 4.81 Updated simulation results-Elastic-1 stage

In the Elastic-2 stage (Figure 4.82), the part was supported from 4 points and a 5N load was applied from the middle point. In this case, a deflection of 0.978 mm was observed.

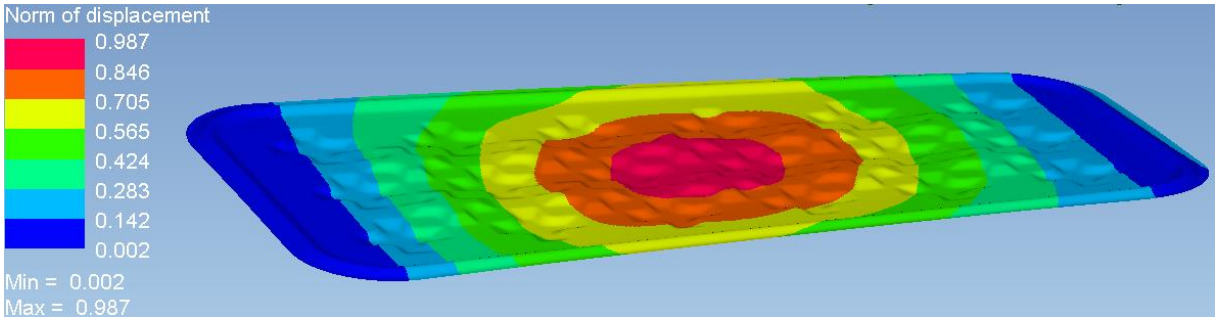

Figure 4.82 Updated simulation results-Elastic-2 stage

As a result of the evaluations, the sheet metal part could not be fully formed. The sheet metal part does not take the shape of the mold exactly. When the simulation results were examined, it was seen that the shape of the part obtained from the experimental results was visually achieved at a pressure value of approximately 0.04-0.05 GPa.

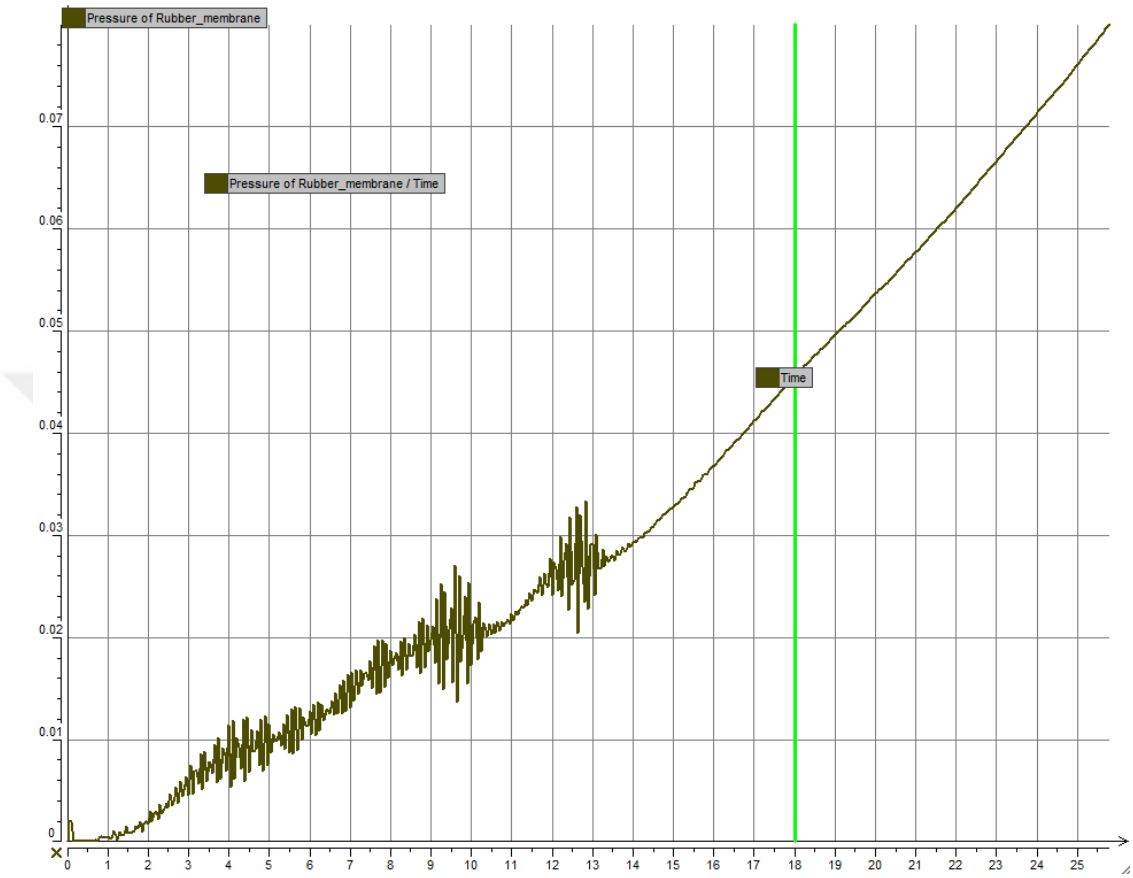

Figure 4.83 Rubber membrane pressure graph

According to the value seen in the graph (Figure 4.83), the shape closest to the part obtained in the experimental phase, as a result of visual inspection, is the shape obtained under 0.04 GPa pressure. In the pictures below (Figure 4.84,4.85 and 4.86), it is the shape that the simulation obtains when it reaches 0.04 GPa pressure. Figure 4.85 is the geometry taken from experimental results.

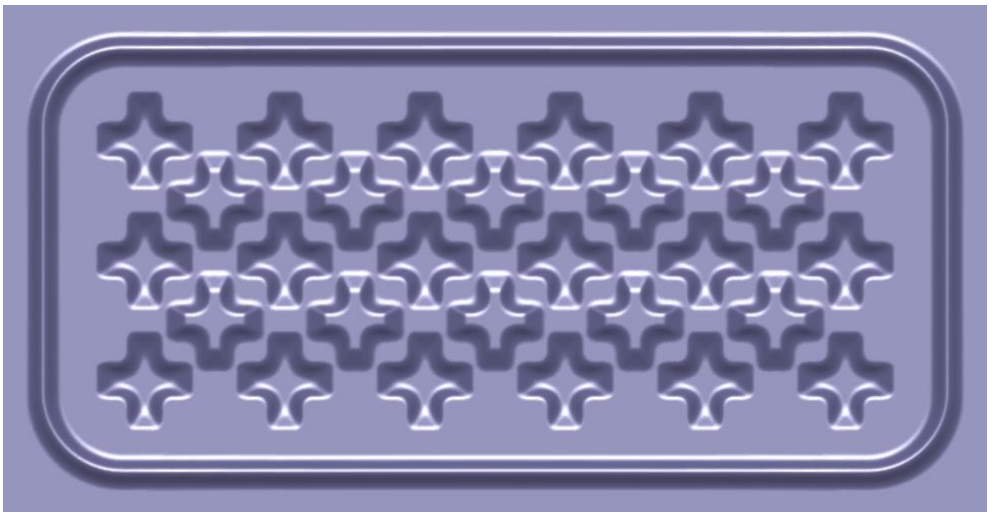

Figure 4.84 Design

Figure 4.85 Deformed sheet

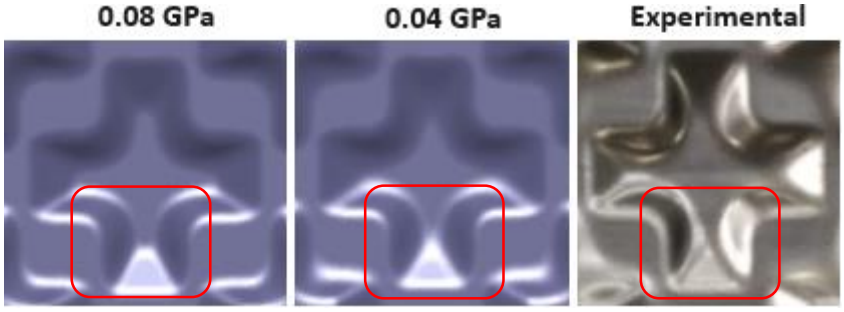

Figure 4.86 The visual inspection of 0.08-0.04 and experimental result

From left to right (Figure 4.86), the desired and obtained shapes appear. The geometry aimed to be achieved is a geometry with sharper corners. However, the deformed part is a part with smoother transitions. When the base area (marked in red) was examined, it was seen that it was not fully formed.

Therefore, a new simulation file was created and a new simulation was made after keeping all conditions the same and setting only the pressure value to 0.04 GPa. Trimming line has also been added in the new simulation (Figure 4.87).

When the pressure value is set to 0.04 GPa, the tapers in the positive direction are almost the same as at 0.08 GPa. However, the thinning distribution in the negative direction has changed (Figure 4.87).

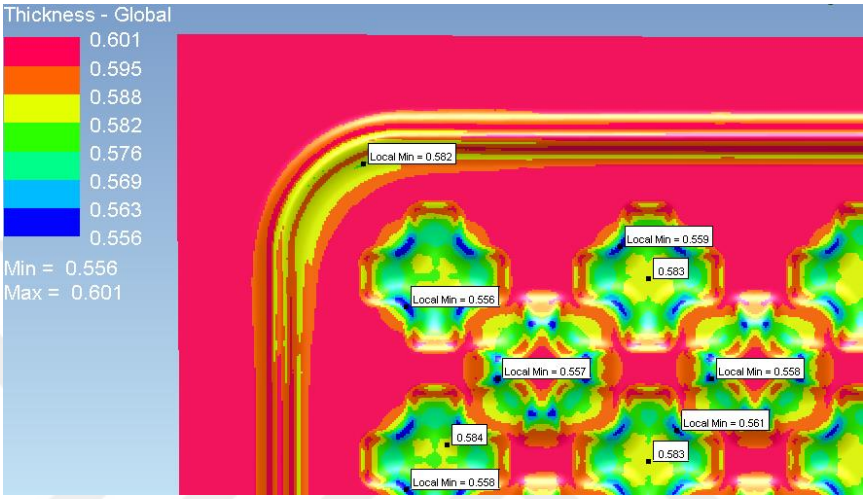

Figure 4.87 Thickness distrubution of 0.04 GPa forming pressure

Figure 4.89 was shaped with 0.04 GPa pressure, and Figure 4.88 was shaped with 0.08 GPa pressure. According to thickness measurements taken from similar points, 0.04 GPa pressure had a different thickness distribution because it could not shape the part fully.

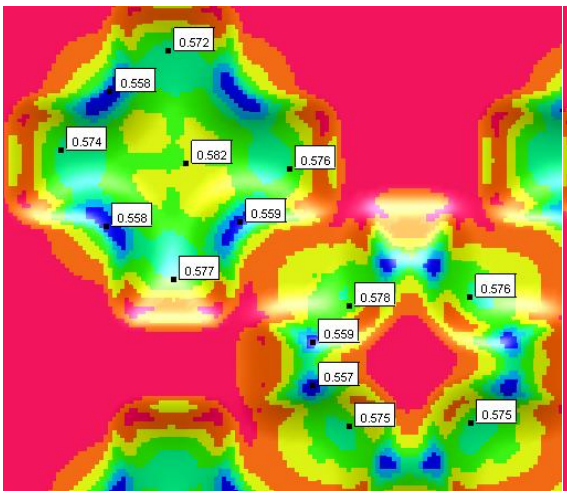

Figure 4.88 0.04 GPa pressure

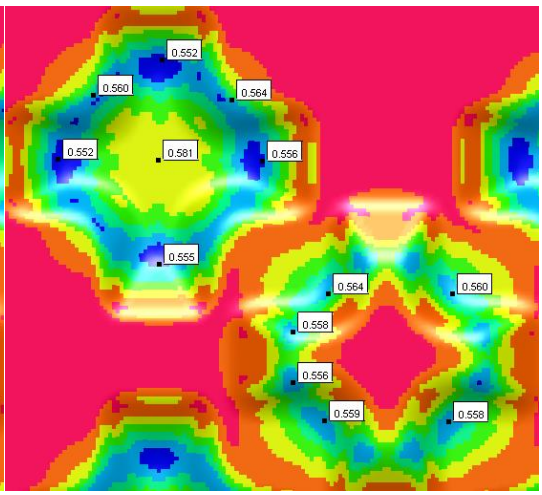

Figure 4.89 0.08 GPa pressure

According to the FLD Graph, there is no risk associated with forming at lower pressure as expected (Figure 4.90).

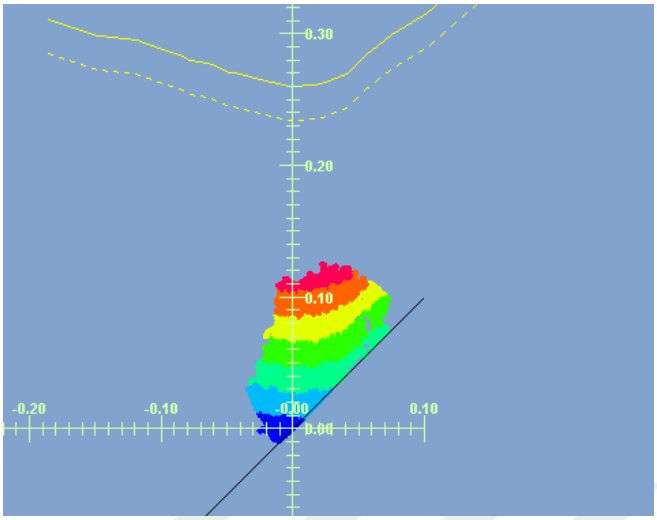

Figure 4.90 FLD graph of 0.04 GPa foming pressure

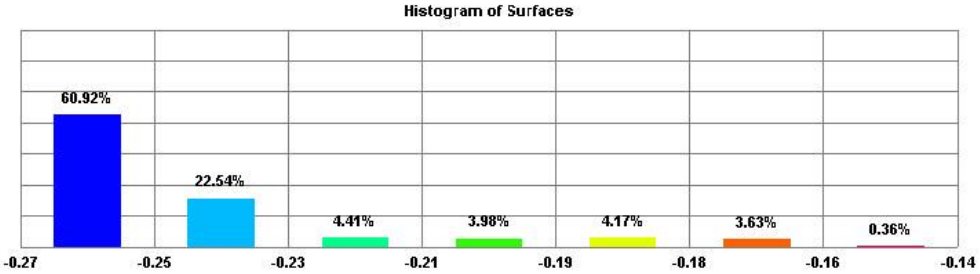

Figure 4.91 Histogram of strain

The highest strain areas are seen in the inner corners in the negative direction (Figure 4.92).

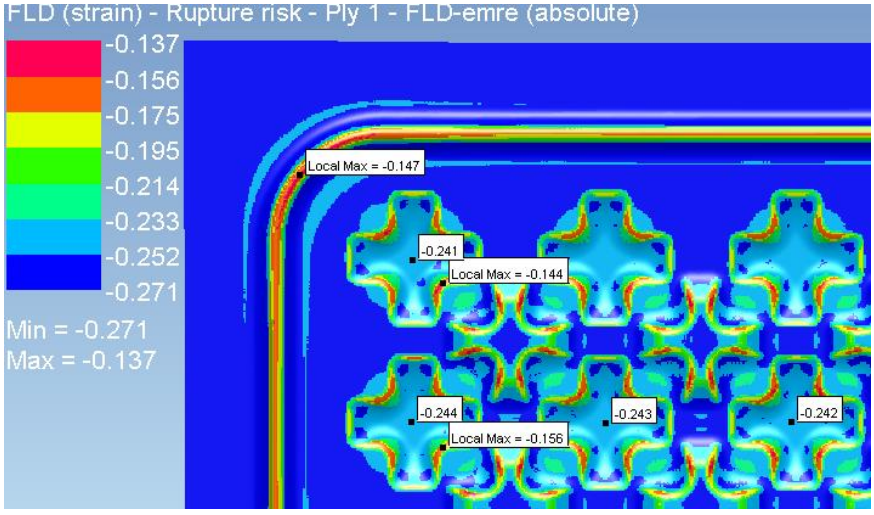

Figure 4.92 Strain distribution

When looking at the FLD Strain distribution, the areas at risk of spring-back and wrinkling are identified as the middle regions of the long and short edges. Experimental results also show this (Figure 4.93).

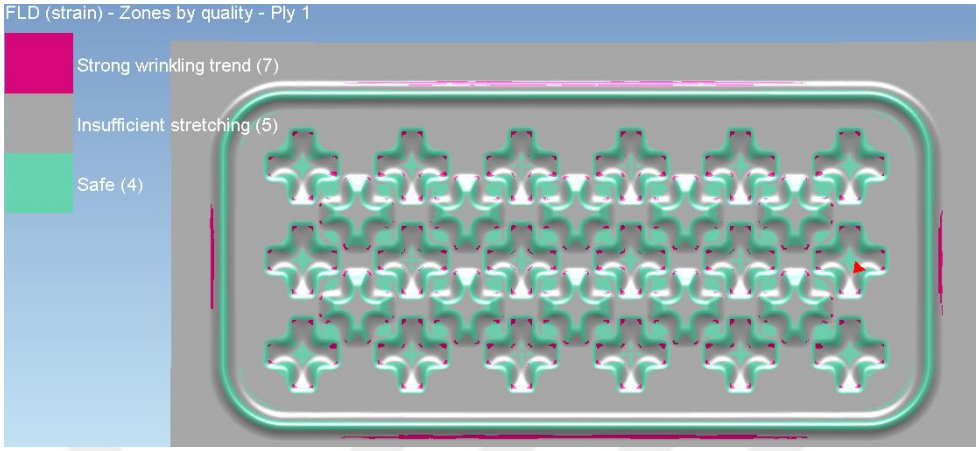

Figure 4.93 Wrinkling trend of simulation which is done with 0.04 GPa forming pressure

While the maximum distance between the mold and the sheet metal part after forming under 0.08 GPa pressure was 0.172 mm, under 0.04 GPa pressure this value became 0.566 mm. This situation shows that the part cannot be shaped completely (Figure 4.94).

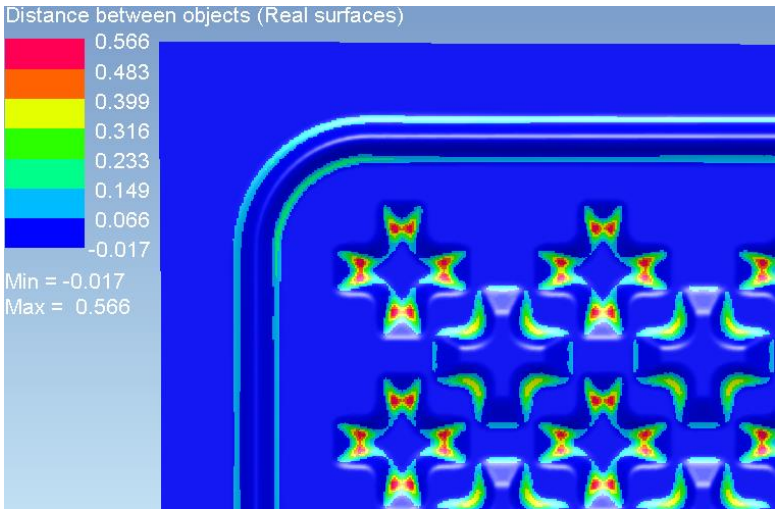

Figure 4.94 The distance in between die and formed part after forming with 0.04 GPa forming pressure

Springback analysis was performed immediately after shaping. Before the springback analysis started, the outer line of the drawbead was automatically offset by 2.5 mm to create a trimming line, and the sheet metal part was trimmed before the simulation

started. Then, springback analysis is performed. While the springback value is 15.314 mm before the sheet metal piece was trimmed, it was 3.150 mm after it was trimmed (Figure 4.95).

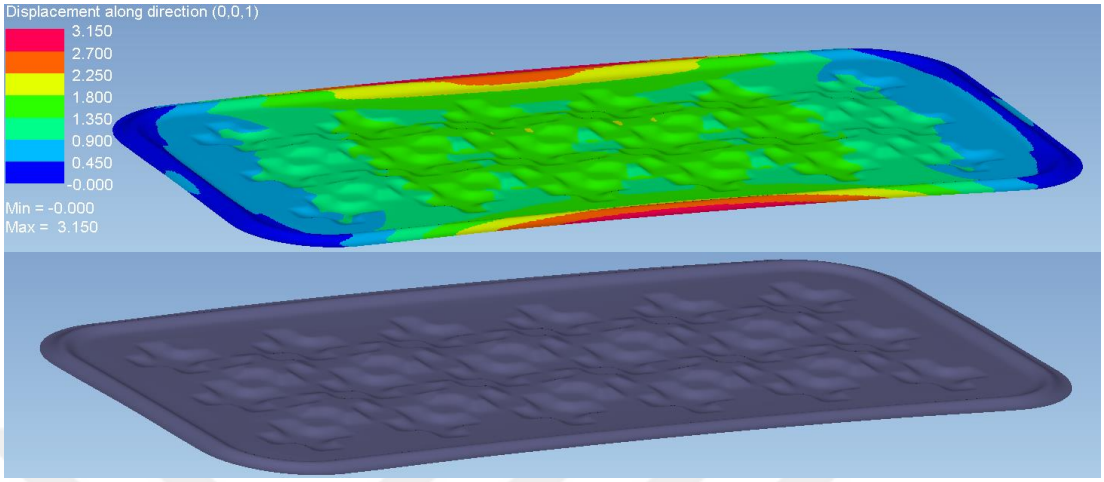

Figure 4.95 Springback result (0.04 GPa pressure)

The Elastic-1 phase comes immediately after springback (Figure 4.96). The aim of this stage is for the material to take its final shape under atmospheric pressure. It has been observed that springback decreases at this stage.

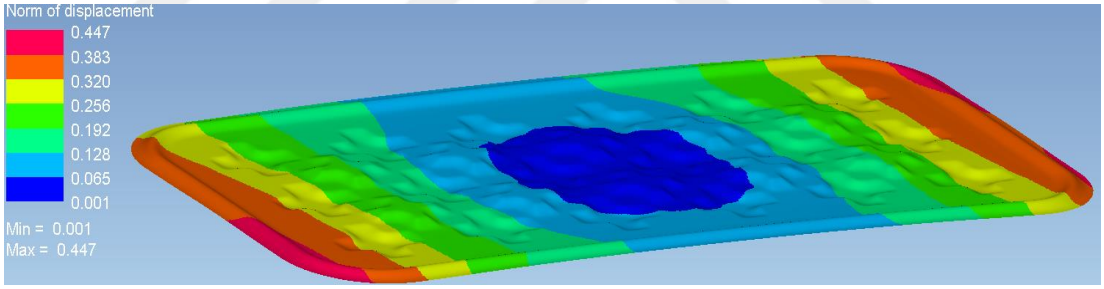

Figure 4.96 Elastic-1 stage (0.04 GPa pressure)

Elastic-2 is the final stage of the simulation (Figure 4.97). The same boundary conditions were used as in previous simulations. The deflection of 1,024 mm occurred with a 5N load from the middle point.

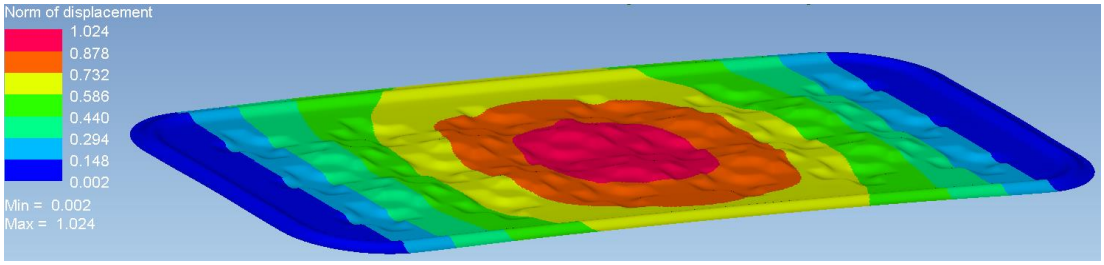

Figure 4.97 Elastic-2 Stage (0.04 GPa pressure)

In this thesis study, a shaping pattern was created and the parts shaped with this pattern were aimed to meet criteria such as minimum thinning and springback. (The test conditions was mentioned in Figure 4.62 Test rig)

Table 4.10 Comparison of Experimental and Simulation results

Deformed Part Deflection Values (5N Load, 0.08 GPa Forming Pressure)		
Exp. No.	**Exp. Results (mm)**	**Sim. Result (mm)**
1	1,02	**0,978**
2	1,05	
3	1,02	
4	0,99	
5	1,02	
Average	**1,02**	

Flat Sheet Metal Part Flexibility Values (5N Load)		
Exp. No.	**Exp. Results (mm)**	**Sim. Result (mm)**
1	11,85	**14,273**
2	11,78	
3	11,90	
4	11,70	
5	11,82	
Average	**11,81**	

Table 4.11 Comparison of Experimental and Simulation results for 0.04 GPa Pressure

Deformed Part Deflection Values (5N Load, 0.04 GPa Forming Pressure)		
Exp. No.	**Experimental Results (mm)**	**Simulation Result (mm)**
1	1,02	**1,024**
2	1,05	
3	1,02	
4	0,99	
5	1,02	
Average	**1,02**	

When the result obtained is interpreted, the deflection value of the shaped part is close to the simulation results. As a result of the examinations, the part could not be fully shaped, as stated in the title of "Resimulation, Results and Comparing the Simulation Data With Scanned Data". Therefore, a reanalysis was made using the visually closest value of 0.04 GPa pressure value as reference.

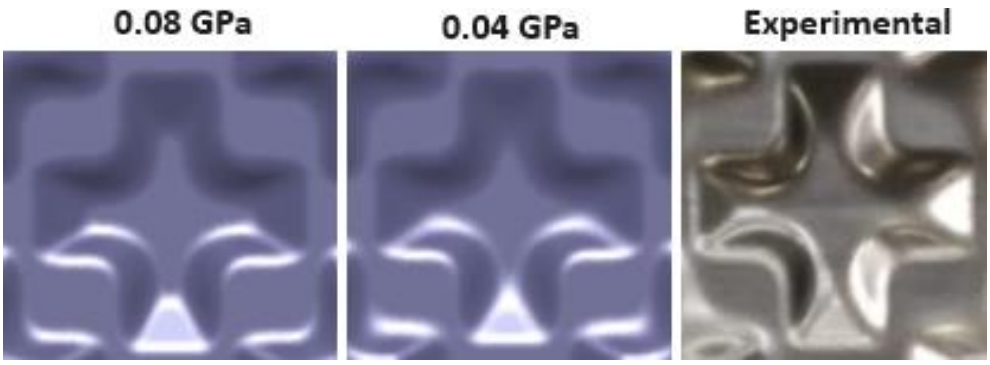

Figure 4.98 The visual inspection of 0.08-0.04 and experimental result

The deflection result in the new analysis and the average of the experimental results successfully overlap. There may be many reasons why the part cannot be shaped completely. These are the most important ones;

1. Approximate Stress-Strain data of the sheet metal part.
2. Hydroforming device cannot reach 800bar pressure
3. Approximate Mooney-Rivlin Coefficients of the rubber part

In order to mathematically evaluate these three possibilities, first a tensile test was applied to a sample of the sheet metal part. According to the results obtained, the material is a softer material than the known results. Values taken from the "Stress-Strain Graph (TAI)" graph were applied in all simulation stages. However, the part was found to be a softer material as a result of the tensile test performed at Atilim University Metal Forming Center of Excellence (MFCE). According to the chart provided by TAI, the highest stress value of the material is 707.44 MPa. However, according to the test results made in MFCE, the highest stress value of the material is 458.38 MPa.

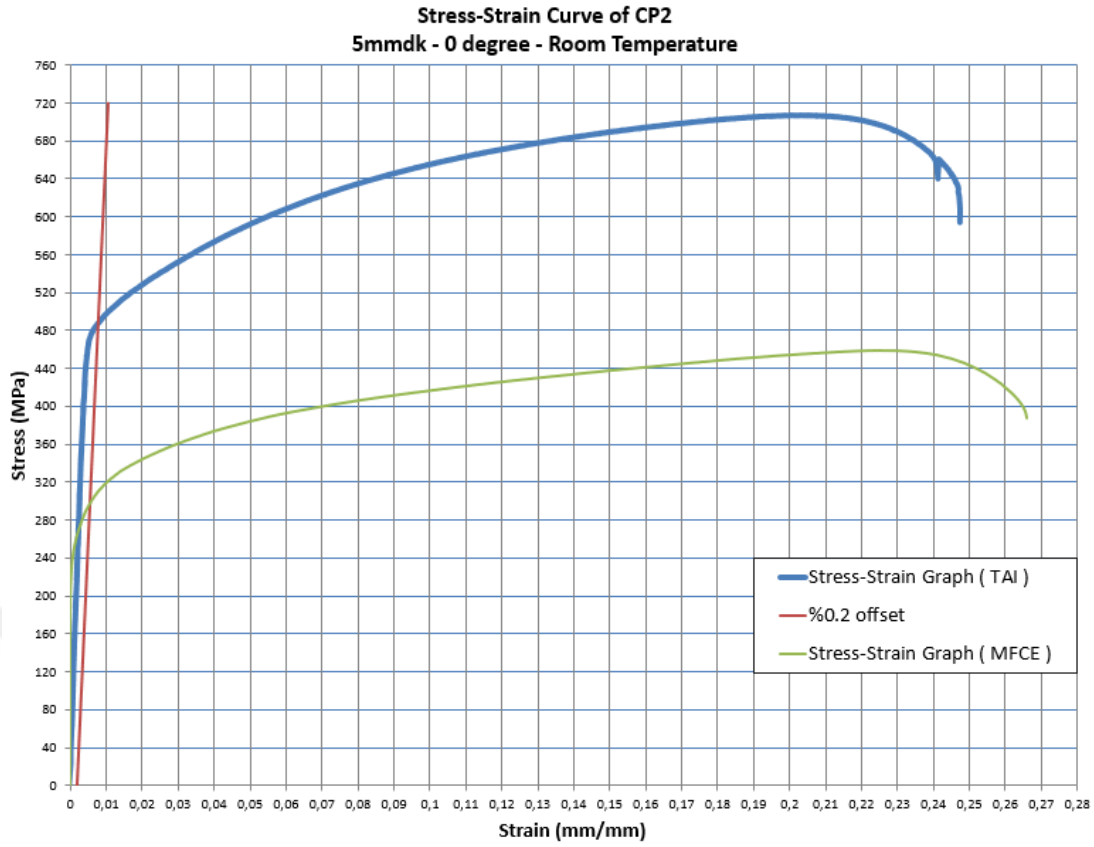

Figure 4.99 Comparison of TAI data and MFCE Stress-Strain graphs

The obtained graphics were compared with GOM Argus measurements, and the lowest thickness obtained in GOM Argus measurements was measured to be approximately 0.54 mm. In the simulation made with 0.04 GPa pressure, the thickness values taken from the same points are as follows.

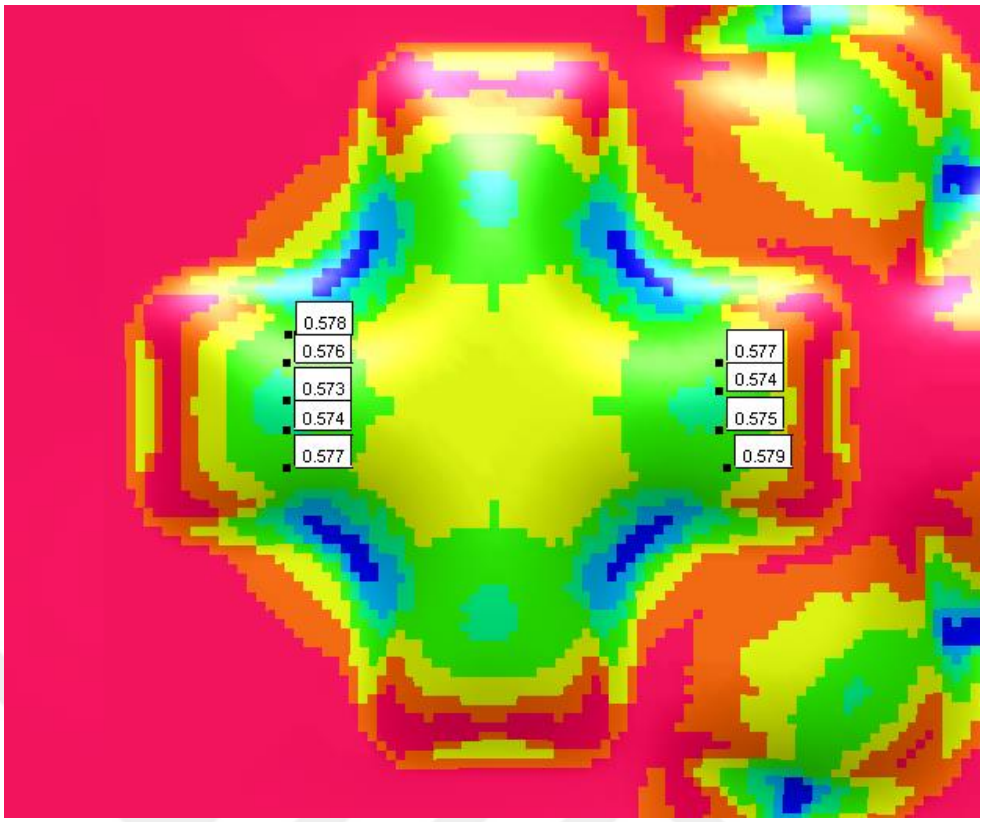

Figure 4.100 GOM measurement and simulation thickness distributions taken from the same points (0.04GPa)

The thickness value of 0.54 mm obtained in the experimental (Figure 4.73- Figure 4.101 and Table 4.9) became an average of 0.57 mm in the simulation (Figure 4.100). The reason for this difference is due to the different material card.

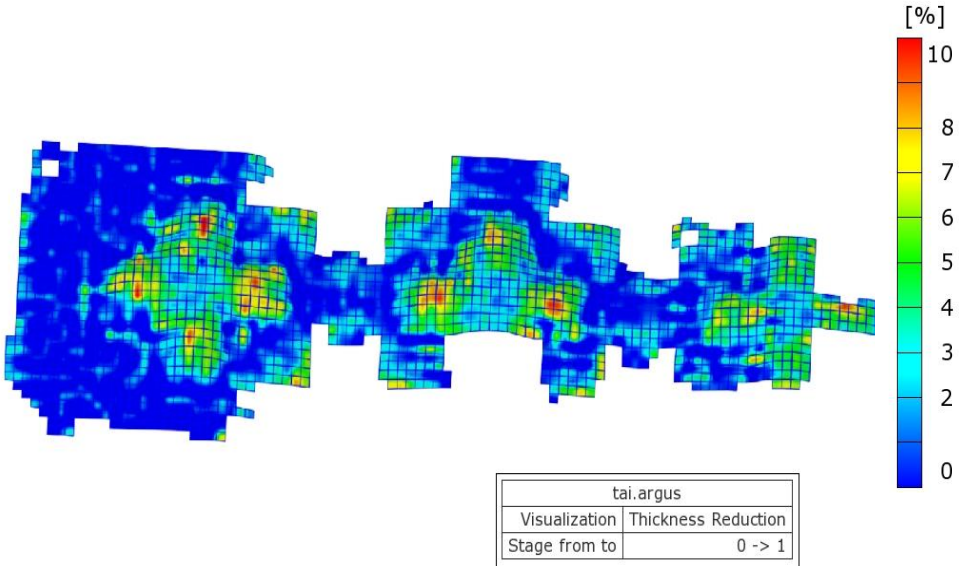

Figure 4.101 GOM Argus thickness measurement result

The second possibility, that the hydroforming device does not reach 800 bar, was also confirmed by the pressure values taken from the device screen. However, the pressure value could not be measured directly from the compression zone. The data provided by the machine is considered correct.

The last possibility, that the Mooney-Rivlin coefficients are wrong, seems to be the only and most valid reason. This is because the material is softer than known. Therefore, lower pressure values should be sufficient for shaping. However, it is still not fully formed. Therefore, the Mooney-Rivlin coefficients of rubber are much higher than known.

According to all these results, when the material was simulated using a pressure value of 0.04 GPa, the simulation and experimental results overlapped and a successful analysis-experiment process was achieved.

When a pressure value of 0.08 GPa was used, very close springback and deflection values were achieved.

4.6.2 Comparing the Deformed Part with Simulation Results

At this stage, the shaped sheet metal part was scanned with the FARO 3D Laser Scanner. The scanned geometry was taken as a point cloud and the meshing operation was performed, then saved as a surface via Catia-V5. The results were examined in two stages. First of all, 0.04 GPa forming pressure was taken as reference (Figure 4.102), then 0.08 GPa forming pressure was taken as reference (Figure 4.103). In two comparisons, the elastic-1 stage in simulation is taken as reference geometry The distance distributions are as follows.

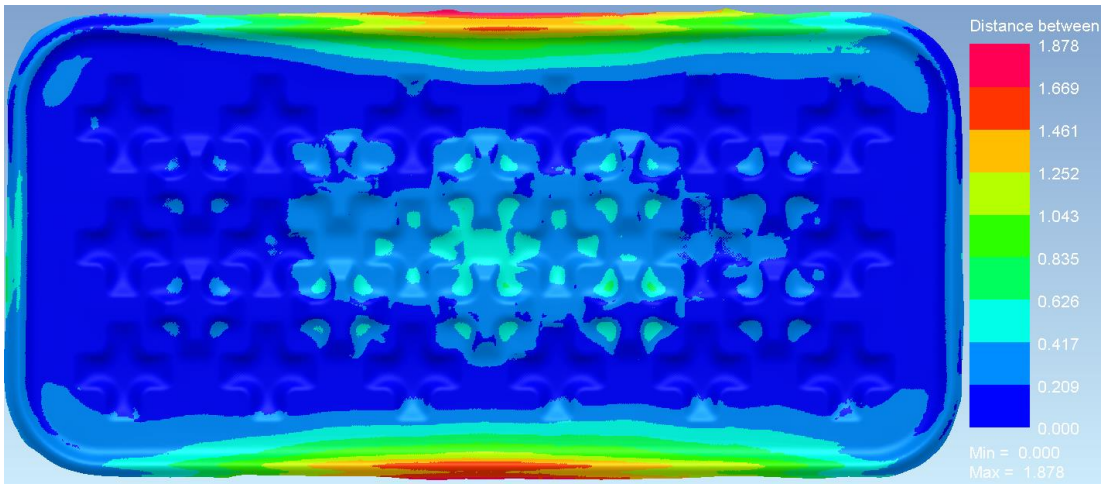

Figure 4.102 Comparison of laser scanning data and simulation result (0.04 GPa pressure)

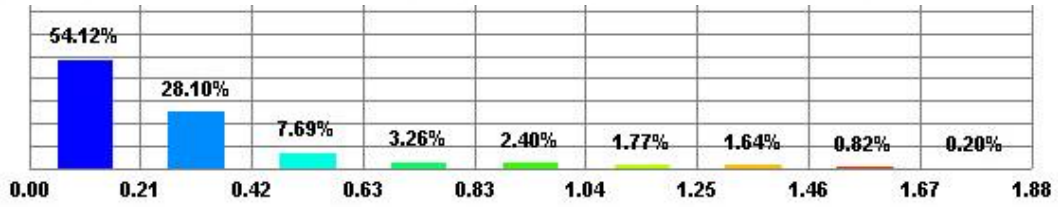

Figure 4.103 Percentage distribution of compared surfaces (0.04 GPa pressure)

The biggest difference is in the drawbead on the long edges with 1.8mm (Figure 4.102)

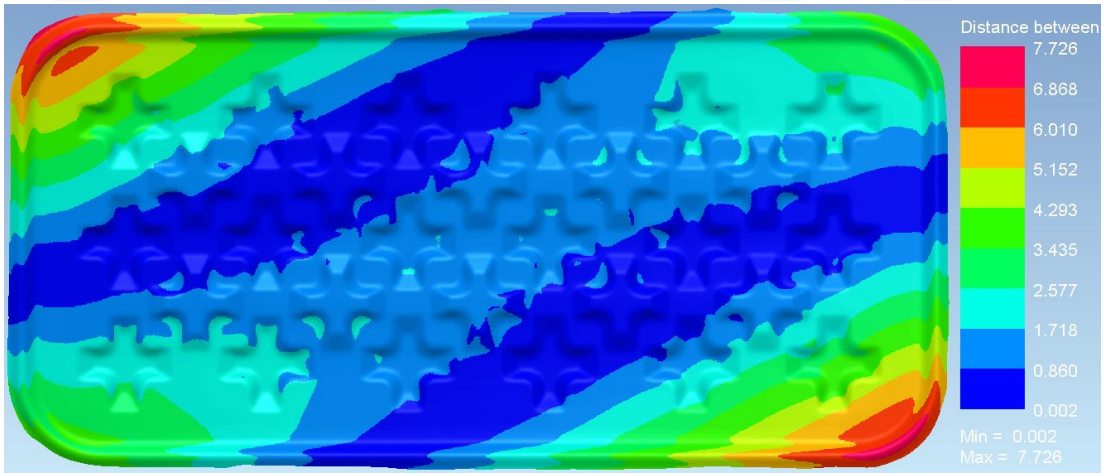

Figure 4.104 Comparison of laser scanning data and simulation result (0.08 GPa pressure)

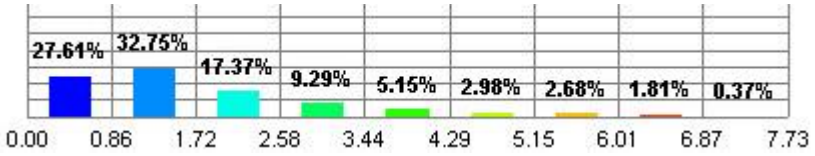

Figure 4.105 Percentage distribution of compared surfaces (0.08 GPa pressure)

As a result of visual inspections, as stated in previous headings, simulations of 0.04 GPa forming pressure will be taken as reference.

4.7 Development Algorithm for Estimation of Deflection of Formed Sheets

One of the purposes of the designed geometry is to provide rigidity to the material. The material that gains a higher second moment of area will become more rigid. This way, it will deflect less. The issue that spent the most time in this thesis was setting up and solving simulations. A formula has been created to get rid of the simulation burden. Thus, it will be possible to determine what kind of flexibility behavior the designed geometry will display if it is lengthened or shortened as needed. This formula was created based on the results obtained from the pressure value of 0.04GPa and 0.08 GPa.

The long side is defined as "b" and the short side is defined as "a". The b/a ratio will be used and the ‘’a’’ value is kept constant (Figure 4.106). In other words, the formulation of the situation in which the part extends along the b axis has been created.

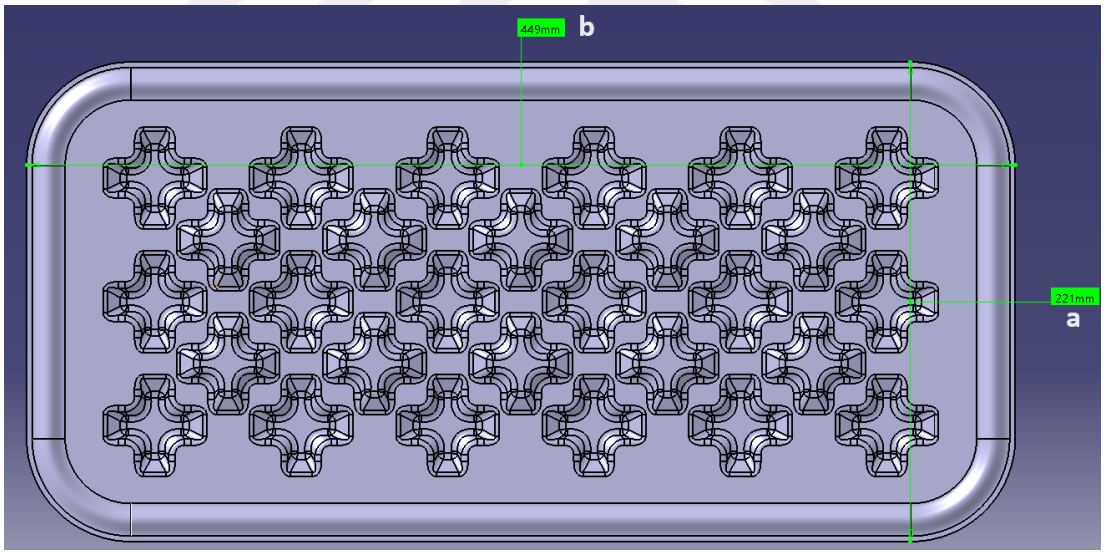

Figure 4.106 Representation of edges b and a

Simulations were carried out with a pressure value of 0.04 GPa and an algorithm was created for this pressure value.

Table 4.12 b/a elastic behavior chart 0.04 GPa Pressure

	b/a Elastic Behavior - 5N Load Applied - Part Formed By 0.04 Gpa Pressure				
No	b (mm)	a (mm)	b/a	Simulation Stretch Result (mm)	Analytical Stretch Result (mm)
1	747,25	221	3,38	7,401	7,140
2	648	221	2,93	4,551	4,304
3	582,87	221	2,64	2,87	2,911
4	448	221	2,03	1,024	1,125
5	383	221	1,73	0,555	0,639
6	281,75	221	1,27	0,247	0,211

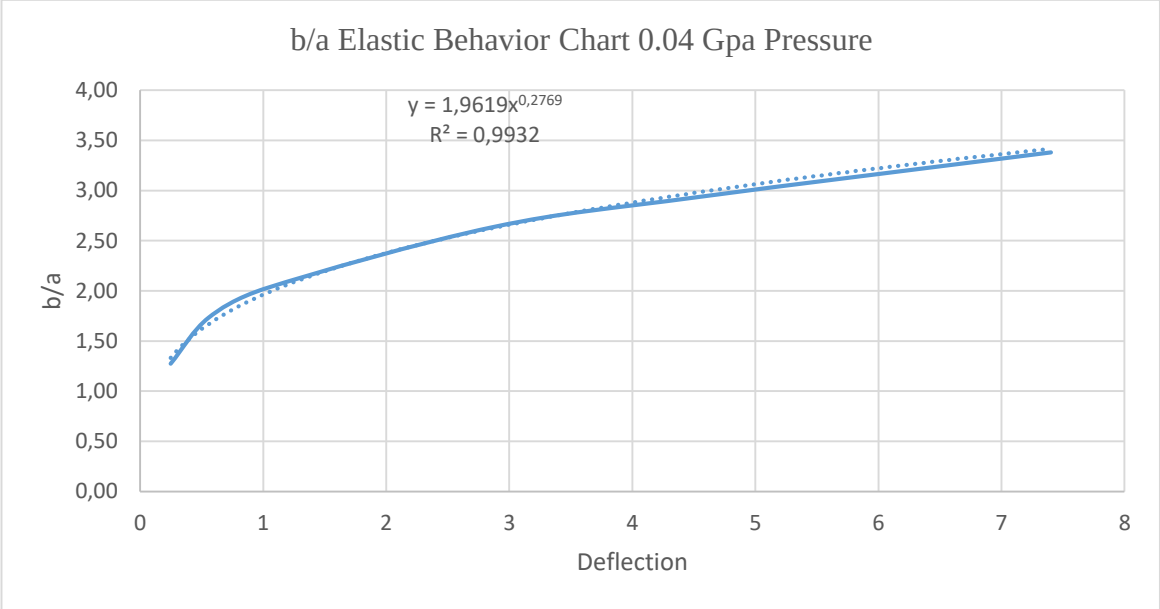

Figure 4.107 b/a elastic behavior chart (0.04 GPa)

$$x = \left(\frac{\frac{b}{a}}{1.9619} \right)^{\left(\frac{1}{0.2769}\right)}$$

Table 4.13 b/a elastic behavior chart 0.08 GPa Pressure

	b/a Elastic Behavior - 5N Load Applied - Part Formed By 0.08 Gpa Pressure				
No	b (mm)	a (mm)	b/a	Simulation Deflection Result (mm)	Analytical Deflection Result (mm)
1	747,25	221	3,38	4,507	4,429
2	648	221	2,93	2,739	2,868
3	582,87	221	2,64	2,16	2,076
4	448	221	2,03	0,98	0,930
5	383	221	1,73	0,504	0,577
6	281,75	221	1,27	0,243	0,226

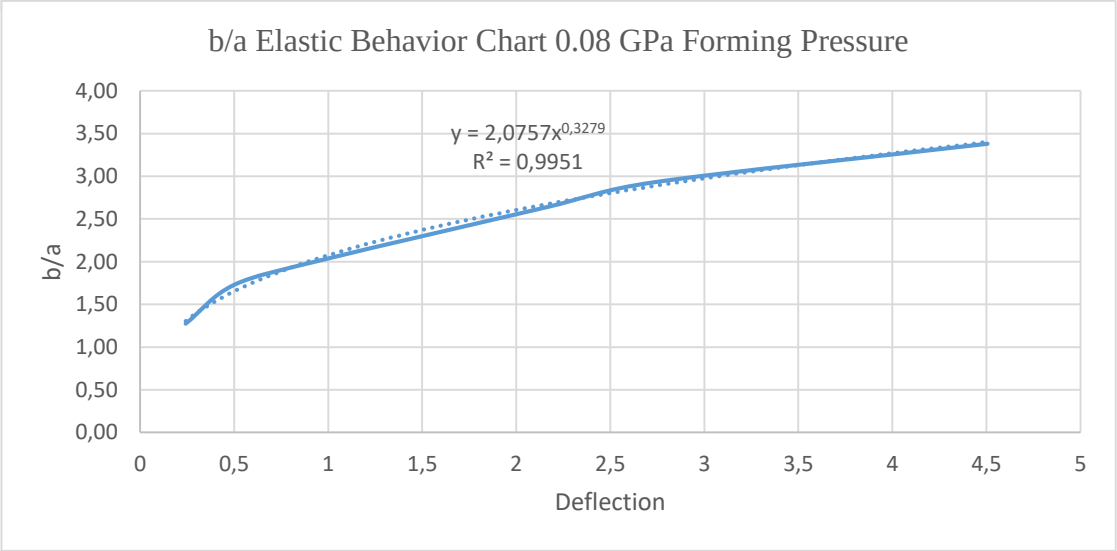

Figure 4.108 b/a elastic behavior chart (0.08 GPa)

As seen in the graph, there is an accuracy rate of 99.51% between b/a ratio 1.25 - 3.38.

$$\mathbf{x} = \left(\frac{\frac{\mathbf{b}}{\mathbf{a}}}{\mathbf{2.0757}} \right)^{\left(\frac{\mathbf{1}}{\mathbf{0.3279}}\right)}$$

CHAPTER 5

5. CONCLUSION

Many experiences and outcomes were obtained in this thesis study. The main goal of the project is to create a shaping pattern. With this shaping pattern, minimum deflection, distortion and maximum 10% thinning in titanium CP2 material are aimed.

At the beginning of the project, mechanical characterization tests of titanium CP2 material were carried out to use in the simulation stages. As a result of these tests, parameters such as the Elastic Modulus (E) and Friction coefficient of the material were determined experimentally. The stress-strain graphs used in the material card creation phase were provided by TAI, who provided material and equipment support for this thesis. These data were used in the interface of the PAM-STAMP program and the most suitable material model was determined. The Krupkowsky (swift) law with the closest match to the experimental graph (98.47%) was selected as the material model.

As a result of preliminary evaluations and research, studies were carried out on plus-shaped forming patterns to provide rigidity in both directions. In order to maximize rigidity, a geometry designed as deep as possible. Since the effect of the second moment of inertia increases with the square of the depth, depth has become one of the most important parameters in determining the geometry. The determined plus shape patterns were applied to the sheet metal plate measuring 490mm x 266mm x 0.6mm and elastic analyzes were carried out using the supporting 4 point with Ansys-Mechanical. The most successful pattern obtained from elastic analysis was accepted as the reference pattern. After this stage, the selected pattern was optimized by carrying out a study in parallel with the design, taking into account the manufacturability, distortion, springback and thinning criteria.

The outputs obtained during the plastic analysis stages, parameters such as radius, draft angles and depth used in the shaping pattern directly affect manufacturability.

Considering all these parameters, the design was optimized during the plastic simulation phase. After the manufacturability of the pattern was ensured, the use of drawbead was tried to further reduce springback, distortion and deflection. It has been observed that the use of a continuous drawbead that completely covers the forming pattern has a significant effect on reducing distortion, springback and deflection. In particular, after the shaping stage, the part was trimmed by offset 2.5 mm from the outer line of the drawbead. After the part was trimmed, distortion and springback decreased significantly. This is another importance of using drawbead. However, in 23.design and 24.design, the entire geometry was designed using drawbead in two different styles. In these two designs, the results were not as efficient as with a drawbead covering the perimeter of the forming pattern. The conclusion obtained here is that the use of drawbead is a very good supporter when used around the shaping pattern.

When the part was examined at the experimental stage, it was seen that perfect shaping could not be achieved. The failure to fully shape the part has been examined under several main headings;

1. Approximate Stress-Strain data of the sheet metal part.

The accuracy of these data used from the TAI library was compared with an additional tensile test performed in MFCE. According to the results, the titanium material used in the experiments and the material in the TAI library were different. However, the material used in the experiments is a softer material. Therefore, it is an easier material to shape.

2. Hydroforming device does not reach 800 bar pressure

The second possibility, that the hydroforming device does not reach 800 bar, was also confirmed by the pressure values taken from the device screen.

3. Approximate Mooney-Rivlin Coefficients of the rubber part

The last possibility, that the Mooney-Rivlin coefficients are wrong, seems to be the only and most valid reason. This is because the material is softer than known. Therefore, lower pressure values should be sufficient for shaping. However, it is still not fully formed. Therefore, the Mooney-Rivlin coefficients of rubber are much higher

than known. According to all these results, when the material was simulated using a pressure value of 0.04 GPa, the simulation and experimental results overlapped and a successful analysis-experiment process was achieved. When a pressure value of 0.08 GPa was used, very close springback and deflection values were achieved.

When the table created in the 4.6 Illustration Stage and Results section (Tables 6 and 8) is examined, it gives 0.978mm deflection with 0.08 GPa forming pressure and 5N point load. In the experimental study, this value was measured as 1.02mm. As a result of the examinations, the part formed with 0.04 GPa forming pressure in the simulation is visually similar to the experimental part, as it cannot be shaped 100%. Under this pressure, the simulation result with 5N point load gives 1,024 mm deflection. The deflection values of the simulation created with both 0.08GPa and 0.04GPa pressures are close to the experimental ones.

With the simulation carried out under heading 4.6.1, the parts produced in the experimental phase were placed on top of each other and it was examined how much the part deviated from the simulation result. 0.04 GPa forming pressure was taken as reference. The reason for this is that, as a result of visual inspections, the result of the simulation with 0.04 GPa forming pressure is very similar to the experimental part. When the results are examined, the largest deviation of the part is in the drawbead section at the long corners with 1.878mm. The deviation in the inner regions is between 0 and 0.55 mm and can be considered low. Therefore, the experimental result and simulation result are close.

As it is known, simulation times are very long. In order to save time, an algorithm has been developed, which is one of the goals of the project. Thanks to this algorithm, the geometry can be kept fixed on one side and the other side can be extended from 280mm to 750mm. Using the algorithm developed for dimensions varying in this range, it can be calculated how rigid the material will remain.

As a result of all the work done, a design that meets requirements such as maximum 10% thinning, minimum deflection, minimum distortion and minimum springback has been created. Design and simulation results supported each other and the project requirements were met.

CHAPTER 6

6. FUTURE WORKS

Many gains have been achieved in this thesis study. Design, analysis and manufacturing processes have been experienced and optimization processes have been carried out. Grade-2 Titanium was chosen as the material. The created and optimized shaping pattern was applied on the titanium sheet.

The first study that can be done in the future is to experimentally test and measure the Mooney-Rivlin coefficients of the rubber material used. In this way, the accuracy rate will increase and both analysis time and additional die costs will be saved.

The second study that can be done is to expand the scope of this thesis and create a forming pattern that can be used in a wider variety of materials by selecting relatively softer and harder materials such as aluminum and steel. Again, using the plus model or by creating a new pattern, this pattern can be applied to materials commonly used in sectors. In this case, design criteria such as depth, radius, etc. should be optimized by taking the softest material as a reference. The advantage of this study will be to get rid of long analysis and design processes by strengthening the parts that require strength.

REFERENCES

[1] ‘’How to Identify If Sheet Metal Hydroforming Is Right For Your Project’’ Internet:https://stampingsimulation.com/how-to-identify-if-sheet-metal-hydroforming-is-right-for-your-project/, Apr, 2014 [Oct.13,2023]

[2] H.A.Hatipoglu, ‘’ EXPERIMENTAL AND NUMERICAL INVESTIGATION OF SHEET METAL HYDROFORMING (FLEXFORMING) PROCESS’’ Master’s thesis, Middle East Technical University, Turkey, 2007

[3] C.-W. Hsu, A. G. Ulsoy and M. Demeri, "Development of process control in sheet metal forming," *Journal of Materials Processing Technology*, vol.127 (3), pp. 362, 2002.

[4] T. Trzepieciński, "Advances in sheet metal forming technologies," Rzeszow University of Technology, pp. 64, 2012.

[5] C. Bell, J. Corney, N. Zuelli and D. Savings, "A state of the art review of hydroforming technology," *International Journal of Material Forming*, pp. 790, 2019.

[6] S. Zhang, J. Danckert, ‘’Development of Hydro-Mechanical Deep Drawing.’’ *Journal of Materials Processing Technology*, vol. 83(1-3), pp. 14-25, 1998

[7] S. Yuan, X. Fan, ‘’Developments and perspectives on the precision forming processes for ultra-large size integrated components’’, *International Journal of Extreme Manufacturing*, vol. 1 pp. 3, 2019

[8] Yadav, A. D. "Process Analysis and Design in Stamping and Sheet Hydroforming." Doctoral dissertation, Ohio State University, USA, 2008

[9] "Quintus,". Internet: https://quintustechnologies.com/knowledge-center/recent-hydroform-and-flexform-development/, 2016 [Nov.23,2023].

[10] H.A.Hatipoglu, ‘’ Experimental And Numerical Investigation Of Sheet Metal Hydroforming (Flexforming) Process’’ Master’s thesis, Middle East Technical University, Turkey, 2007

[11] "The Analysis of the application of hydroforming technology in automobile industry,"Internet:http://www.hydroforming1688.com/article/autopartforming.html. [Aug.11,2023]

[12] Tolazzi, M., ‘’Hydroforming applications in automotive: a review’’ *International Journal of Material Forming*, vol. 3(1), pp. 89, 2010.

[13] S. M. Kulkarni, V. V. Ruiwale, M. S. Jadhao, A. A. Kadam, S. R. Kale"A review on Hydroforming Processes," *International Journal of Current Engineering and Technology*, pp. 161, 2004.

[14] E. Erdin, ‘’Deep Draw Hydroforming Process’’ Internet:https://americanhydroformers.com/deep-draw-hydroforming-process/, July 24, 2014, [May.11,2023]

[15] E.Erdin,‘’Sac Şekillendirme İşlemleri’’ Internet: https://web.hitit.edu.tr/dosyalar/materyaller/eminerdin@hititedutr300420180H7S9C0E.pdf, [Sept.13,2023]

[16] "Wikipedia," Internet: https://en.wikipedia.org/wiki/Hydroforming#cite_note-7 [Sept.13,2023]

[17] "HydroformingTechnology,"Internet:https://www.aws-schaefer.de/en/products/hydroforming-technology/. [Sep.13,2023]

[18] "Tube Hydroforming: Part Two," Internet: https://www.totalmateria.com/page.aspx?ID=CheckArticle&site=kts&LN=TR&NM=363, Jan 2012.[May.20,2023].

[19] Inoxveneta," TUBE HYDROFORMING’’, Internet:https://www.inoxveneta.it/en/tube-hydroforming/. [Sep.18,2023]

[20] S. Yuan, F. Wang, Z. Wang,‘’Safety analysis of 200 m3 LPG spherical tank manufactured by the dieless hydro-bulging technology’’, *Journal of Materials Processing Technology*, vol. 70, pp. 1, 1997.

[21] Z. Wang, G. Liu, S. Yuan, B. Teng and Z. He, ‘’Progress in shell hydroforming.’’ *Journal of Materials Processing Technology*, *vol. 167*, pp. 232, 2005

[22] Q.Zhang, Z. Wang, ‘’Shape improvement of a dieless hydro-bulged sphere made of hexagonal and pentagonal shaped panels.’’ *Journal of Materials Processing Technology*, vol. 220, pp. 87-95, 2015

[23] "An Engineers’ Guide to Sheet Metal Bending," Internet:https://www.komaspec.com/about-us/blog/guide-to-sheet-metal-bending/. 2021. [Dec.17,2023].

[24] "Deep Drawing," Internet: https://www.stm-ag.ch/en/deep-drawing/. [Dec.17,2023].

[25] S. Benson, "Bending Basics: The hows and whys of springback and springforwar,"Internet:https://www.thefabricator.com/thefabricator/article/bending/bending-basics-the-hows-and-whys-of-springback-and-springforward, July 2016, [Dec.17,2023]

[26] "Distortion & Warping," Internet: https://galvanizeit.org/design-and-fabrication/design-considerations/distortion-and-warping, 2017 [Apr.22,2023].

[27] S. Zhou, Y. Chen, D. Zhang and J. Xie, ‘’Classification of surface defects on steel sheet using convolutional neural networks.’’ *Materiali in Tehnologije, vol. 51*, pp. 126, 2017.

[28] L. Perumal and D. T. T. Mon, ‘’Finite elements for engineering analysis: A brief review’’ *International Proceedings of Computer Science and Information Technology*, vol. 10, pp.66, 2011.

[29] A. S.Tohamy, "Critical Shear Stresses for Webs of Plate Girder Subjected to Shear Loading and Contained Cut-outs," Master’s thesis, Beni Suef University, Egypt, 2015.

[30] Y. Jun and M. Lee,’’ Adaptive Mesh Refinement for Dealing with Shock Wave Analysis.’’ *Korean Journal of Computational Design and Engineering, vol.18*, pp. 462, 2013.

[31] D. Giuntoli, "Understanding Finite Element Analysis and Its Benefits for Your Medical Device," Internet: https://www.mindflowdesign.com/insights/finite-element-analysis-medical-product-benefits/, Jun. 25, 2015. [Apr. 26,2023]

[32] "Mesh Topologies," Internet:https://www.ansys.com/. [Jun. 26,2023].

[33] G.R. Liu, T. Nguyen-Thoi , K.Y., ‘’Lam An edge-based smoothed finite element method (ES-FEM) for static, free and forced vibration analyses of solids.’’ *Journal of Sound and Vibration*, vol. 320, pp. 1101, 2009.

[34] J. M. Nogué, "Mandibular biomechanics as a key factor to understand diet in mammals," *Mammalian teeth. Form and function*, pp. 63, 2021.

[35] "MATERIAL PROPERTIES,". Internet:https://myesi.esi-group.com/downloads/software-documentation/pam-stamp-2021.0-reference-manual-online. Jun. 2021 [Sep. 21,2023]

[36] S. K. Paul, ‘’Theoretical analysis of strain- and stress-based forming limit diagrams.’’ *The Journal of Strain Analysis for Engineering Design*, vol. 48, pp. 178, 2013.

[37] "Main Takeaways on Stress and Strain," Internet:https://ocw.tudelft.nl/course-readings/1-1-6-main-takeaways-on-stress-and-strain/, [Sep.21,2023]

[38] "Engineering Stress/Strain vs True Stress/Strain," Internet: https://yasincapar.com/tr/engineering-stress-strain-vs-true-stress-strain-2/, [Dec. 21,2023].

[39] O. Bahr, P. Schaumann, B. Bollen, J. Bracke, ‘’Young’s modulus and Poisson’s ratio of concrete at high temperatures: Experimental investigations.’’ *Materials & Design*, vol. 45, pp. 423, 2013.

[40] "Mechanical Properties," Internet:https://ahssinsights.org/forming/mechanical-properties/mechanical-properties/ [Sep. 21,2023].

[41] "polymerdatabas," Internet:https://polymerdatabase.com/polymer%20physics/Stress-Strain%20Behavior.html, 2019 [Dec. 11,2023].

[42] "HALANDER," Internet: https://www.helandermetal.com/the-hydroforming-process-how-does-it-work/ [Dec. 11,2023].

APPENDIX

Parallel to Rolling Direction (0°) – Repeat 1.

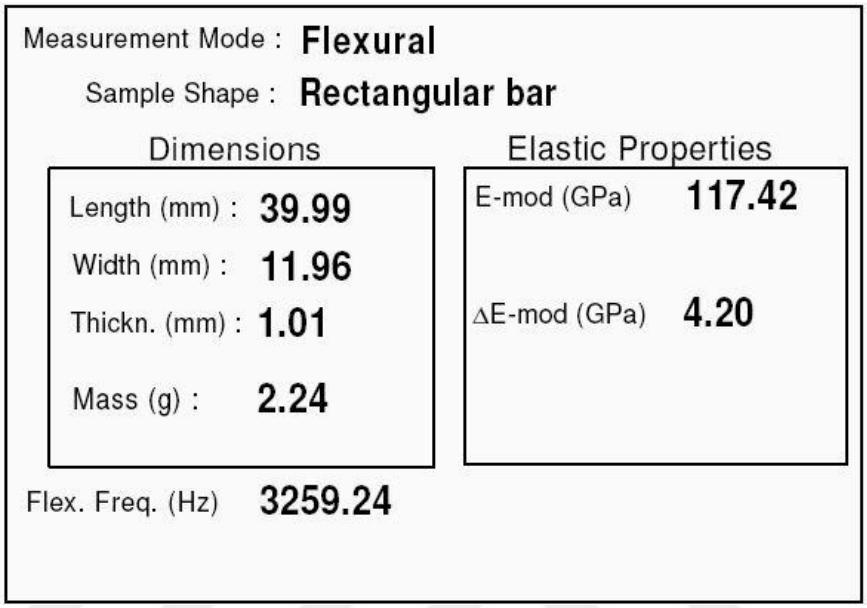

Parallel to Rolling Direction (0°) – Repeat 2

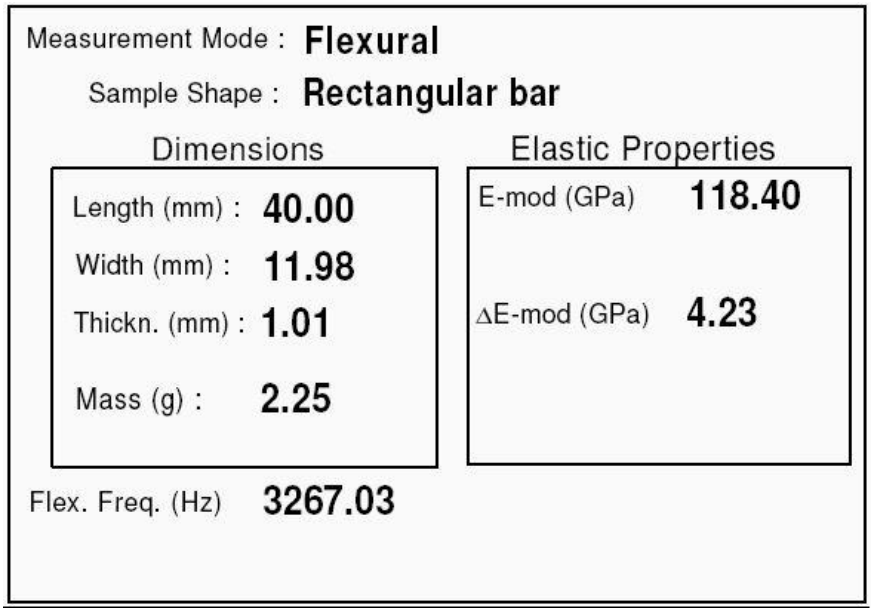

Parallel to Rolling Direction (0°) – Repeat 3

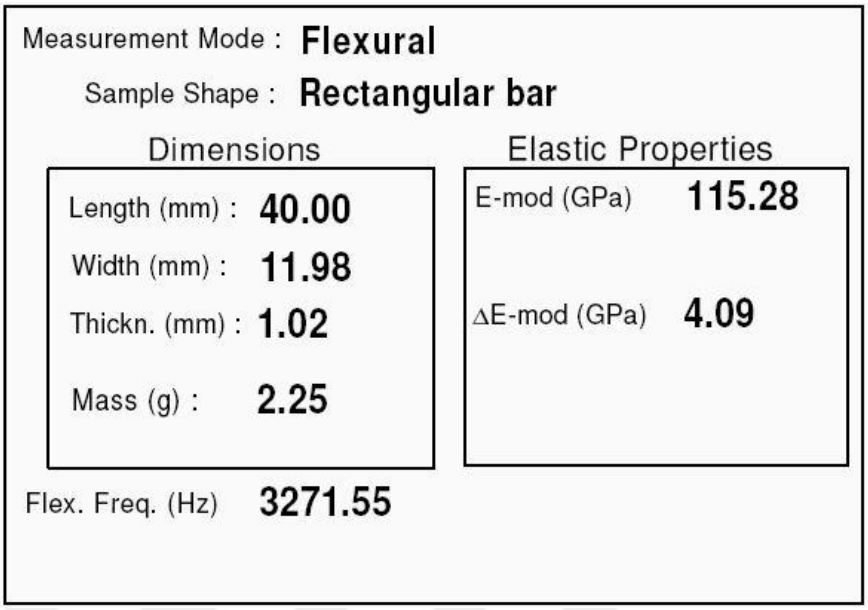

Rolling Direction (45°) – Repeat 1

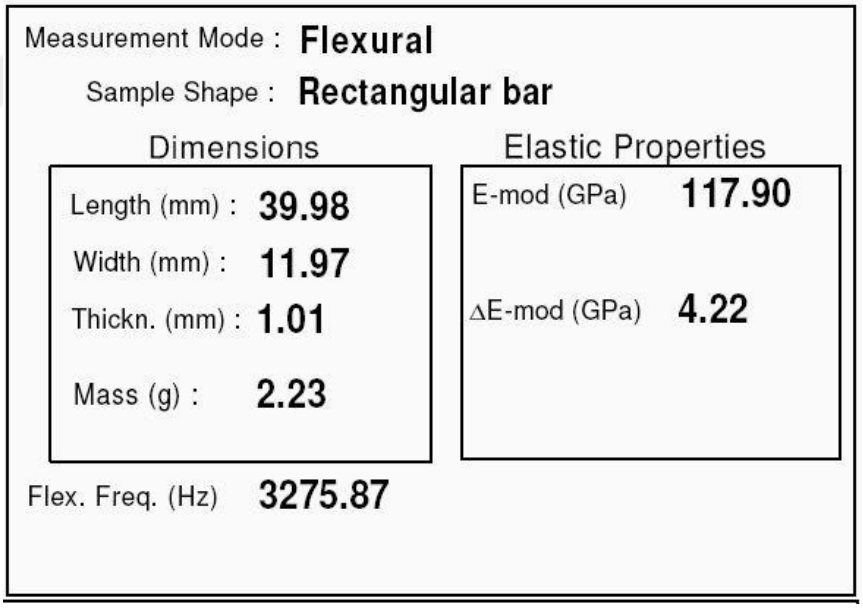

Rolling Direction (45°) – Repeat 2

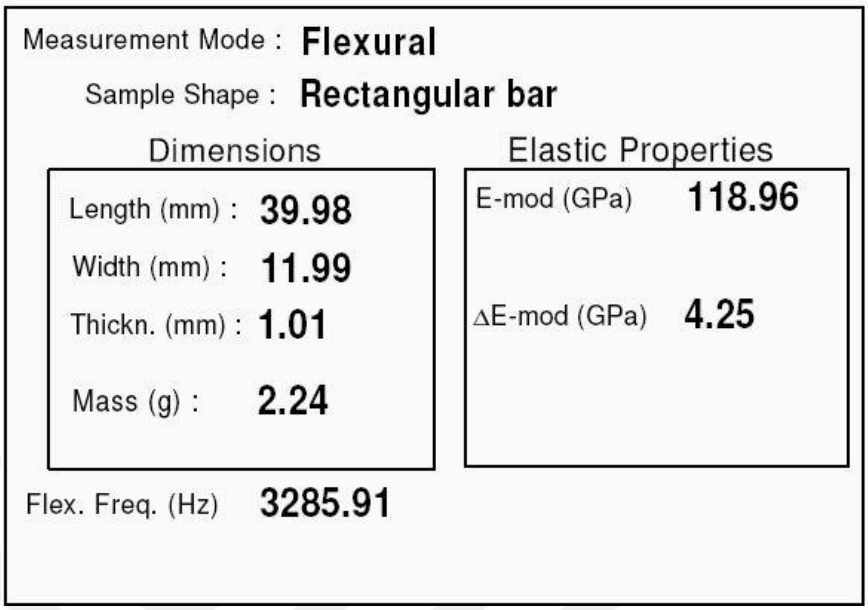

Rolling Direction (45°) – Repeat 3

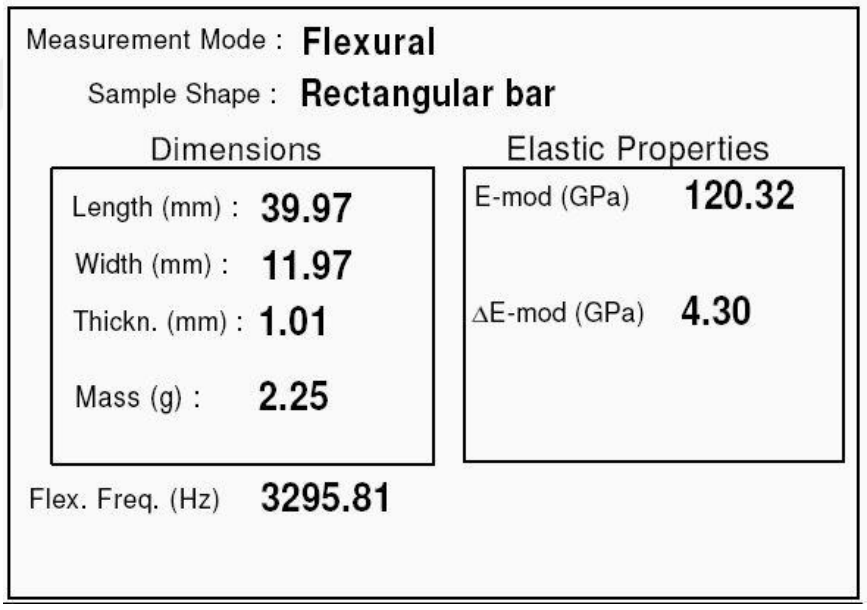

Rolling Direction (90°) – Repeat 1

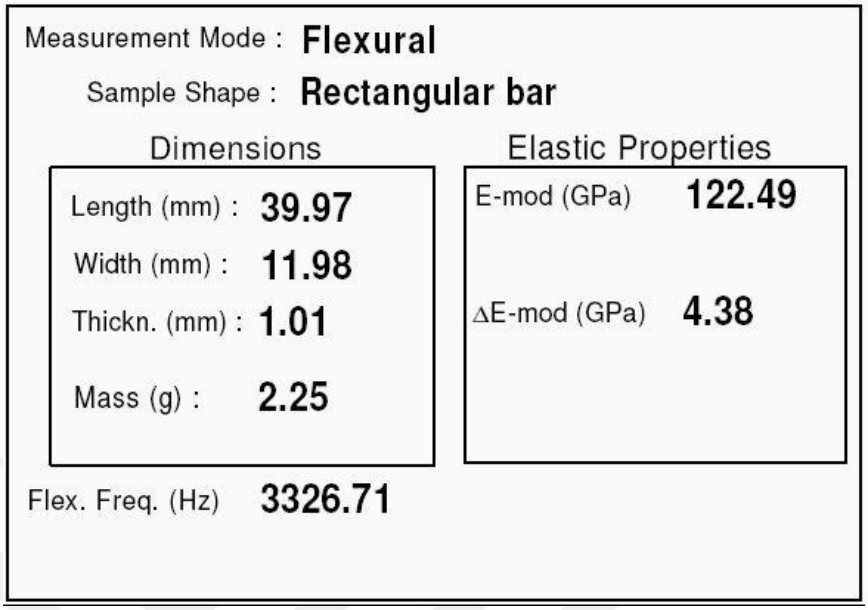

Rolling Direction (90°) – Repeat 2

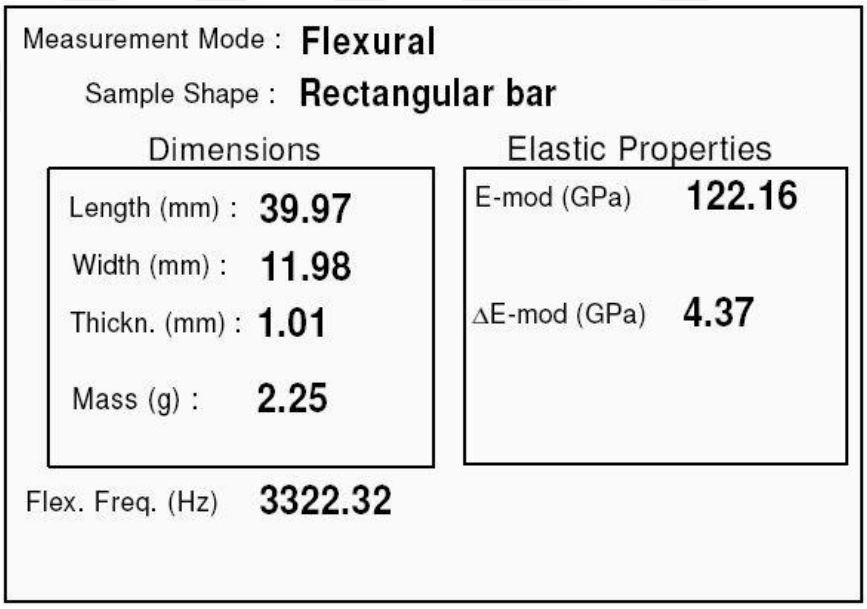

Rolling Direction (90°) – Repeat 3